Florida State University Libraries

2004

Supersymmetry at pp̄, pp and e+e# Colliders in Light of Wmap Measurements of the Dark Matter Density of the Universe

Tadas Krupovnickas

THE FLORIDA STATE UNIVERSITY

COLLEGE OF ARTS AND SCIENCES

SUPERSYMMETRY AT $p\bar{p}$, pp AND e^+e^- COLLIDERS IN LIGHT OF
WMAP MEASUREMENTS OF THE DARK MATTER DENSITY OF THE
UNIVERSE

By

TADAS KRUPOVNICKAS

A Dissertation submitted to the
Department of Physics
in partial fulfillment of the
requirements for the degree of
Doctor of Philosophy

Degree Awarded:
Summer Semester, 2004

The members of the Committee approve the dissertation of Tadas Krupovnickas defended on May 19, 2004.

Howard Baer
Professor Directing Thesis

Ettore Aldrovandi
Outside Committee Member

Laura Reina
Committee Member

Todd Adams
Committee Member

Jorge Piekarewicz
Committee Member

The Office of Graduate Studies has verified and approved the above named committee members.

ACKNOWLEDGEMENTS

I thank my advisor foremost for being a great person, not only an equally great scientist.

I would also like to thank my other collaborators: Csaba Balázs, Alexander Belyaev and Xerxes Tata.

And I thank the committee members for active participation in my presentations and being so helpful with the paperwork.

I strongly suspect that the recommendations written by Howard Baer, Laura Reina and Xerxes Tata immensely helped me to get a such a good postdoc. Many thanks to you all!

TABLE OF CONTENTS

LIST OF TABLES

LIST OF FIGURES

ABSTRACT

The Standard Model (SM) describes almost all the particle physics experiments with a high accuracy. However, the SM has a lot of conceptual problems (spontaneous symmetry breaking is introduced by hand, the Higgs boson mass has to be very finely fine-tuned, there is no explanation for the number of generations or particle quantum numbers, there are at least 19 arbitrary model parameters). Therefore, it is reasonable to search for theories solving some or all of the problems that the SM has. One class of such theories is based on an assumption that at some large energy scale Nature chooses the maximal possible space-time symmetry, called supersymmetry (SUSY).

Once the theory is constructed, it has to be tested against the experiment. This dissertation explores various collider signals in the framework of minimal Supergravity model (mSUGRA) and gaugino mediated SUSY breaking model (inoMSB). We calculate whether the signal predicted by these models could be detected at the Fermilab Tevatron and at the CERN LHC hadronic colliders, and also explore the capabilities of a future e^+e^- Linear Collider. We show the collider reach contours in the mSUGRA parameter space, combined with constraints from other experiments. We also devise new cuts, optimizing the signal to background ratio in the regions where no such work was previously done.

CHAPTER 1

INTRODUCTION

1.1   The Standard Model

Almost all known particle physics experiments to date are very well described by the Standard Model (SM) (to explain neutrino oscillations one needs to modify the SM). However, there are reasons to believe that the SM cannot be a fundamental physical theory and it is only an approximation at a certain energy scale.

The SM is a quantum field theory that is based on the gauge symmetry $SU(3)_C \times SU(2)_L \times U(1)_Y$ [1]. Here $SU(3)_C$ represents the symmetry group of strong interactions, and $SU(2)_L \times U(1)_Y$ is the symmetry group of the electroweak interactions.

The fermionic sector of the SM is organized in the following three families with identical properties except for mass:

$$\begin{pmatrix} u \\ d \end{pmatrix}_L, \ u_R, \ d_R \quad ; \quad \begin{pmatrix} \nu_e \\ e \end{pmatrix}_L, \ e_R \tag{1.1}$$

$$\begin{pmatrix} c \\ s \end{pmatrix}_L, \ c_R, \ s_R \quad ; \quad \begin{pmatrix} \nu_\mu \\ \mu \end{pmatrix}_L, \ \mu_R \tag{1.2}$$

$$\begin{pmatrix} t \\ b \end{pmatrix}_L, \ t_R, \ b_R \quad ; \quad \begin{pmatrix} \nu_\tau \\ \tau \end{pmatrix}_L, \ \tau_R. \tag{1.3}$$

The gauge sector of the SM is composed of eight gluons (gauge bosons of $SU(3)_C$) and the γ, $W^\pm$ and Z^0 particles (four gauge bosons of $SU(2)_L \times U(1)_Y$).

The Lagrangian of the SM (before the spontaneous electroweak symmetry breaking) consists of the gauge boson (GB), Higgs boson (H), fermion (F) and Yukawa (Y) terms:

$$\mathcal{L}_{GB} = -\frac{1}{4}(F^a_{\mu\nu})^2 - \frac{1}{4}(F_{\mu\nu})^2 - \frac{1}{4}\left(G^A_{\mu\nu}\right)^2, \tag{1.4}$$

$$\mathcal{L}_H = |D_\mu\phi|^2 + \mu^2\phi^\dagger\phi - \lambda(\phi^\dagger\phi)^2, \tag{1.5}$$

$$\mathcal{L}_F = \bar{E}_L(i\,\slashed{D}')E_L + \bar{e}_R(i\,\slashed{D}')e_R + \bar{Q}_L(i\,\slashed{D})Q_L + \bar{u}_R(i\,\slashed{D})u_R + \bar{d}_R(i\,\slashed{D})d_R, \tag{1.6}$$

$$\mathcal{L}_Y = -\lambda_e\bar{E}_L\cdot\phi e_R + h.c. - \lambda_d\bar{Q}_L\cdot\phi d_R - \lambda_u\epsilon^{ab}\bar{Q}_{La}\phi^\dagger_b u_R + h.c. \tag{1.7}$$

Here

$$\phi = \begin{pmatrix}\phi^+\\ \phi^0\end{pmatrix}, \tag{1.8}$$

$$F_{\mu\nu} = \partial_\mu A_\nu - \partial_\nu A_\mu, \tag{1.9}$$

$$F^a_{\mu\nu} = \partial_\mu A^a_\nu - \partial_\nu A^a_\mu + gf^{abc}_{SU(2)}A^b_\mu A^c_\nu, \tag{1.10}$$

$$G^A_{\mu\nu} = \partial_\mu G^A_\nu - \partial_\nu G^A_\mu + g_s f^{ABC}_{SU(3)}G^B_\mu G^C_\nu, \tag{1.11}$$

$$D'_\mu = \partial_\mu - igA^a_\mu T^a - ig'YB_\mu, \tag{1.12}$$

$$D_\mu = \partial_\mu - igA^a_\mu T^a - ig'YB_\mu - ig_s\frac{\lambda_A}{2}G^A_\mu, \tag{1.13}$$

$$\slashed{D} = \gamma^\mu D_\mu, \qquad \slashed{D}' = \gamma^\mu D'_\mu. \tag{1.14}$$

$f^{abc}_{SU(2)}$ are the structure constants of the $SU(2)$ group and $f^{ABC}_{SU(3)}$ are the structure constants of the $SU(3)$ group.

The scalar sector of the SM is not experimentally confirmed yet. The fact that the weak gauge bosons $W^\pm$ and Z^0 are massive particles and the photon γ is massless, indicates that $SU(2)_L \times U(1)_Y$ is not the symmetry of the vacuum but $U(1)_{em}$ is. The electroweak symmetry must be spontaneously broken via the Higgs mechanism which requires us to include a weak doublet of complex scalar fields in the SM. As a result the symmetry is broken (although rather *ad hoc*), the weak gauge bosons acquire mass, and the theory predicts the existence of a new electrically neutral scalar particle - the Higgs boson.

All this said, there are aspects of the SM which are generally perceived as important disadvantages. It does not explain the particle quantum numbers, such as weak isospin, hypercharge and color, and does not explain why just three generations are present. The SM contains at least 19 arbitrary parameters. At least 9 more parameters must be included to explain the neutrino oscillations [2]. Also, spontaneous symmetry breaking is introduced by setting the Higgs mass parameter to the wrong-sign by hand. That hardly has a satisfactory theoretical basis. The SM does not include gravitational interaction. We also encounter

fine-tuning problem. For the huge hierarchy between the electroweak and Planck scales to exist the parameters in the Higgs sector must be tuned to one part in 10^{34} [3]. New physics near the electroweak scale can stabilize this hierarchy.

1.2   Supersymmetry

One solution to some of the SM problems is to introduce an additional spacetime symmetry, called supersymmetry (SUSY).

1.2.1   The Symmetry of Spacetime

According to the Coleman-Mandula theorem [4], under some physically reasonable assumptions the largest non-trivial spacetime symmetry group of quantum field theory is the Poincaré group. Therefore all internal symmetries, such as gauge symmetries can only be realized as a direct product of the internal symmetry group with the Poincaré symmetry group. However, in their analysis Coleman and Mandula did not consider the possibility of anti-commuting spinorial charges. One can upgrade Poincaré algebra to the super-Poincaré algebra, which includes not only the commutators but also the anti-commutators of the generators of the new group.

The Poincaré group is formed by combining rotations, boosts and translations. The commutation relations between the generators of translations in space and time P_μ and the generators of rotations and boosts $M_{\mu\nu}$ are:

$$[P_\mu, P_\nu] = 0, \tag{1.15}$$

$$[M_{\mu\nu}, P_\lambda] = i\left(g_{\nu\lambda}P_\mu - g_{\mu\lambda}P_\nu\right), \tag{1.16}$$

$$[M_{\mu\nu}, M_{\rho\sigma}] = -i\left(g_{\mu\rho}M_{\nu\sigma} - g_{\mu\sigma}M_{\nu\rho} - g_{\nu\rho}M_{\mu\sigma} + g_{\nu\sigma}M_{\mu\rho}\right). \tag{1.17}$$

The Casimir operators of the Poincaré group are P^2 and the Pauli-Lubanski four-vector $(W_\mu = \frac{1}{2}\epsilon_{\mu\nu\rho\sigma}P^\nu M^{\rho\sigma})$ square W^2. The eigenvalues of the Casimir operators are used to classify the representations of the Poincaré group. The physically realized unitary representations include

- Massive particles: $P^2 = m^2 > 0$, with $W^2 = -m^2 s(s+1)$, where s denotes the spin quantum number $s = 0, \frac{1}{2}, 1, ...$

3

- Massless particles: $P^2 = 0$, with $W^2 = 0$. Here $W_\mu = \lambda P_\mu$ and λ is the helicity value. $\lambda = \pm s$, $s = 0, \frac{1}{2}, 1, ...$

It is possible to add the anti-commuting Majorana spinorial generators Q_a, $a = 1, ..., 4$ to the Poincaré group. Then we arrive at the super-Poincaré algebra with the commutation relations:

$$[P_\mu, Q_a] = 0, \tag{1.18}$$

$$[M_{\mu\nu}, Q_a] = -(\sigma_{\mu\nu})_{ab} Q_b, \tag{1.19}$$

$$\{Q_a, \bar{Q}_b\} = 2(\gamma^\mu)_{ab} P_\mu. \tag{1.20}$$

Since Q_a is a Majorana spinor charge, the anti-commutators

$$\{Q_a, Q_b\} = -2(\gamma^\mu C)_{ab} P_\mu, \tag{1.21}$$

$$\{\bar{Q}_a, \bar{Q}_b\} = 2(C^{-1}\gamma^\mu)_{ab} P_\mu \tag{1.22}$$

follow from the last two equations.

The supersymmetric algebra presented above is called a graded Lie algebra, since it contains the anti-commutators. It was shown [5] that the presented algebra is the most general graded Lie algebra, satisfying some physical assumptions (except for the possibility of more than one spinorial charge Q). Further on we will assume that there is only one super-charge Q_a, as low energy models with more than one super-charge lead to phenomenologically excluded conclusions.

In the case of the super-algebra P^2 is still the Casimir operator, but W^2 is not. Therefore, the particles in the super-multiplet have the same masses but may have different spins.

The supermultiplets of massive particles are labeled by (m, j), where m is the mass and $j = 0, \frac{1}{2}, 1, ...$ is an index, related to the spin of the particles. Each supermultiplet with mass m contains two particles with spins $j \pm \frac{1}{2}$ and two particles with spin j. The number of helicity states for spin j objects is $2(2j + 1)$, and it is equal to the combined number of helicity states for spin $j + \frac{1}{2}$ and $j - \frac{1}{2}$ objects: $2(j + \frac{1}{2}) + 1 + 2(j - \frac{1}{2}) + 1$. In other words, the number of bosonic helicity states is equal to the number of fermionic helicity states.

In the case of massless supermultiplets one can show that each supermultiplet contains the states with helicities j and $j - \frac{1}{2}$. Due to Lorentz invariance the same multiplet will have to contain the states with helicities $-j$ and $-j + \frac{1}{2}$.

4

1.2.2 Superfields

If one assumes SUSY to be the fundamental space-time symmetry, then it is possible to write a general superfield combining the bosonic and fermionic fields:

$$
\begin{aligned}
\hat{\Phi}(x,\theta) &= \mathcal{S} - i\sqrt{2}\bar{\theta}\gamma_5\psi - \frac{i}{2}(\bar{\theta}\gamma_5\theta)\mathcal{M} + \frac{1}{2}(\bar{\theta}\theta)\mathcal{N} + \frac{1}{2}(\bar{\theta}\gamma_5\gamma_\mu\theta)\mathrm{V}^\mu \\
&+ i(\bar{\theta}\gamma_5\theta)[\bar{\theta}(\lambda + \frac{i}{\sqrt{2}}\,\slashed{\partial}\psi)] - \frac{1}{4}(\bar{\theta}\gamma_5\theta)^2[\mathcal{D} - \frac{1}{2}\Box\mathcal{S}].
\end{aligned} \tag{1.23}
$$

Here we have introduced a new Majorana spinor θ with anti-commuting Grassmann numbers θ_a, $a = 1, ..., 4$ as it's components:

$$
\{\theta_a, \theta_b\} = 0. \tag{1.24}
$$

We assume that

$$
\{\theta_a, \psi_b\} = 0. \tag{1.25}
$$

The coefficients in the superfield expansion (1.23) consist of scalars $\mathcal{S}, \mathcal{M}, \mathcal{N}, \mathcal{D}$, vector V^μ and spinor fields ψ and λ.

One could prove that the general superfield (1.23) can be reduced to the left chiral superfield, which transforms into itself under supersymmetric transformation, and the right chiral superfield with similar properties:

$$
\hat{S}_L = \mathcal{S} + i\sqrt{2}\bar{\theta}\psi_\mathrm{L} + i\bar{\theta}\theta_\mathrm{L}\mathcal{F} + \frac{i}{2}(\bar{\theta}\gamma_5\gamma_\mu\theta)\partial^\mu\mathcal{S} - \frac{1}{\sqrt{2}}\bar{\theta}\gamma_5\theta\bar{\theta}\,\slashed{\partial}\psi_\mathrm{L} + \frac{1}{8}(\bar{\theta}\gamma_5\theta)^2\Box\mathcal{S}, \tag{1.26}
$$

$$
\hat{S}_R = \mathcal{S} - i\sqrt{2}\bar{\theta}\psi_\mathrm{R} - i\bar{\theta}\theta_\mathrm{R}\mathcal{F} - \frac{i}{2}(\bar{\theta}\gamma_5\gamma_\mu\theta)\partial^\mu\mathcal{S} - \frac{1}{\sqrt{2}}\bar{\theta}\gamma_5\theta\bar{\theta}\,\slashed{\partial}\psi_\mathrm{R} + \frac{1}{8}(\bar{\theta}\gamma_5\theta)^2\Box\mathcal{S}. \tag{1.27}
$$

Here, as usual,

$$
\psi_R = \frac{1 + \gamma_5}{2}\psi, \tag{1.28}
$$

$$
\psi_L = \frac{1 - \gamma_5}{2}\psi, \tag{1.29}
$$

and $\mathcal{F}$ is a complex scalar field, which replaced the fields $\mathcal{M}$ and $\mathcal{N}$ in the reduction procedure (namely, we took $\mathcal{N} = i\mathcal{M} \equiv i\mathcal{F}$).

$\hat{S}_L^\dagger$ has the form of the right chiral scalar superfield. Therefore it is possible to write the Lagrangian in terms of $\hat{S}_L$ and $\hat{S}_L^\dagger$ without losing generality.

1.2.3 The Master Lagrangian

The variation of the Lagrangian density can be only a total derivative under supersymmetric transformations. It can be shown that the coefficient of $(\bar{\theta}\gamma_5\theta)^2$ (D-term) of any superfield and the coefficient of $\bar{\theta}\theta_L$ of a left chiral superfield (F-term) transforms as a total derivative under a SUSY transformation. These terms are the candidates for the Lagrangian.

We construct two functions $K(\hat{S}_{Li}^\dagger, \hat{S}_{Lj})$ (Kähler potential) and $f(\hat{S}_{Li})$ (superpotential). The D-term of the Kähler potential and the F-term of the superpotential are candidates for a SUSY Lagrangian. After requiring that the theory is renormalizable and eliminating the auxilliary fields one arrives at the following expression of the master Lagrangian for chiral scalar superfields:

$$\mathcal{L} = \sum_i (\partial_\mu S_i)^\dagger (\partial^\mu S_i) \;+\; \frac{i}{2}\sum_i \bar{\psi}_i \,\slashed{\partial}\psi_i - \left|\frac{\partial f}{\partial \hat{S}_i}\right|^2_{\hat{S}_i=S}$$
$$-\; \frac{1}{2}\sum_{ij}\left[\frac{\partial^2 f}{\partial \hat{S}_i \partial \hat{S}_j}\bigg|_{\hat{S}_i=S} \bar{\psi}_i \frac{1-\gamma_5}{2}\psi_j + h.c.\right] \tag{1.30}$$

The Lagrangian (1.30) contains only scalar and spinor fields, and there is no gauge symmetry imposed on it. However, the supersymmetric theory has to evolve to the SM at low energies, and therefore we may expect that the Lagrangian of a supersymmetric theory will incorporate the local gauge invariance principle.

The master Lagrangian for SUSY gauge theories has the form:

$$\mathcal{L} = \sum_i (D_\mu S_i)^\dagger (D^\mu S_i) + \frac{i}{2}\sum_i \bar{\psi}_i \,\slashed{D}\psi_i + \frac{i}{2}\sum_{\alpha A} \bar{\lambda}_{\alpha A}(\slashed{D}\lambda)_{\alpha A} - \frac{1}{4}\sum_{\alpha A} F_{\mu\nu\alpha A} F_{\alpha A}^{\mu\nu}$$
$$-\; \sqrt{2}\sum_{i\alpha A}\left(S_i^\dagger g_\alpha t_{\alpha A}\bar{\lambda}_{\alpha A}\frac{1-\gamma_5}{2}\psi_i + h.c.\right)$$
$$-\; \frac{1}{2}\sum_{\alpha A}\left[\sum_i S_i^\dagger g_\alpha t_{\alpha A} S_i + \xi_{\alpha A}\right]^2 - \sum_i \left|\frac{\partial f}{\partial \hat{S}_i}\right|^2_{\hat{S}_i=S}$$
$$-\; \frac{1}{2}\sum_{ij}\bar{\psi}_i\left[\frac{\partial^2 f}{\partial \hat{S}_i \partial \hat{S}_j}\bigg|_{\hat{S}_i=S}\frac{1-\gamma_5}{2} + \left(\frac{\partial^2 f}{\partial \hat{S}_i \partial \hat{S}_j}\right)^\dagger\bigg|_{\hat{S}_i=S}\frac{1+\gamma_5}{2}\right]\psi_j, \tag{1.31}$$

where the covariant derivatives are given by:

$$D_\mu S = \partial_\mu S + i \sum_{\alpha A} g_\alpha t_{\alpha A} V_{\mu\alpha A} S, \tag{1.32}$$

$$D_\mu \psi = \partial_\mu \psi + i \sum_{\alpha A} g_\alpha t_{\alpha A} V_{\mu\alpha A} \psi_L - i \sum_{\alpha A} g_\alpha t^*_{\alpha A} V_{\mu\alpha A} \psi_R, \tag{1.33}$$

$$(\slashed{D}\lambda)_{\alpha A} = \slashed{\partial}\lambda_{\alpha A} + i g_\alpha (t^{adj}_{\alpha B} \slashed{V}_{\alpha B})_{AC} \lambda_{\alpha C}, \tag{1.34}$$

$$F_{\mu\nu\alpha A} = \partial_\mu V_{\nu\alpha A} - \partial_\nu V_{\mu\alpha A} - g_\alpha f_{\alpha ABC} V_{\mu\alpha B} V_{\nu\alpha C}. \tag{1.35}$$

$t_{\alpha A}$ is the representation of the gauge group generator, g_α is the gauge coupling constant (index α allows for several gauge couplings if the gauge group is not simple), $\xi_{\alpha A}$ is a coupling constant which enters the Fayet-Illiopoulos D-term.

The first line of the Lagrangian (1.31) contains the gauge invariant kinetic energies for the components of the chiral and gauge superfields. The second line describes the interactions of gauginos $\lambda_{\alpha A}$ with the scalar and fermion components of chiral superfields. The third line describes the scalar potential. The last line shows the interactions of matter and Higgs fields, and also the fermion mass terms. The Yukawa interactions of the SM would arise from the terms in this line.

The Lagrangian (1.31) is exactly supersymmetric. SUSY is not observed in nature, and therefore has to be broken. However, there is no compelling theory of SUSY breaking. The way to bypass this problem is to introduce SUSY breaking terms into the Lagrangian by hand. Thus our ignorance is masked by a number of input parameters, which a full theory would be able to predict from the first principles. One can only add the *soft* SUSY breaking terms to the Lagrangian (the terms which do not introduce quadratic divergences into the theory) to preserve one of its main advantages over the SM.

1.2.4 The Minimal Supersymmetric Standard Model

The next step is to supersymmetrize the SM. The gauge bosons are promoted to gauge superfields:

$$B_\mu \rightarrow \hat{B} \ni (\lambda_0, \mathcal{B}_\mu, \mathcal{D}_B), \tag{1.36}$$

$$W_{A\mu} \rightarrow \hat{W}_A \ni (\lambda_A, W_{A\mu}, \mathcal{D}_{WA}), \quad A = 1, 2, 3, \tag{1.37}$$

$$g_{A\mu} \rightarrow \hat{g}_A \ni (\tilde{g}_A, g_{A\mu}, \mathcal{D}_{gA}), \quad A = 1, ..., 8. \tag{1.38}$$

The matter content is written in terms of just the left-handed fermions and their conjugates (since the right-handed fermions are related to the conjugates of the left-handed fermions). The matter superfields are:

$$\begin{pmatrix} \nu_{iL} \\ e_{iL} \end{pmatrix} \quad \rightarrow \quad \hat{L}_i \equiv \begin{pmatrix} \hat{\nu}_i \\ \hat{e}_i \end{pmatrix}, \tag{1.39}$$

$$(e_R)^c \quad \rightarrow \quad \hat{E}_i^c, \tag{1.40}$$

$$\begin{pmatrix} u_{iL} \\ d_{iL} \end{pmatrix} \quad \rightarrow \quad \hat{Q}_i \equiv \begin{pmatrix} \hat{u}_i \\ \hat{d}_i \end{pmatrix}, \tag{1.41}$$

$$(u_R)^c \quad \rightarrow \quad \hat{U}_i^c, \tag{1.42}$$

$$(d_R)^c \quad \rightarrow \quad \hat{D}_i^c. \tag{1.43}$$

Index $i = 1, 2, 3$ refers to the generation number in the above expressions.

For the case of electron the superfields have the form:

$$\hat{e} = \tilde{e}_L(\hat{x}) + i\sqrt{2}\bar{\theta}\psi_{eL}(\hat{x}) + i\bar{\theta}\theta_L\mathcal{F}_e(\hat{x}), \tag{1.44}$$

$$\hat{E}_c = \tilde{e}_R^\dagger(\hat{x}) + i\sqrt{2}\bar{\theta}\psi_{E^cL}(\hat{x}) + i\bar{\theta}\theta_L\mathcal{F}_{E^c}(\hat{x}) \tag{1.45}$$

and similarly for the quarks. $\mathcal{F}_e$ and $\mathcal{F}_{E^c}$ are auxilliary fields, which are eliminated via the application of Euler-Lagrange equations. $\tilde{e}_L$ and $\tilde{e}_R$ are complex scalar fields, superpartners of the electron.

ψ_e and ψ_{E^c} are Majorana spinors. It is generally more convenient to work with Dirac spinors. The Dirac field may be constructed out of two Majorana spinors in the following way (provided Majorana spinors have the same charge):

$$e = P_L\psi_e + P_R\psi_{E^c}. \tag{1.46}$$

The SM doublet of the Higgs fields is promoted to a doublet of left chiral superfields:

$$\phi = \begin{pmatrix} \phi^+ \\ \phi^0 \end{pmatrix} \rightarrow \hat{H}_u = \begin{pmatrix} \hat{h}_u^+ \\ \hat{h}_u^0 \end{pmatrix}. \tag{1.47}$$

The superfield $\hat{h}_u^0$ carries weak hypercharge $Y = 1$. It generates the masses of the up-type fermions via the Yukawa interactions in the superpotential. However, the superfield $\hat{h}_u^{0\dagger}$ with $Y = -1$, which could generate the masses of the down-type fermions, can not be included

in the superpotential, as the superpotential depends only on left chiral superfields. One is led to introduce a second left chiral scalar doublet superfield,

$$\hat{H}_d = \begin{pmatrix} \hat{h}_d^- \\ \hat{h}_d^0 \end{pmatrix}. \tag{1.48}$$

which has weak hypercharge $Y = -1$.

The introduction of the second Higgs doublet also solves the anomaly cancellation problem, which would occur if there were only one Higgs doublet. In that case the theory would contain hypercharge $Y = 1$ fermions: higgsinos $\psi_{h_u^+}$ and $\psi_{h_u^0}$. By adding the second Higgs doublet, we also add the higgsinos $\psi_{h_d^-}$ and $\psi_{h_d^0}$ with $Y = -1$, and triangle anomalies succesfully cancel.

The superpotential for the MSSM is taken to be

$$\hat{f} = \mu \hat{H}_u^a \hat{H}_{da} + \sum_{ij=1,2,3} \left[(\mathbf{f}_e)_{ij} \hat{L}_i^a \hat{H}_{da} \hat{E}_j^c + (\mathbf{f}_u)_{ij} \epsilon_{ab} \hat{Q}_i^a \hat{H}_u^b \hat{U}_j^c + (\mathbf{f}_d)_{ij} \hat{Q}_i^a \hat{H}_{da} \hat{D}_j^c \right] \tag{1.49}$$

Here $a, b = 1, 2$ are $SU(2)$ doublet indices. Color indices on the quark superfields have been suppressed. The $\mathbf{f}_{ij}$s are elements of the Yukawa coupling matrices.

To summarize we show the field content of the MSSM and the corresponding quantum numbers for a single generation.

Table 1.1. The matter and Higgs superfield content of the MSSM and the corresponding gauge transformation properties and weak hypercharge quantum numbers.

Field	$SU(3)_c$	$SU(2)_L$	$U(1)_Y$
$\hat{L}_i = \begin{pmatrix} \hat{\nu}_i \\ \hat{e}_i \end{pmatrix}$	1	2	-1
$\hat{E}_c$	1	1	2
$\hat{Q}_i = \begin{pmatrix} \hat{u}_i \\ \hat{d}_i \end{pmatrix}$	3	2	$\frac{1}{3}$
$\hat{U}_c$	3*	2	$-\frac{4}{3}$
$\hat{D}_c$	3*	2	$\frac{2}{3}$
$\hat{H}_u = \begin{pmatrix} \hat{h}_u^+ \\ \hat{h}_u^0 \end{pmatrix}$	1	2	1
$\hat{H}_d = \begin{pmatrix} \hat{h}_d^- \\ \hat{h}_d^0 \end{pmatrix}$	1	2*	-1

It is possible to write down renormalizable interactions which violate baryon and lepton number conservation in the MSSM. Since such interactions must be very suppressed, we will not include terms of this type.

An additional constraint is implemented in the MSSM by defining matter parity

$$R = (-1)^{3(B-L)+2s},$$
(1.50)

and requiring that no terms in the Lagrangian violate it. It is easy to see that normal matter (the SM content and the second doublet of Higgs fields) is even and supersymmetric matter (the remaining fields, entering the superfields listed in Table 1.1) is odd under the R-parity transformation. R-parity conservation is just a simplification. There are phenomenologically viable models in which R-parity is not conserved.

The final step is to list all gauge invariant soft SUSY breaking terms:

$$
\begin{aligned}
\mathcal{L}_{soft} = & -\sum_{ij} \Big[\tilde{Q}_i^\dagger \mathbf{m}_{Q_{ij}}^2 \tilde{Q}_j + \tilde{d}_{Ri}^\dagger \mathbf{m}_{D_{ij}}^2 \tilde{d}_{Rj} + \tilde{u}_{Ri}^\dagger \mathbf{m}_{U_{ij}}^2 \tilde{u}_{Rj} \\
& + \tilde{L}_i^\dagger \mathbf{m}_{L_{ij}}^2 \tilde{L}_j + \tilde{e}_{Ri}^\dagger \mathbf{m}_{E_{ij}}^2 \tilde{e}_{Rj} + m_{H_u}^2 |\tilde{H}_u|^2 + m_{H_d}^2 |\tilde{H}_d|^2 \Big] \\
& - \frac{1}{2} \left[M_1 \bar{\lambda}_0 \lambda_0 + M_2 \bar{\lambda}_A \lambda_A + M_3 \bar{\tilde{g}} \tilde{g} \right] \\
& - \frac{i}{2} \left[M_1' \bar{\lambda}_0 \gamma_5 \lambda_0 + M_2' \bar{\lambda}_A \gamma_5 \lambda_A + M_3' \bar{\tilde{g}} \gamma_5 \tilde{g} \right] \\
& + \left[(\mathbf{a}_u)_{ij} \epsilon_{ab} \tilde{Q}_i^a H_u^b \tilde{u}_{Rj}^\dagger + (\mathbf{a}_d)_{ij} \tilde{Q}_i^a H_{da} \tilde{d}_{Rj}^\dagger + (\mathbf{a}_e)_{ij} \tilde{L}_i^a H_{da} \tilde{e}_{Rj}^\dagger + h.c. \right] \\
& + \left[(\mathbf{c}_u)_{ij} \epsilon_{ab} \tilde{Q}_i^a H_d^{b*} \tilde{u}_{Rj}^\dagger + (\mathbf{c}_d)_{ij} \tilde{Q}_i^a H_{ua}^* \tilde{d}_{Rj}^\dagger + (\mathbf{c}_e)_{ij} \tilde{L}_i^a H_{ua}^* \tilde{e}_{Rj}^\dagger + h.c. \right] \\
& + \left[b H_u^a H_{da} + h.c. \right].
\end{aligned}
$$
(1.51)

The $SU(3)$ color indices were suppressed in this formula. The 3×3 scalar mass squared matrices are Hermitian, so each contains 6 real and 3 imaginary independent parameters. The gaugino mass parameters M_i's and M_i''s are real and there are 6 of them. The $\mathbf{a}$ and $\mathbf{c}$ are general complex matrices with 18 independent parameters in each. The bilinear term b can, in general, be complex.

To continue the count of the MSSM parameters one needs to add the free parameters entering the superpotential (1.49). The main contribution to the count comes from the 3×3 generally complex Yukawa coupling matrices. Omitting the details, there are 178 parameters in our version of the MSSM (and that's after requiring the R-parity invariance and B and L number conservation). If one excludes the $\mathbf{c}$ terms in the soft SUSY breaking Lagrangian (as they are strongly supresed by the experimental constraints in many models), then 124 parameters still remain.

For comparison, the SM contains 19 free parameters: three gauge couplings g_1, g_2 and g_3, the parameter θ_{QCD}, μ and λ from the Higgs potential, six quark and three lepton masses, three CKM mixing angles, and one phase in the CKM matrix.

It is not very surprising that the MSSM contains such a huge (compared to the SM) number of parameters. The MSSM is not a fundamental theory, but rather an extension of the SM, which itself is considered to be an effective theory. However, to make phenomenological analysis viable, one could simplify the MSSM using some reasonable assumptions.

One of the most important motivations for the weak scale SUSY was the elimination of quadratic divergencies, which introduce a huge fine-tuning into the SM. But this goal can only be achieved by requiring that the SUSY breaking parameters and μ are of the order of the weak scale, or at most a few TeV. This requirement restricts the SUSY particle masses to be not overly large.

The higher order corrections to the CP and flavor violating processes, which include sparticles in the loops, depend on the sparticle masses. Experimental constraints on the CP and flavor violation are very strict, so the way to agree with the experiment is either to increase the sparticle masses (but we already restricted them to be not too heavy) or drop the CP and flavor violating terms in the supersymmetric sector.

In the following, we set the **c** terms to zero. We will also assume that squark and slepton soft mass matrices as well as **a** matrices are diagonal in the same basis that the fermion Yukawa couplings are diagonal.

We also neglect the Yukawa couplings for the first and second generations. Including the third generation Yukawa couplings, the matrices are approximated by

$$\mathbf{f}_e \sim \begin{pmatrix} 0 & 0 & 0 \\ 0 & 0 & 0 \\ 0 & 0 & f_\tau \end{pmatrix}, \quad \mathbf{f}_u \sim \begin{pmatrix} 0 & 0 & 0 \\ 0 & 0 & 0 \\ 0 & 0 & f_t \end{pmatrix}, \quad \mathbf{f}_d \sim \begin{pmatrix} 0 & 0 & 0 \\ 0 & 0 & 0 \\ 0 & 0 & f_b \end{pmatrix}. \qquad (1.52)$$

Matrices **a** are taken to be proportional to the Yukawa coupling matrices:

$$\mathbf{a}_e \sim \begin{pmatrix} 0 & 0 & 0 \\ 0 & 0 & 0 \\ 0 & 0 & f_\tau A_\tau \end{pmatrix}, \quad \mathbf{a}_u \sim \begin{pmatrix} 0 & 0 & 0 \\ 0 & 0 & 0 \\ 0 & 0 & f_t A_t \end{pmatrix}, \quad \mathbf{a}_d \sim \begin{pmatrix} 0 & 0 & 0 \\ 0 & 0 & 0 \\ 0 & 0 & f_b A_b \end{pmatrix}. \qquad (1.53)$$

A_τ, A_t and A_b are called trilinear couplings. Bilinear coupling b is taken to be real and written as $b = B\mu$. This parametrization of the **a** and b terms is motivated by gravity mediated models.

The constructed theory still respects the electroweak symmetry. It has to be spontaneously broken. The (tree level) scalar potential consists of three parts:

$$V_F = \sum_i \left| \frac{\partial \hat{f}}{\partial \hat{S}_i} \right|_{\hat{S}=S}, \tag{1.54}$$

$$V_D = \frac{1}{2} \sum_A \left[\sum_i S_i^\dagger g t_A S_i \right]^2, \tag{1.55}$$

$$V_{soft} = \sum_i m_{\phi_i}^2 |\phi_i|^2 - B\mu(H_d H_u + h.c.). \tag{1.56}$$

Index i runs over all the scalar fields.

We rotate the *vev* of H_u to its lower component, which is defined to be neutral. It can be proved that minimization of the potential with respect to the other component of H_u gives $< h_d^- >= 0$. We only have to minimize the scalar potential for the neutral Higgs fields:

$$\begin{aligned} V_{scalar} &= (m_{H_u}^2 + \mu^2)|h_u^0|^2 + (m_{H_d}^2 + \mu^2)|h_d^0|^2 \\ &- B\mu(h_u^0 h_d^0 + h.c.) + \frac{1}{8}(g^2 + g'^2)(|h_u^0|^2 - |h_d^0|^2)^2. \end{aligned} \tag{1.57}$$

The first derivatives of the potential with respect to the conjugate fields are set to zero:

$$\frac{\partial V}{\partial h_u^{0*}} = (m_{H_u}^2 + \mu^2)h_u^0 - B\mu h_d^{0*} + \frac{1}{4}(g^2 + g'^2)h_u^0(|h_u^0|^2 - |h_d^0|^2) = 0, \tag{1.58}$$

$$\frac{\partial V}{\partial h_d^{0*}} = (m_{H_d}^2 + \mu^2)h_d^0 - B\mu h_u^{0*} - \frac{1}{4}(g^2 + g'^2)h_d^0(|h_u^0|^2 - |h_d^0|^2) = 0. \tag{1.59}$$

The same condition applies to the derivatives of the scalar potential with respect to the fields.

We are not interested in the trivial solution $< h_u^0 >=< h_d^0 >= 0$ (no EW symmetry breaking). To insure that we reach the minimum of the potential, the determinant of the matrix of second derivatives is required to be negative at the origin. Since we are evaluating

the derivatives at the origin of the field space, only the bilinear terms contribute, and we have

$$(B\mu)^2 > (m_{H_u}^2 + \mu^2)(m_{H_d}^2 + \mu^2). \tag{1.60}$$

The quartic term vanishes in the direction of the field space where $|h_u^0| = |h_d^0|$. In other directions the quartic term is large and dominant, and therefore the potential is bounded from below. In the direction of $|h_u^0| = |h_d^0|$ we require the scalar potential to be positive, so that a local minimum would occur:

$$m_{H_u}^2 + m_{H_d}^2 + 2\mu^2 > 2B\mu. \tag{1.61}$$

If these conditons are met, then the scalar potential develops a well-defined local minimum, where electroweak symmetry is spontaneously broken. We write $< h_u^0 > \equiv v_u$, $< h_d^0 > \equiv v_d$ and define a parameter

$$\tan\beta \equiv \frac{v_u}{v_d}. \tag{1.62}$$

Using the relation

$$M_Z^2 = \frac{g^2 + g'^2}{2}(v_u^2 + v_d^2), \tag{1.63}$$

one can arrive at the tree level minimization conditions:

$$B\mu = \frac{(m_{H_u}^2 + m_{H_d}^2 + 2\mu^2)\sin 2\beta}{2}, \tag{1.64}$$

$$\mu^2 = \frac{m_{H_d}^2 - m_{H_u}^2 \tan^2\beta}{\tan^2\beta - 1} - \frac{M_Z^2}{2}. \tag{1.65}$$

Now we can list the sparticle content of the MSSM. The gluon's superpartner is called the gluino $\tilde{g}$. Each quark has a squark as a superpartner, and the same is true for the leptons (the superpartners are generally denoted by the same symbol as partners with a tilde on the top). The superpartners of the electroweak gauge bosons mix with the superpartners of two Higgs doublet fields and produce four neutral gauginos called neutralinos $\tilde{Z}_i^0$ ($i = 1, ..., 4$) and two charged gauginos called charginos $\tilde{W}_j^\pm$ ($j = 1, 2$). There are four Higgs bosons in the MSSM: light scalar h^0, pseudoscalar A^0, heavy scalar H^0, and the charged Higgs boson $H^\pm$.

The squarks and sleptons are scalars, but the quarks and leptons are fermions with four independent components. Since the number of degrees of freedom is supposed to be the

same in the fermionic and bosonic sector of the supersymmetric theory, there have to be two scalar partners (each having two independent components) for each fermion of the SM. So, for example, top quark t has two superpartners $\tilde{t}_L$ and $\tilde{t}_R$. These scalar fields do not represent the mass matrix eigenstates, and therefore they can mix. The mass eigenstates are called $\tilde{t}_1$ and $\tilde{t}_2$, $m_{\tilde{t}_1} < m_{\tilde{t}_2}$. Since the mixing angle depends on the Yukawa coupling, mixing is generally neglected for the first two generations, for which the Yukawa coupling is small.

Even in the final presented form, the MSSM still contains a lot of parameters. The assumptions which were made to reduce the number of parameters are not justified by the MSSM itself, but rather by the experimental results. SUSY breaking is introduced by hand. All these shortcomings lead to consider models with fewer parameters, which are based on some deeper theoretical insights and try to explain the SUSY breaking.

1.2.5 Models of SUSY Breaking

All attempts to introduce spontaneous SUSY breaking at the TeV scale into the supersymmetric theories fail due to phenomenological problems. For example, in O'Raifeartaigh's model [7] with F-type SUSY breaking one gets the lightest massive boson lighter than the lightest massive fermion, the fact not observed in the experiments. That led people to consider some other types of models, where SUSY is generally broken in a hidden sector, and then mediated to the visible sector (containing the MSSM fields) via the messenger fields.

Historically the first to appear and still the most commonly used models were inspired by supergravity. The main idea behind such models is promoting SUSY transformations from global to local transformations. Then the requirement of the invariance under supersymmetric transformations leads to the appearance of the same terms as in the Lagrangian of general relativity. The full supersymmetric Lagrangian for gauge theories was first presented in [8].

When local SUSY is broken, the resulting Goldstino is absorbed by the otherwise massless gravitino (the superpartner of the graviton). The gravitino becomes massive with a mass of

$$m_{3/2} = e^{G_0/2} M_P, \tag{1.66}$$

where G_0 is the *vev* of the Goldstino.

The hidden sector is assumed to contain only the fields which are gauge singlets under the observable sector gauge symmetries. Thus hidden sector fields interact with the visible sector fields only via gravitational interactions. If the scale of SUSY breaking in the hidden sector is $\sim 10^{11}$ GeV, then the soft SUSY breaking terms in the visible sector all have magnitude ~ 1 TeV, just as we required in the MSSM.

Taking a flat Kähler metric for the chiral scalar fields of the hidden sector leads to a common mass for all scalars: $m_0^2 = m_{3/2}^2 + V_0$. V_0 is the minimum of the scalar potential. Universal scalar masses solve the problems of SUSY flavor and CP violation. Also, common gaugino masses $m_{1/2}$ may be obtained by making additional assumptions. In such case, the model is called mSUGRA or CMSSM (Constrained MSSM). mSUGRA has only 5 parameters in addition to the SM parameters:

$$m_0, \quad m_{1/2}, \quad A_0, \quad \tan\beta, \quad sign\mu. \tag{1.67}$$

The above parameters (with the exception of $\tan\beta$) are defined at the GUT (grand unified theory) scale, where all three SM couplings unify, rather than the Planck scale. A_0 is the common value of the trilinear couplings A_t, A_b and A_τ at the GUT scale. The absolute value of μ is fixed by the other parameters.

The other SUSY breaking models include the anomaly mediated SUSY breaking (AMSB) [9], the gauge mediated SUSY breaking (GMSB) [10] and the gaugino mediated SUSY breaking (inoMSB) [11].

The AMSB is based on the fact that there is an additional contribution to the soft SUSY breaking terms in the visible sector, which originates in the super-Weyl anomaly. Such contribution can dominate in models without SM gauge singlet superfields that can acquire a Planck scale vev.

The parameter space of the AMSB model consists of

$$m_0, \quad m_{3/2}, \quad \tan\beta, \quad sign\mu. \tag{1.68}$$

The gaugino masses are determined by the other parameters.

In the GMSB model the messenger superfields themselves carry the $SU(3)_C \times SU(2)_L \times U(1)_Y$ quantum numbers, while the hidden sector superfields do not. Soft SUSY breaking terms in the visible sector are generated radiatively, with the messenger fields in the loops.

The GMSB model has the following parameters:

$$\Lambda, \quad M, \quad n_5, \quad \tan\beta, \quad sign\mu, \quad C_{grav}. \tag{1.69}$$

Here $\Lambda = <F_S> / <S>$ is the ratio of the components of the hidden sector superfield, M is the mass scale associated with the messenger fields, n_5 is a parameter which enters the expressions of the gaugino and scalar masses, and C_{grav} gives the ratio $<F_{grav}> / <F_S>$, where $<F_{grav}>$ is the F-term responsible for giving gravitino a mass.

The inoMSB models are inspired by the string theory. They are based on an idea that the visible sector is confined to one brane in the space with extra dimensions, and the hidden sector is confined to another brane. The messenger superfields (which include gauge and gravity superfields) propagate in the bulk and couple to both branes. One can take a particular realization of this model, where we specify the symmetry group of the visible sector at the GUT scale. The compactification scale M_c ($M_{GUT} < M_c \leq M_P$) is introduced, at which the boundary conditions for the soft SUSY breaking parameters of the MSSM are taken to be

$$m_0 = A_0 = B_0 = 0. \tag{1.70}$$

Then the model has the following parameters:

$$m_{1/2}, \quad M_c, \quad \tan\beta, \quad sign\mu. \tag{1.71}$$

1.2.6 Sparticle Production at Colliders

At hadronic colliders the superpartners of the SM particles are produced via the collisions of partons - gluons and quarks. Depending on the particle masses and underlying model parameters, one can expect to see different signals above the SM background. The dominant scenarios, occuring in mSUGRA, are described below and further in the manuscript.

If at least some of the squarks are sufficiently light to be produced, then the pair production of squarks, where squarks subsequently decay to quarks and gauginos, can give rise to high multiplicity jets. If R-parity is conserved, then the lightest supersymmetric particle would escape detection and therefore squark production would also be accompanied by a large missing transverse energy.

In case of the dominant gluino production, and gluino being heavier than squarks, one would observe lengthy cascade decays, with gluino decaying to squarks and quarks, and squarks decaying into quarks and gauginos.

If only gauginos can be produced, the dominant process may be $\tilde{W}_1\tilde{Z}_2$ or $\tilde{W}_1\tilde{W}_1$ production. If $\tilde{W}_1$ can only decay in three body mode, then one could search for multilepton signals. However, this case is usually quite swamped by the background.

At the linear collider the background is much reduced, but the center of mass energy is usually lower too. The discovery capabilities of a linear collider are generally determined by the masses of particles. In the subsequent chapters we show that usually the signal can be disentangled from the background by using proper cuts if there is sufficient energy to create the sparticle pair.

CHAPTER 2

REACH OF THE FERMILAB TEVATRON FOR MINIMAL SUPERGRAVITY IN THE REGION OF LARGE SCALAR MASSES

2.1 Introduction

Run 2 of the Fermilab Tevatron $p\bar{p}$ collider has begun at center of mass energy $\sqrt{s} = 1.96$ TeV, and already the CDF and D0 experiments have gathered over 300 pb^{-1} of integrated luminosity. Projections are to acquire anywhere from 2-10 fb^{-1} of integrated luminosity before turn on of the CERN LHC. One prominent goal of Tevatron experiments is to discover the Higgs boson, which may well be within reach according to analyses of electroweak radiative corrections. Another prominent goal is to obtain evidence for weak scale supersymmetric matter.

The search for supersymmetry is somewhat model dependent. In this chapter, we adopt the paradigm minimal supergravity model (mSUGRA)[12], with parameters

$$m_0, \ m_{1/2}, \ A_0, \ \tan\beta, \ sign(\mu). \tag{2.1}$$

In models such as mSUGRA, with gaugino mass unification and a weak scale gravitino mass, the gluino to chargino mass ratio is $m_{\tilde{g}}/m_{\widetilde{W}_1} \sim 3.7$, so that bounds from LEP2 ($m_{\widetilde{W}_1} > 103.5$ GeV)[13] likely place gluino pair production out of reach of Tevatron experiments. Since squark masses are usually comparable to or greater than $m_{\tilde{g}}$, it is likely that squark pair production is beyond the Tevatron reach as well. An exception occurs for third generation squarks- the top and bottom squarks- since these might have much lower masses[14]. In addition, slepton pair production occurs at low enough rates in these models that they are unlikely to be directly observable[15].

18

However, charginos and neutralinos may well be within the kinematic reach of the Tevatron, and can be produced with observable cross sections. Important pair production reactions include

- $p\bar{p} \to \widetilde{W}_1 \widetilde{Z}_1 X$,

- $p\bar{p} \to \widetilde{W}_1^+ \widetilde{W}_1^- X$ and

- $p\bar{p} \to \widetilde{W}_1 \widetilde{Z}_2 X$,

where X represents assorted hadronic debris. The purely hadronic final states suffer large QCD backgrounds, while the leptonic final states have more manageable electroweak backgrounds. The first of these reactions can lead to single lepton plus missing energy states, which suffer large backgrounds from $W \to \ell\nu_\ell$ production (here, $\ell = e$, μ and τ). The second chargino pair reaction suffers large backgrounds from WW and $Z \to \tau\bar{\tau}$ production. The last of these– $\widetilde{W}_1 \widetilde{Z}_2$ production– can lead to clean (non-jetty) trilepton plus $\not{E}_T$ final states which can be above SM background levels for significant regions of model parameter space.

The clean trilepton signature was suggested as long ago as 1983[16], and explicit collider calculations for production via on-shell gauge bosons were performed in Refs.[17, 18], including spin correlations between initial and final states. Arnowitt and Nath pointed out that rates may be detectable even for production via off-shell gauge bosons[19]. More detailed projections (based on partial neutralino branching fraction calculations) yielded a pessimistic assessment of the Tevatron reach[20]. Improved sparticle production and decay calculations however showed that in fact the reach of Fermilab Tevatron experiments could extend well past LEP2 for significant regions of model parameter space[21]. This was followed by a number of calculations[22] and collider simulations of clean trilepton detection rates considered against SM backgrounds arising mainly from WZ production[23, 24, 25, 26], with results being extended to large $\tan\beta$ in Ref. [27]. Especially for large $\tan\beta$, it was found that the greatest reach was obtained via the inclusive trilepton channel, with jetty events allowed into the trilepton sample[28, 29]. At the Fermilab Tevatron SUSY/Higgs workshop (concluded in year 2000), it was found that in fact the largest backgrounds came from off-shell W^*Z^* and $W^*\gamma^*$ production[30]. These backgrounds were calculated, and cuts were modified to show that in fact the inclusive trilepton signal was still observable over

large portions of mSUGRA model parameter space[28, 29, 31, 32, 33]. Reach calculations were made in the m_0 *vs.* $m_{1/2}$ plane extending out to m_0 values as high as 1 TeV.

Since these previous calculations, a greater emphasis has been placed on mSUGRA model parameter space at large m_0 values. It has been noticed that as m_0 increases, ultimately the superpotential μ parameter, as derived from radiative electroweak symmetry breaking (REWSB), becomes small in magnitude shortly before encountering the region where REWSB breaks down[34]. Chan *et al.*[35], adopting effectively μ^2/M_Z^2 as a fine-tuning parameter, emphasized that the entire region of small μ^2 at large m_0 may be considered to have low fine tuning; they dubbed the region as the "hyperbolic branch". Later, using more sophisticated fine tuning calculations, Feng *et al.*[36] showed that just the low $m_{1/2}$ portion of the hyperbolic branch has low fine tuning. The peculiar focussing behavior of the RG running of the soft breaking Higgs mass $m_{H_u}^2$ in this region led to the characterization as the "focus point" region. In this chapter, we will refer to the large m_0 region with small $|\mu|$ as the hyperbolic branch/focus point (HB/FP) region.

The large m_0 region of parameter space has received renewed attention as well due to several experimental developments. First, improved evaluations of the neutralino relic density[37, 38, 39, 40, 41] show four viable regions of mSUGRA model parameter space consistent with recent WMAP and other data sets[42]. These include 1.) the bulk region at low m_0 and $m_{1/2}$ where neutralinos may annihilate in the early universe via t-channel slepton exchange, 2.) the stau co-annihilation region where $m_{\widetilde{Z}_1} \simeq m_{\tilde{\tau}_1}$[37], 3.) the axial Higgs A annihilation corridor at large $\tan\beta$[38] and 4.) the HB/FP region where the neutralino has a significant higgsino component and can readily annihilate to WW and ZZ pairs in the early universe[39]. A fifth region of squark-neutralino co-annihilation can exist as well for particular values of the A_0 parameter that give rise, for instance, to $m_{\tilde{t}_1} \simeq m_{\widetilde{Z}_1}$[40].

The bulk region of relic density, which originally seemed most compelling, is difficult to reconcile with LEP2 limits on the Higgs mass, the $b \to s\gamma$ branching fraction, and for $\mu < 0$, the muon anomalous magnetic moment[43, 44]. The stau co-annihilation region is viable, but unless the parameters are just right, the relic density can become either too large or too small. The A-annihilation corridor is also viable, but requires large $\tan\beta$, and usually sparticle masses are beyond the reach of Tevatron searches. The HB/FP region remains viable for almost all $\tan\beta$ values, and since scalar sparticles are typically in the multi-TeV

regime, gives a value of $b \to s\gamma$ and a_μ in close accord with SM predictions[43, 44]. Since $|\mu|$ is small in the HB/FP region, then charginos and neutralinos are expected to be light, and hence signals such as the trilepton one may be accessible to Tevatron collider searches.

2.2   Calculational Procedure and the Results

For these reasons, in this chapter we extend the trilepton search results presented in Ref. [28] to large values of $m_0 > 1$ TeV, including the HB/FP region. For our signal calculations, we use Isajet v7.66[45]. This version of Isajet contains 1-loop corrections to all sparticle masses[46], and treats the Higgs potential in the RG-improved one loop effective potential approximation. It yields good overall agreement with other publicly available codes, as documented by Allanach *et al.*[47], including the location of the HB/FP region. We note, however, that the location of the HB/FP region is very sensitive to the value of m_t adopted in the calculation. To illustrate this, we show in Fig. 2.1 the boundary of parameter space in the m_0 *vs.* $m_{1/2}$ plane for $A_0 = 0$, $\tan\beta = 10$, $\mu > 0$, and for $m_t = 172.5, \ 175, \ 177.5$ and 180 GeV. The right-hand boundary, which dictates the location of the HB/FP region, ranges from 2-20 TeV depending on m_t and $m_{1/2}$.

We adopt the SM background calculation as presented in Ref. [28]. The backgrounds evaluated include WZ ($Z \to \tau\bar{\tau}$) production, Z^*Z^* production, $t\bar{t}$ production and trilepton production through a variety of $2 \to 4$ Feynman graphs including $W^*\gamma^*$ and W^*Z^* production, as calculated using Madgraph[48]. In Ref. [28], a variety of cuts were proposed to reduce background compared to signal. Here, we adopt set SC2 from Ref. [28], which generally gave a reach in accord with calculations from Refs. [29, 31]. For these cuts, the total $3\ell + \not{E}_T$ background level was found to be 1.05 fb.

Our first results are shown in Fig. 2.2, where we show the m_0 *vs.* $m_{1/2}$ plane for $\tan\beta = 10$, $A_0 = 0$ and $\mu > 0$. Here, and in the rest of this chapter, we fix $m_t = 175$ GeV. The red regions are excluded by lack of REWSB (right side) and presence of a stau LSP (left side). The magenta shaded regions are excluded by the LEP2 bound $m_{\widetilde{W}_1} > 103.5$ GeV.[1] In addition, the region below the magenta contour has $m_h < 114.1$ GeV, in violation of LEP2 limits on the search for a SM Higgs boson. We also show the Tevatron reach

---

[1]LEP experiments exclude charginos up to 91.9 GeV even if $m_{\widetilde{W}_1} - m_{\widetilde{Z}_1}$ is as small as 3 GeV, so that the LEP excluded region is unlikely to be much altered even in the HB/FP part of parameter space.
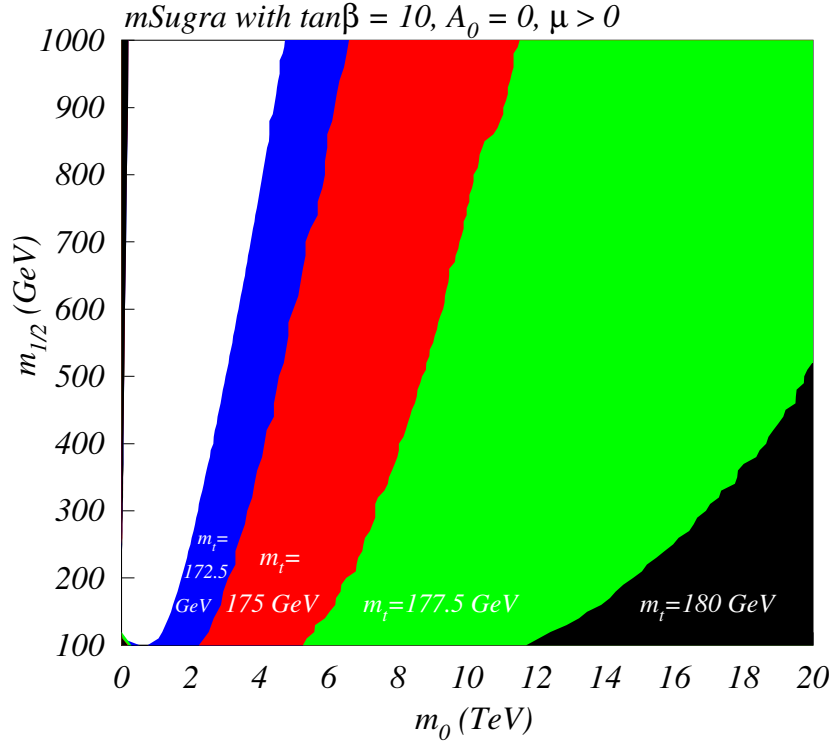
Figure 2.1. Boundary of the m_0 *vs.* $m_{1/2}$ parameter plane of the mSUGRA model, with $\tan\beta = 10$, $A_0 = 0$ and $\mu > 0$, for $m_t = 172.5$, 175, 177.5 and 180 GeV.

contours requiring a 5σ signal for 10 fb^{-1} of integrated luminosity (solid contour), and a more optimistic contour for a 3σ signal for 25 fb^{-1} (dashed contour). These correspond to signal cross sections rates of 1.62 fb and 0.61 fb, respectively, after application of cuts SC2 of Ref. [28].

The first feature to note is that the LEP2 bound on m_h now excludes essentially all the region that was previously mapped out in Refs. [28, 29, 31]. There is some uncertainty of a few GeV with respect to the calculation of m_h (see *e.g.* Ref. [47]), so the magenta contour is not a solid bound on mSUGRA parameter space. In any case, the reach region of the Fermilab Tevatron separates into two regions. The first, for very low m_0 values where sleptons are light, has the $\widetilde{Z}_2 \to \tilde{\ell}\ell$ and $\widetilde{W}_1 \to \tilde{\ell}\nu$ two body decay modes allowed, which dominate the $\widetilde{Z}_2$ and $\widetilde{W}_1$ branching fractions. The large leptonic branching fractions give rise
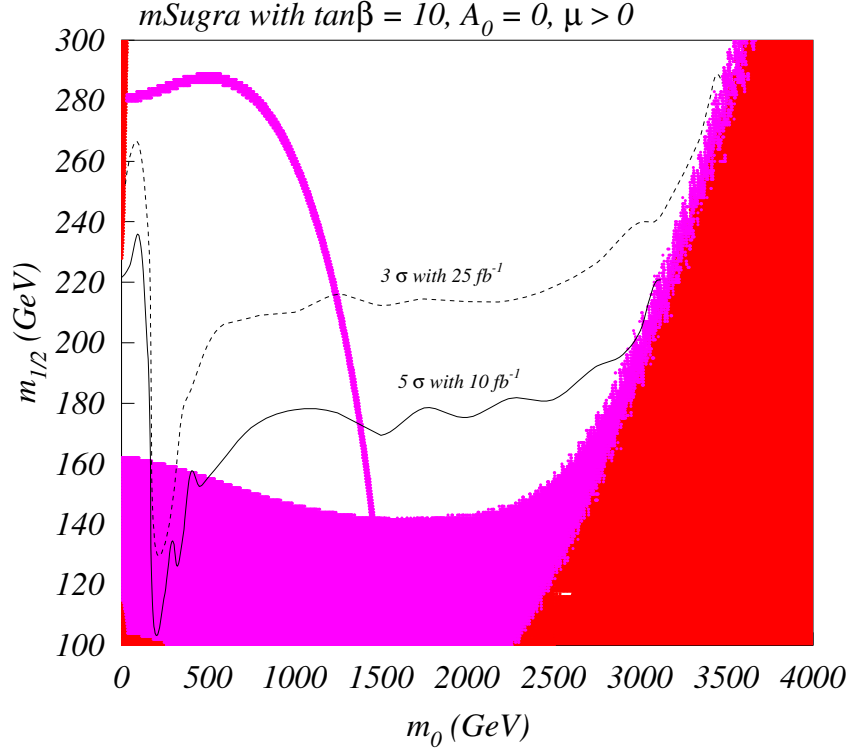
Figure 2.2. The reach of Fermilab Tevatron in the m_0 *vs.* $m_{1/2}$ parameter plane of the mSUGRA model, with $\tan\beta = 10$, $A_0 = 0$ and $\mu > 0$, assuming a 5σ signal at 10 fb^{-1} (solid) and a 3σ signal with 25 fb^{-1} of integrated luminosity (dashed). The red (magenta) region is excluded by theoretical (experimental) constraints. The region below the magenta contour has $m_h < 114.1$ GeV, in violation of Higgs mass limits from LEP2.

to high rates for trileptons. The second region occurs for $m_0 \gtrsim 300$ GeV. As m_0 increases, the slepton masses also increase so that two-body chargino and neutralino decay modes become forbidden. In the region of moderate $m_0 \sim 200$ GeV, three-body decays such as $\widetilde{Z}_2 \to \ell\bar{\ell}\widetilde{Z}_1$ can occur, but interference between slepton- and Z-mediated decay graphs give rise[21] to a very tiny leptonic branching fraction for the $\widetilde{Z}_2$, and hence a sharp drop in the Tevatron reach for SUSY via trileptons. As m_0 increases further, the slepton mediated decay diagrams for $\widetilde{Z}_2$ three-body decay are increasingly suppressed, and the decay rate becomes dominated by the Z exchange graph. Ultimately, the branching fraction $\widetilde{Z}_2 \to e^+e^-\widetilde{Z}_1$ increases to $\sim 3\%$, *i.e.* the same as the Z branching fraction to electrons. Thus the reach of Fermilab
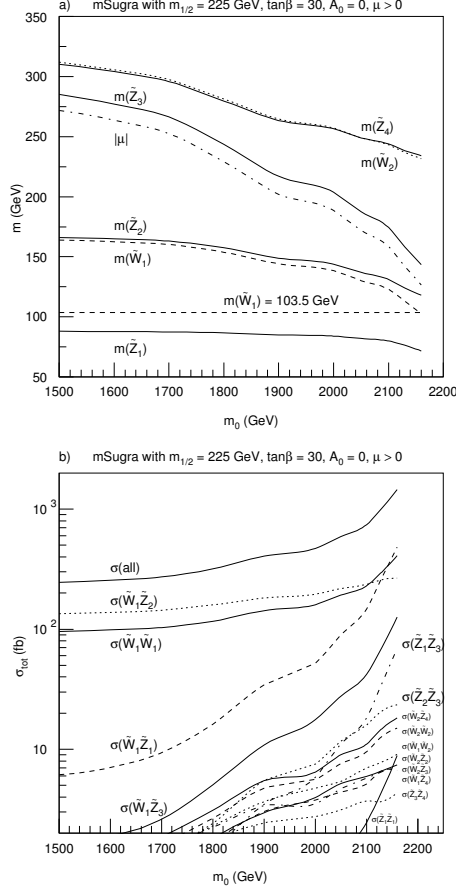
Figure 2.3. In *a.*), we show selected sparticle masses versus m_0 in the HB/FP region. In *b.*), the corresponding total cross sections are shown.

Tevatron experiments increases and levels off as m_0 becomes large. However, for very large m_0 values, then we enter the HB/FP region, where $|\mu|$ become small. In this case, chargino and neutralino masses decrease, and the production cross sections rise, yielding an increased reach at very large m_0. From Fig. 2.2, we see that the 5σ reach for 10 fb^{-1} reaches $m_{1/2} \sim 175$ GeV for $m_0 \sim 1000 - 2000$ GeV, corresponding to a reach in $m_{\widetilde{W}_1}$ $(m_{\tilde{g}})$ of 125 (525) GeV. The observability of the 3σ signal for 25 fb^{-1} of integrated luminosity extends to values of $m_{1/2} \sim 210$ GeV, corresponding to values of $m_{\widetilde{W}_1}$ $(m_{\tilde{g}}) \sim 150$ (600) GeV. In the HB/FP region, this extends to $m_{1/2} \sim 270$ GeV, corresponding to a reach in $m_{\tilde{g}} \sim 750$ GeV.

24
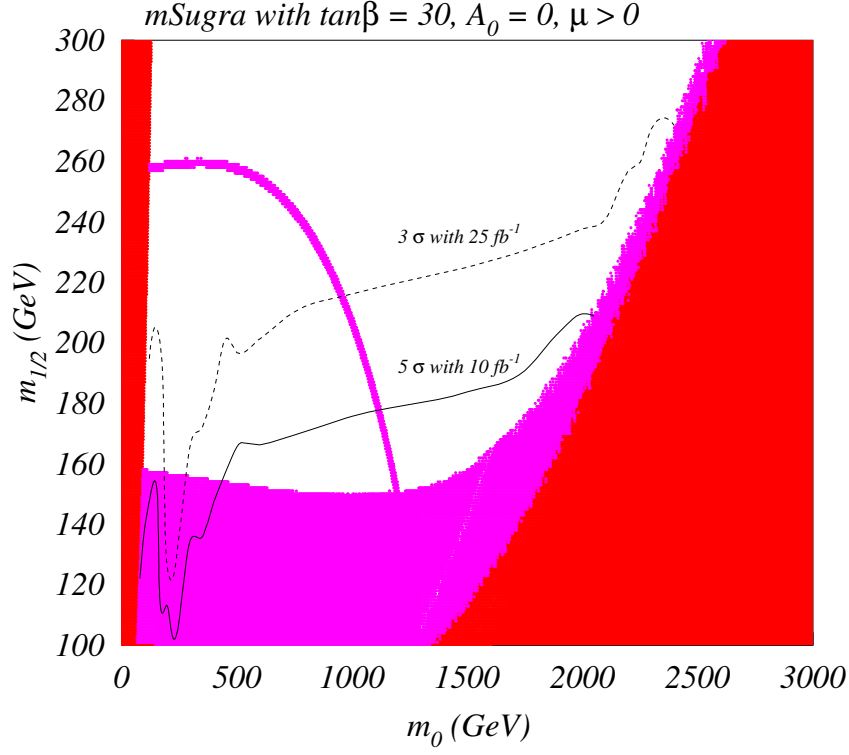
Figure 2.4. The reach of Fermilab Tevatron in the m_0 *vs.* $m_{1/2}$ parameter plane of the mSUGRA model, with $\tan\beta = 30$, $A_0 = 0$ and $\mu > 0$. The red (magenta) region is excluded by theoretical (experimental) constraints. The region below the magenta contour has $m_h < 114.1$ GeV, in violation of Higgs mass limits from LEP2.

To gain a better understanding of what's happening in the HB/FP region, in Fig. 2.3a.) we plot the masses of various charginos and neutralinos and the μ parameter as a function of m_0 for fixed $m_{1/2} = 225$ GeV, $A_0 = 0$, $\tan\beta = 30$ and $\mu > 0$. Initially, for $m_0 \sim 1500 - 1700$ GeV, the $\widetilde{W}_1$, $\widetilde{Z}_1$ and $\widetilde{Z}_2$ masses are essentially constant with m_0, as might be expected. As we approach the large m_0 HB/FP region, the value of μ drops, and consequently the light chargino and neutralino masses drop, as they become increasingly higgsino-like. As $\mu \to 0$, $m_{\widetilde{W}_1} - m_{\widetilde{Z}_1}$ also approaches zero. However, the LEP2 limit of $m_{\widetilde{W}_1} = 103.5$ is reached before the $\widetilde{W}_1$ and $\widetilde{Z}_1$ become nearly degenerate.

In Fig. 2.3b.), we also show various chargino and neutralino cross sections versus m_0 for the same parameters as in Fig. 2.3a.). For intermediate values of m_0, $\sigma(\widetilde{W}_1\widetilde{Z}_2)$ and
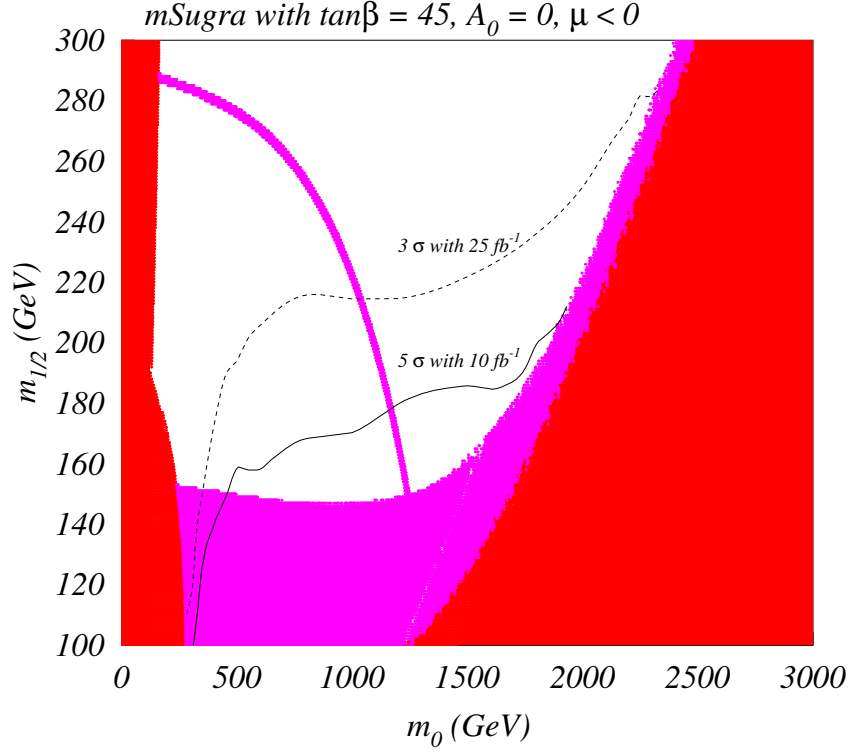
Figure 2.5. The reach of Fermilab Tevatron in the m_0 *vs.* $m_{1/2}$ parameter plane of the mSUGRA model, with $\tan\beta = 45$, $A_0 = 0$ and $\mu < 0$. The red (magenta) region is excluded by theoretical (experimental) constraints. The region below the magenta contour has $m_h < 114.1$ GeV, in violation of Higgs mass limits from LEP2.

$\sigma(\widetilde{W}_1^+ \widetilde{W}_1^-)$ are dominant. As one increases m_0 and approaches the HB/FP region, the various chargino and neutralino masses drop, and the production cross sections increase, giving rise to an increased reach by Tevatron experiments. At the highest m_0 values, actually $\sigma(\widetilde{W}_1 \widetilde{Z}_1)$ production has become dominant. In addition, a variety of cross sections such as $\sigma(\widetilde{Z}_1 \widetilde{Z}_3)$, $\sigma(\widetilde{Z}_2 \widetilde{Z}_3)$, $\sigma(\widetilde{W}_2 \widetilde{Z}_4)$, $\cdots$ are increasing, and their sum can be non-negligible. These heavier -ino states in general have lengthier cascade decays, and can lead to complicated signals including multileptons which may be at the edge of observability.

Fig. 2.4 shows the Tevatron reach in the m_0 *vs.* $m_{1/2}$ plane for $\tan\beta = 30$, $A_0 = 0$ and $\mu > 0$. In this case, the reach at large m_0 remains large as in the $\tan\beta = 10$ case from Fig. 2.2. However, the reach at low m_0 has diminished somewhat, which is an effect
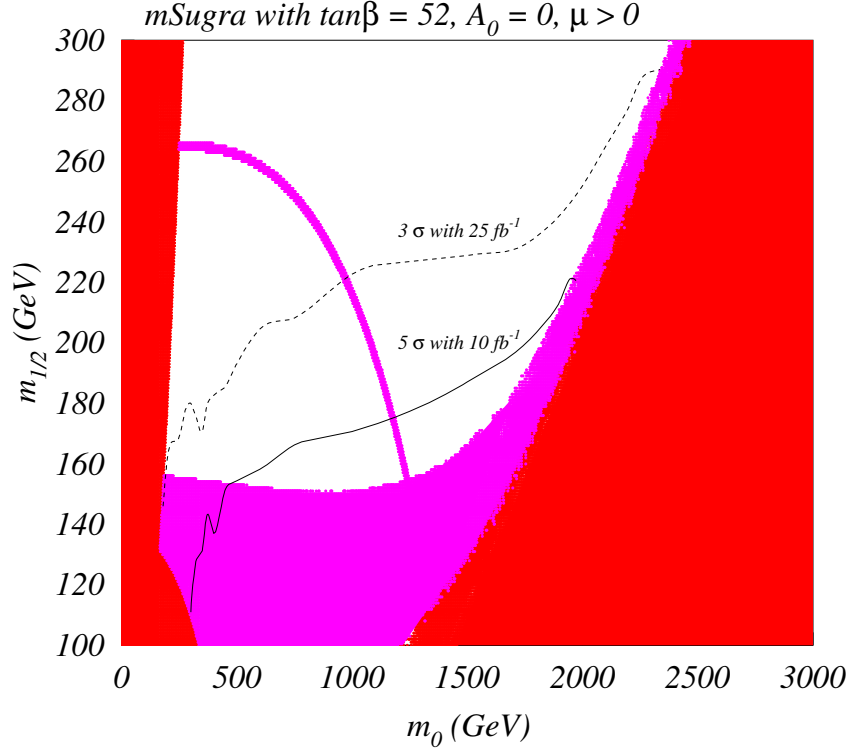
Figure 2.6. The reach of Fermilab Tevatron in the m_0 *vs.* $m_{1/2}$ parameter plane of the mSUGRA model, with $\tan\beta = 52$, $A_0 = 0$ and $\mu > 0$. The red (magenta) region is excluded by theoretical (experimental) constraints. The region below the magenta contour has $m_h < 114.1$ GeV, in violation of Higgs mass limits from LEP2.

of large $\tan\beta$ where the τ and b Yukawa couplings become large, and the $\tilde{\tau}_1$ mass becomes lighter than that of other sleptons. The enhanced chargino and neutralino decays to taus in this region comes at the expense of decays to es and μs, so that the low m_0 3ℓ reach is diminished[27].

The m_0 *vs.* $m_{1/2}$ plane is shown for $\tan\beta = 45$, with $\mu < 0$ in Fig. 2.5. The plot shows even greater reach suppression at low m_0 due to the increase in $\tan\beta$, where an even greater suppression of chargino and neutralino decays to es and μs occurs at the expense of decays to τs. Irregardless, as m_0 increases, sleptons, smuons and staus all decouple from the decay calculations, so that results are relatively insensitive to $\tan\beta$, and the reach remains large in the HB/FP region.

Finally, in Fig. 2.6, we show the mSUGRA plane for $\tan\beta = 52$, $A_0 = 0$ and $\mu > 0$. Again, the reach is diminished for low m_0, but remains substantial for large m_0, especially in the HB/FP region. As with the previous figures, the reach extends to $m_{1/2} \sim 270$ GeV, corrresponding to a value of $m_{\tilde{g}} \sim 750$ GeV.

2.3   Summary

In summary, we have evaluated the reach of the Fermilab Tevatron collider for supersymmetry in the framework of the mSUGRA model. The best signature for SUSY appears to be trilepton events orginating from chargino/neutralino production, with subsequent leptonic decays. We have extended previous analyses into the large m_0 region, where significant regions of parameter space are accessible to Tevatron search experiments. This region includes the intriguing HB/FP region, where squarks and sleptons are heavy (thus ameliorating the SUSY flavor and CP problems), while possibly maintaining naturalness[36]. In this region, since μ is decreasing, sparticle production cross sections increase, and Tevatron experiments may be able to find evidence for SUSY out to $m_{1/2}$ values as high as 200-280 GeV depending on the ultimate integrated luminosity which is achieved.

CHAPTER 3

UPDATED REACH OF CERN LHC AND CONSTRAINTS FROM RELIC DENSITY, $b \to s\gamma$ AND a_μ IN THE MSUGRA MODEL

3.1 Introduction

The search for supersymmetric (SUSY) matter is one of the primary objectives of experiments at high energy colliders[49]. SUSY matter may reveal itself through indirect effects[50], as in contributions to rare decays such as $b \to s\gamma$, $b \to s\ell\bar{\ell}$ or $B_s \to \mu^+\mu^-$, or via contributions to electric or magnetic moments such as the electric dipole moment of the electron or neutron or $(g-2)_\mu$. It is possible that relic SUSY cold dark matter (CDM) has already been detected gravitationally, and recent analyses of WMAP and other data sets indicate that the relic density $\Omega_{CDM}h^2 = 0.1126^{+0.0161}_{-0.0181}(2\sigma$ CL)[42], with a baryonic density about six times smaller. Both direct and indirect searches for relic SUSY CDM are underway[51]. Detection of a signal in any of these experiments would provide evidence for physics beyond the standard model, but the results may have both supersymmetric as well as non-supersymmetric interpretations.

The definitive discovery of SUSY matter will likely have to come from experiments operating at high energy colliders. Already, negative searches for SUSY by the LEP2 experiments have resulted in significant bounds: for instance, the light chargino $\widetilde{W}_1$ must have mass $m_{\widetilde{W}_1} > 103.5$ GeV[52], while a SM-like higgs boson must have mass $m_h > 114.1$ GeV[53]. The reach of the Fermilab Tevatron collider has been examined as well. In the context of the minimal supergravity model (mSUGRA)[12], with parameters

$$m_0, \ m_{1/2}, \ A_0, \ \tan\beta, \ sign(\mu), \tag{3.1}$$

$m_{1/2}$ values of up to 250 GeV (corresponding to $m_{\tilde{g}} \overset{<}{\sim} 600$ GeV) can be probed with 25 fb^{-1} for $m_0 \overset{<}{\sim} 200$ GeV[25] and small values of $\tan\beta$. Then, the best reach is obtained via the clean trilepton channel.

The CERN LHC is expected to begin operating in 2007 with pp collisions at $\sqrt{s} = 14$ TeV. While the initial luminosity is expected to be ~ 10 fb^{-1} per year, an integrated luminosity of at least several hundred fb^{-1} is ultimately anticipated. The reach of the LHC for supersymmetric matter has been evaluated in the mSUGRA model for low[34, 57, 58, 59] and high[60, 57, 58] values of $\tan\beta$, for slepton[61] and chargino-neutralino production[62], and even in the experimentally unfavorable case where the lightest supersymmetric particle (LSP) decays hadronically via R-parity violating interactions[63]. The LHC reach has also been evaluated for models with non-universal soft terms as given by non-minimal $SU(5)$ SUSY GUTs[64] and gaugino mediation models[65]. Finally, the LHC reach has been evaluated for gauge-mediated[66] (GMSB) and anomaly-mediated (AMSB) SUSY breaking models[67].

In studies evaluating the reach of the LHC, the signal channels have been classified by the number of isolated leptons present in each event. The isolated leptons usually arise as end products of cascade decays of gluinos, squarks or other massive SUSY particles[68]. At large values of the parameter $\tan\beta$, the b and τ Yukawa couplings become large, so that cascade decays to final states containing b-jets and τ-leptons are enhanced[27].

In this chapter, we update the reach projections for the CERN LHC for several reasons.

- We calculate the sparticle production and cascade decay events using ISAJET v7.64[45]. This version includes a variety of radiative corrections and improvements to the sparticle mass spectrum that were not present in earlier ISAJET versions, including two-loop evolution of all RGEs. ISAJET 7.64 gives good agreement with spectra generated by the Suspect, SoftSUSY and Spheno codes, as compiled by Allanach, Kraml and Porod[47]. In addition, 3-body decay matrix elements are included[54, 69], so that decay product energy distributions are more accurately modeled.

- We adopt the code CMSJET v4.801 to model the CMS detector. This gives a more accurate portrayal of CMS than the toy detector models used in Ref. [34].

- We include additional channels to our reach projections, including events containing a reconstructed $Z \to \ell^+\ell^-$ candidate ($\ell = e$ or μ)[70], and events containing isolated

photons. The photonic events may arise from radiative neutralino decay[71, 72] $\widetilde{Z}_2 \rightarrow \widetilde{Z}_1 \gamma$ which is enhanced in the low μ[34] HB/FP[73, 74] region of parameter space.

- Our parameter space scans extend over a wider range than earlier reach projections. We are motivated to do so to cover the HB/FP region with small μ where SUSY phenomenology can be significantly different. Further, we adopt a higher integrated luminosity value of 100 fb^{-1} than earlier studies; this integrated luminosity should be achieved after several years of LHC operation.

- We identify regions of mSUGRA parameter space consistent with recently updated constraints[50] from $b \rightarrow s\gamma$, $(g-2)_\mu$ and $\Omega_{\widetilde{Z}_1} h^2$ calculations as well as the most recent constraints from the LEP2 experiments, and where there should be observable signals at the LHC.

In Sec. 3.2, we present the details of our computer calculations, cuts and detector simulation. In Sec. 3.3, we show our results for the LHC reach projections in the m_0 $vs.$ $m_{1/2}$ plane, and identify parameter regions consistent with all exerimental constraints. We summarize our results in Sec. 3.4.

3.2 Calculational details

We use the CMSJET (version 4.801) fast MC package[75] for the CMS detector response simulation. Both SM background and signal events were generated using ISAJET 7.64 which has undergone numerous upgrades since ISAJET 7.37 used in the last study[60]. The improvements include the incorporation of matrix elements for the calculation of three body decays of gluinos, charginos and neutralinos, two loop renormalization group evolution of all couplings and soft SUSY breaking parameters, inclusion of 1-loop self energies for third generation fermions, and improved evaluation of m_A which, in turn, significantly moves the boundary of the allowed parameter space of the mSUGRA model.

We have computed SM backgrounds from the following sources : $t\bar{t}$, QCD $2 \rightarrow 2$ including $c\bar{c}$ and $b\bar{b}$ production, $W + jets$ and $Z + jets$. Backgrounds from vector boson pair production are negligible to the jetty signals that we consider in this study[34]. For the photonic signal

we also included backgrounds from $W\gamma$ and $Z\gamma$ production, but found these to be negligible after hard cuts. Since the cross section of events with low p_T is much larger than that of events with high p_T, we generated the background events in several bins of p_T. We followed the division described in [57]. We have also adopted the cuts suggested in this study for E_T^{miss}, 0 lepton, 1 lepton, 2 opposite sign and same sign leptons, 3 lepton and ≥ 4 isolated lepton signals. We regard a lepton or a photon to be isolated if

- it has no charged particle with $p_T > 2$ GeV in a cone with $\Delta R < 0.3$ around the direction of the lepton.

- ΣE_T^{cell} in the region with $0.05 < \Delta R < 0.3$ around the lepton's direction has to be less than 10% of the lepton transverse energy.

For the convenience of the reader, we present these cuts in this chapter. All events have to pass the following pre-cuts:

- $E_T^{miss} > 200$ GeV;

- Number of jets, $N_j \geq 2$.

We use a modified UA1-jetfinder routine GLOBJF, implemented in CMSJET, to identify calorimeter jets. A cluster of particles is labeled as a jet if it has transverse momentum p_T greater than 40 GeV and $|\eta| < 3$. Leptons are required to satisfy the following pre-cuts:

- $p_T > 10$ GeV for the muons, $p_T > 20$ GeV for the electrons, $|\eta| < 2.4$ for both muons and electrons.

- Electrons have to be isolated. Muon isolation is not required as part of the pre-cuts. We call an electron or muon non-isolated even if it satisfies the lepton isolation criteria but is part of a jet, or if it is isolated in the calorimeter, but non-isolated in the tracker. Naturally, if it is not isolated in the calorimeter then the lepton is called non-isolated.

The pre-cuts for the photons are:

- $p_T > 20$ GeV in $|\eta| < 2.4$.

- photons have to be isolated.

After events pass the pre-cuts, we impose 90% lepton detection efficiency for each lepton.

The events which pass the pre-cuts are divided into signal types according to the number of leptons (or photons for the isolated γ signal). In the case of the E_T^{miss} signal there can be any number of leptons, 0 lepton signal has no leptons, 1 lepton signal has 1 lepton, 2 OS lepton signal has 2 opposite sign leptons, 2 SS lepton signal has 2 same sign leptons, 3 lepton signal has 3 leptons, ≥ 4 lepton signal has more than 3 leptons, $Z \to \ell^+\ell^-$ signal has at least 2 OS, same flavor leptons with the invariant mass of this pair within the interval $(M_Z - \Delta M_Z, M_Z + \Delta M_Z)$ (ΔM_Z is varied during the optimization procedure). Finally, the isolated γ signal has any number of leptons plus at least one photon (the cut on the number of photons is varied during the optimization procedure). Since muon isolation has not been included as part of the pre-cuts, if we impose the muon isolation during the optimization procedure, the number of events for some signal types can change.

A signal in any channel is considered to be observable if after our optimization procedure described below,

- the number of signal events $S \geq 10$ for an integrated luminosity of 100 fb^{-1}, and

- $S \geq 5\sqrt{B}$, where B is the corresponding number of background events.

We optimize the signal in each channel by imposing additional cuts. The set of cuts that we examined for this purpose are listed in Table 3.1. For the optimization of the $Z \to \ell^+\ell^-$ signal, we have an additional cut: the invariant mass of the pair of opposite sign same flavor lepton pair has to be in the interval $(M_Z - \Delta M_Z, M_Z + \Delta M_Z)$ and ΔM_Z is taken to be $3, 6, 9, ..., 30$ GeV. For the case of the isolated photon signal, in addition to the optimization using the cuts in Table 3.1, we also vary the number of photons which can be $1, 2, 3, 4, \geq 5$. However, for large values of m_0 and $m_{1/2}$, events with $N_\gamma^{iso} > 1$ are generally too rare to pass the requirement of $S > 10$.

For each mSUGRA point that we analyze, we pass the various signals through each one of the complete set of cuts just discussed. If the signal satisfies our observability criterion for any one of these cut choices, we consider it to be observable.[1]

---

[1]When more than one cut choices lead to an observable signal, we retain the choice that maximizes the quantity $S/\sqrt{S + B}$.

Table 3.1. The set of cuts that we have examined for the optimization of the SUSY signal. Except for the muon isolation, the numbers refer to the lower bound on the quantity listed in the first column.

Variable(s)	Values
N_j	2, 3, 4, ..., 10
E_T^{miss}	200, 300, 400, ..., 1400 GeV
E_T^{j1}	40, 150, 300, 400, 500, 600, 700, 800, 900, 1000 GeV
E_T^{j2}	40, 80, 200, 200, 300, 300, 400, 400, 500, 500 GeV
$\Delta\phi\ (p_T^l, E_T^{miss})$	0, 20 deg.
Circularity	0, 0.2
μ isolation	on, off

3.3   Results

3.3.1   Reach of the LHC in various channels

Since sparticle masses are largely determined by the parameters m_0 and $m_{1/2}$ the $m_0 - m_{1/2}$ plane is a convenient arena for simultaneously displaying the SUSY reach of future experimental facilities together with regions already excluded by current data. Many previous calculations for the LHC reach are, therefore, presented in this plane (for various choices of other parameters) starting with $\tan\beta = 2$; this low of a $\tan\beta$ value is now largely excluded by the LEP2 bound on m_h[53]. We begin our presentation with $\tan\beta = 10$, in Fig. 3.1. The red-shaded region on the left is excluded because either electroweak symmetry is not properly broken, or $\tilde{\tau}_1$ is the LSP, while that on the right is excluded because radiative electroweak symmetry breaking (REWSB) does not occur. The magenta region in the lower left is excluded by LEP2 bounds on $m_{\widetilde{W}_1} > 103.5$ GeV, and $m_h > 114.1$ GeV (for a SM-like light Higgs h). The maximum reach is shown by the E_T^{miss} contour, where the signal events include all isolated lepton possibilities. Also shown for reference are contours of $m_{\tilde{g}} = 2$ TeV, and $m_{\tilde{q}} = 2$ TeV. The maximum reach in $m_{1/2}$ occurs for low m_0, where squark masses are somewhat lighter than gluinos, so that $\tilde{q}\tilde{q}$, $\tilde{q}\tilde{g}$ and $\tilde{g}\tilde{g}$ production processes all have large rates. Gluinos as heavy as ~ 3 TeV may be detectable at the LHC if squarks are somewhat lighter. As m_0 increases, squark masses increase, so gluino pair production becomes the dominant sparticle production mechanism. At very large values of m_0, the squarks (and

Figure 3.1. The reach of CERN LHC in the m_0 *vs.* $m_{1/2}$ parameter plane of the mSUGRA model, with $\tan\beta = 10$, $A_0 = 0$ and $\mu > 0$, assuming 100 fb^{-1} of integrated luminosity. The red (magenta) regions are excluded by theoretical (experimental) constraints discussed in the text. We show the reach in the 0ℓ, 1ℓ, OS, SS, 3ℓ, $\geq 4\ell$, γ and Z channels, as well as in the "inclusive" $E\!\!\!/_T$ channel.

also sleptons) essentially decouple, and the reach contours flatten out, since $m_{\tilde{g}}$ is roughly constant for each value of $m_{1/2}$. The maximal reach for 100 fb^{-1} of integrated luminosity is $m_{1/2} \sim 700$ GeV, corresponding to a gluino mass value of $m_{\tilde{g}} \sim 1800$ GeV.

The reach for SUSY signals in the individual channels introduced in the last section are shown by the various contours labelled by the corresponding topology in Fig. 3.1. For low values of m_0, sleptons and squarks are relatively light, and $\tilde{g}\tilde{g}$, $\tilde{g}\tilde{q}$ and $\tilde{q}\tilde{q}$ production processes all occur at large rates; direct slepton and sneutrino pair production rates are much smaller. However, left-squarks $\tilde{q}_L$ decay frequently into the heavier chargino and heavier neutralinos, which in turn may decay to sleptons. These cascade decays frequently terminate in isolated

leptons, which together with leptons from decays from tops and stops in SUSY processes, result in large rates for leptonic signals. For a fixed value of $m_{1/2}$, as m_0 increases, $\tilde{g}$ decay to $\tilde{q}_L$ becomes suppressed, and $BF(\tilde{g} \to \tilde{q}_R)$ increases. Since $\tilde{q}_R \to q\widetilde{Z}_1$ most of the time, cascade decays then give rise to a higher fraction of $\not{E}_T + jets$ events, and the leptonic signal from the decay of gluinos is reduced. Furthermore, since squarks become heavier relative to gluinos as m_0 is increased, the leptonic signal from directly produced $\tilde{q}_L$ also becomes smaller. As m_0 increases even further, $\tilde{g} \to \tilde{q}_R q$ also becomes suppressed or even forbidden, and $\tilde{g} \to \tilde{t}_1 t$ (and possibly $\tilde{g} \to b\tilde{b}_{1,2}$) dominates. The decays through tops and stops gives rise again to leptonic states due to $\tilde{t}_1$ and t leptonic decays. This results in an increased reach at moderate m_0 values via leptonic modes such as SS and OS dileptons, and 3ℓ events. As m_0 increases even more, $\tilde{g}$ two-body decays become completely forbidden, and three-body decays dominate, and the leptonic reach contours tend to level off.

Finally, we show a contour that marks the signal reach for events including $\not{E}_T + jets$ plus at least one isolated photon. In evaluating this reach, we have only retained physics backgrounds in our calculation. Detector-dependent backgrounds where a jet fakes a photon may be significant.[2] In most of the parameter space, the additional photon arises from $h \to \gamma\gamma$ decay, where the h is produced copiously in sparticle cascade decays, especially from $\widetilde{Z}_2 \to \widetilde{Z}_1 h$. In these regions, in fact, if we require *two* isolated photons, then we can reconstruct a di-photon invariant mass. This is illustrated in Fig. 3.2 for the parameter space point $m_0 = m_{1/2} = 500$ GeV, $A_0 = 0$, $\tan\beta = 30$ and $\mu > 0$. It is amusing to note that the $h \to \gamma\gamma$ signal should be visible in SUSY events for 100 fb^{-1} of integrated luminosity. We see that (for these parameters) the highest possible luminosity is needed for the detection of this severely rate-limited, but essentially SM background-free, signal. A detection of h in this manner would nicely confirm its detection via $gg \to h \to \gamma\gamma$, where the signal would be picked out as a small peak above an enormous continuum background. A Higgs signal in the multijet plus $\gamma\gamma + E_T^{miss}$ channel would also suggest the supersymmetric origin of the Higgs production process.

---

[2]If we take the probability for a jet to fake a photon to be 5×10^{-4} and assume that the hard scattering events have ~ 10 30-40 GeV "jets" in them, about one in 500 background events will also appear to have an isolated photon. Assuming that this fake photon background can be estimated by reducing the physics background in the inclusive E_T^{miss} channel by 500, we find that this background is somewhat smaller, but of the same order of magnitude as the physics background that we have evaluated. A real evaluation of this detector-dependent background is beyond the scope of our analysis.
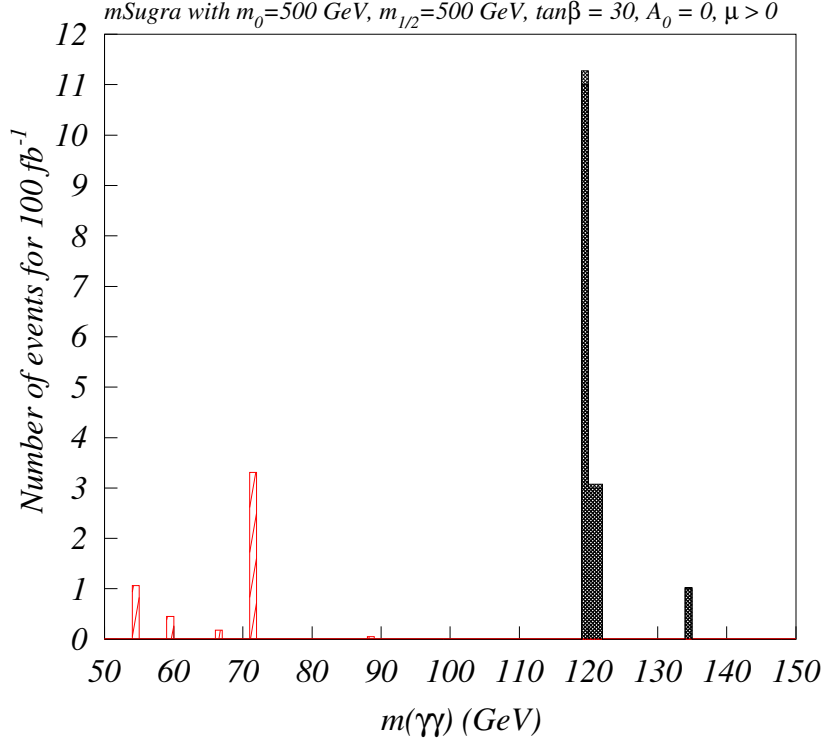
Figure 3.2. The diphoton invariant mass in SUSY events with two isolated photons. The shaded histogram is for diphotons from SUSY events, while the hatched histogram represents corresponding events of SM origin. The background has been obtained by scaling a Monte Carlo run for a lower value of integrated lumnosity.

As m_0 becomes very large, and the region of low $|\mu|$ is approached, the radiative decay $\widetilde{Z}_2 \to \widetilde{Z}_1 \gamma$ becomes enhanced[72]. In this HB/FP region, the isolated photon contour likewise turns up, to reflect the increase in isolated photon activity from neutralino radiative decay.

As we move to larger values of the parameter $\tan \beta$, as in Fig. 3.3 for $\tan \beta = 30$, the first thing to notice is that the left red-shaded region, where $\tilde{\tau}_1$ is the LSP, has expanded. This is because as $\tan \beta$ increases, both the τ (and also b) Yukawa couplings become non-negligible. This results in a reduction of stau and sbottom soft breaking masses via RGE running, and also in greater $L - R$ mixing, which again reduces the mass of the lightest eigenstates. The negative results of searches for heavy isotopes of hydrogen (or other elements) results in limits that are many orders of magnitude below their expected relic density in big-bang
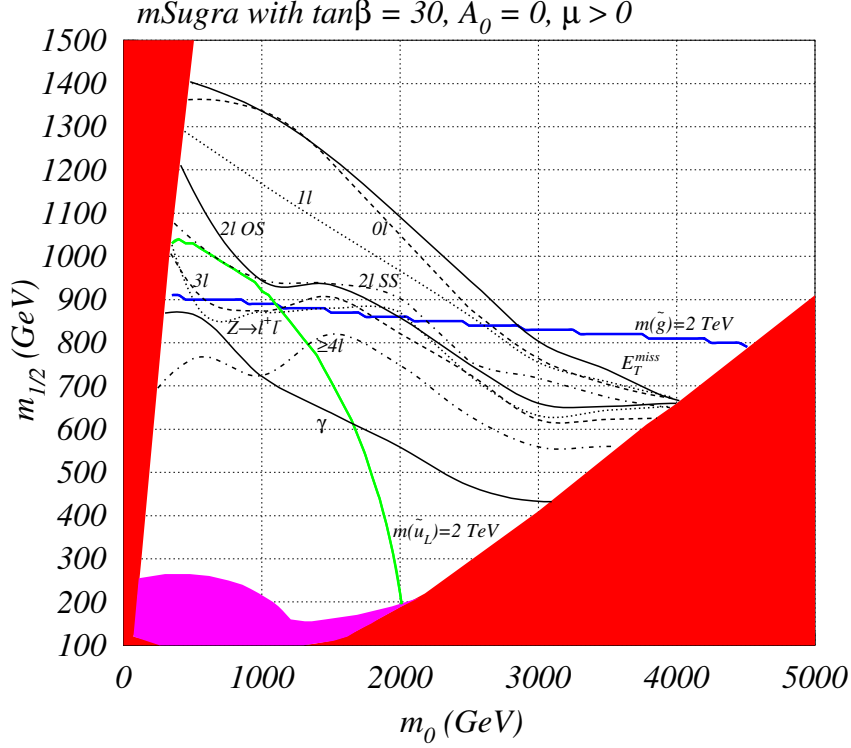
Figure 3.3. The reach of CERN LHC in the m_0 *vs.* $m_{1/2}$ parameter plane of the mSUGRA model, with $\tan\beta = 30$, $A_0 = 0$ and $\mu > 0$, assuming 100 fb^{-1} of integrated luminosity. The red (magenta) regions are excluded by theoretical (experimental) constraints discussed in the text. We show the reach in the 0ℓ, 1ℓ, OS, SS, 3ℓ, $\geq 4\ell$, γ and Z channels, as well as in the "inclusive" $\not{E}_T$ channel.

cosmology, so that this possibility is strongly excluded. Finally, the large values of f_b and f_τ together with the reduction of the corresponding sfermion masses relative to the first two generations mentioned above, increases various three body sparticle decays to b-quarks and τ leptons, at the expense of their first and second generation counterparts[27]. The net effect of this is to enhance sparticle cascade decays to final states containing b-quarks and τ-leptons in the low m_0 region. This results in a diminution of the reach in isolated lepton channels at low m_0, as compared with Fig. 3.1. The large b and τ Yukawa couplings hardly affect the $\not{E}_T + jets$ and 0ℓ signals, and so the ultimate reach of the LHC changes little in proceeding from $\tan\beta = 10$ to $\tan\beta = 30$.
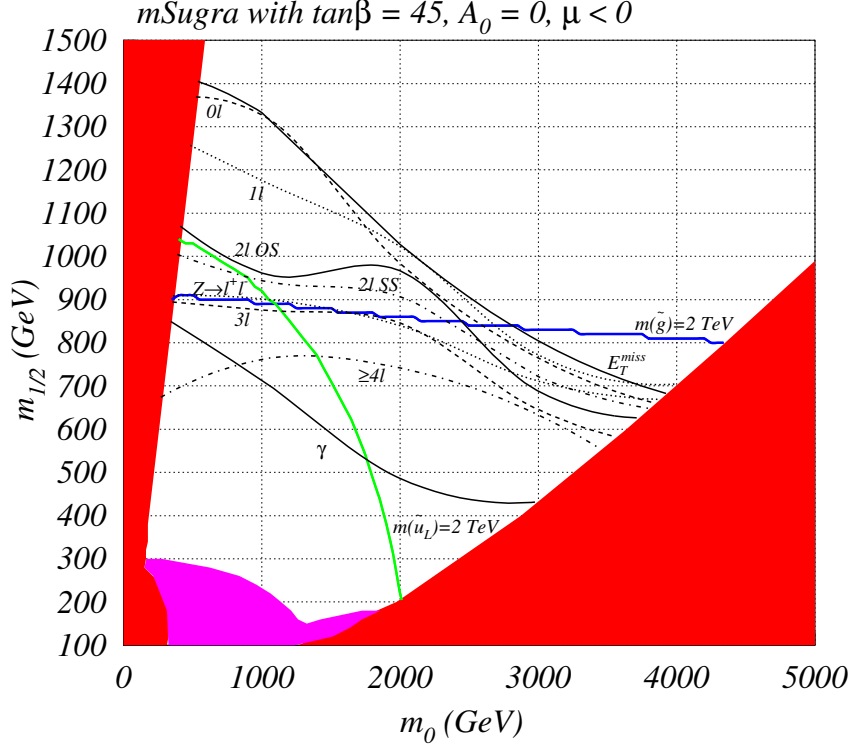
Figure 3.4. The reach of CERN LHC in the m_0 $vs.$ $m_{1/2}$ parameter plane of the mSUGRA model, with $\tan\beta = 45$, $A_0 = 0$ and $\mu < 0$, assuming 100 fb^{-1} of integrated luminosity. The red (magenta) regions are excluded by theoretical (experimental) constraints discussed in the text. We show the reach in the 0ℓ, 1ℓ, OS, SS, 3ℓ, $\geq 4\ell$, γ and Z channels, as well as in the "inclusive" $\not{E}_T$ channel.

In Fig. 3.4, we show the m_0 $vs.$ $m_{1/2}$ plane for $\tan\beta = 45$ and $\mu < 0$. The large b and τ Yukawa coupling effects are accentuated even more in this figure: a larger region is excluded at low m_0, and the reach via multi-lepton channels is further diminished for small m_0 values where squarks and sleptons still play a role in determining cascade decay patterns. However, again, the overall reach in the $\not{E}_T + jets$ and 0ℓ channels is hardly affected. If we increase $\tan\beta$ much beyond about 50 for $\mu < 0$, the parameter space begins to close up fast due to a breakdown in REWSB.

In Fig. 3.5, we show the m_0 $vs.$ $m_{1/2}$ plane for $\tan\beta = 52$ and $\mu > 0$. In this case, the overall reach in the $\not{E}_T + jets$ and 0ℓ channels is similar to the cases at lower $\tan\beta$. However,
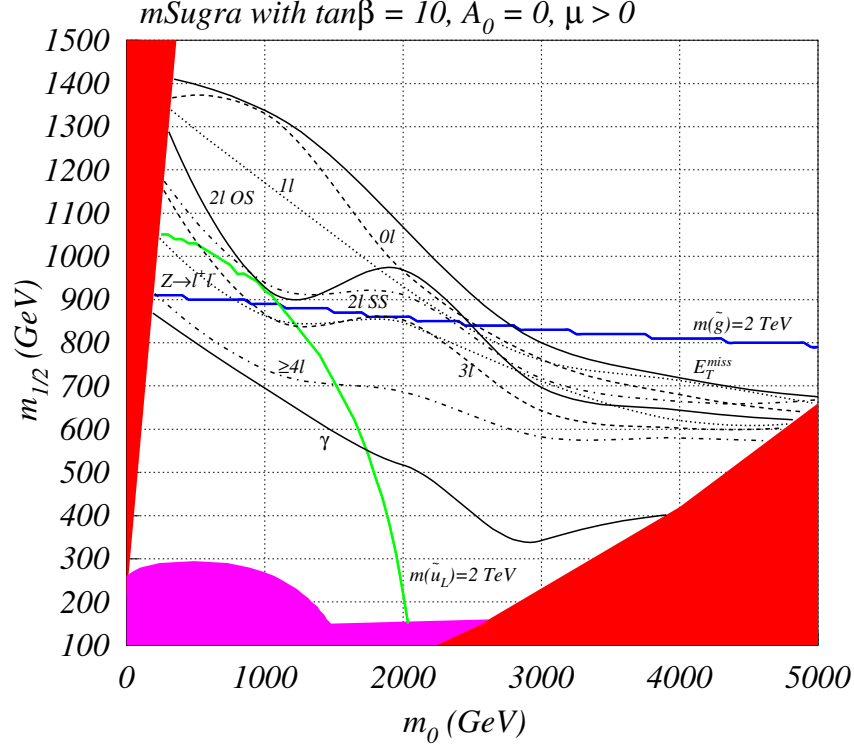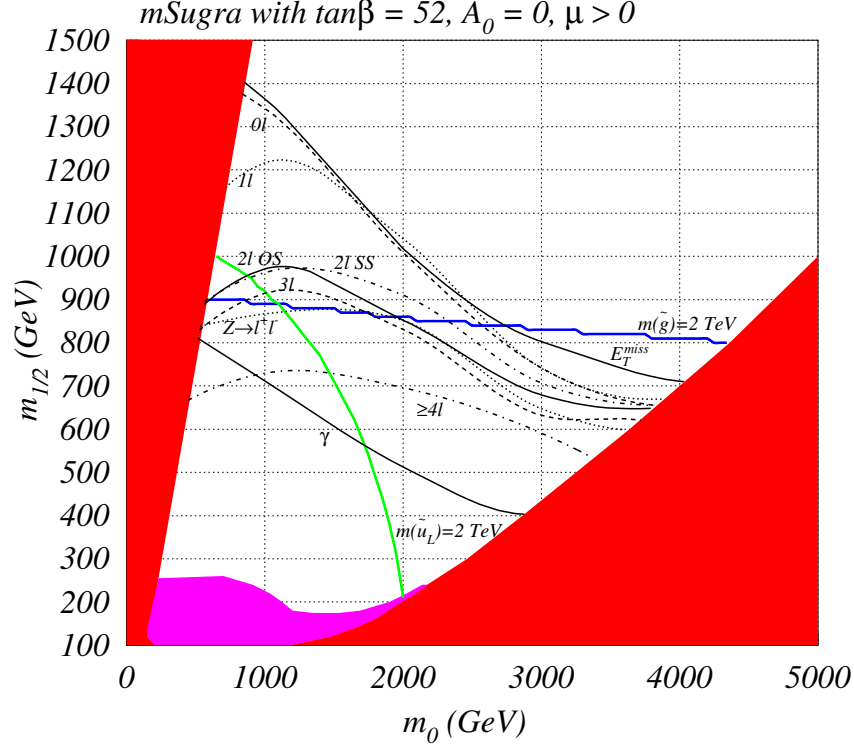
Figure 3.5. The reach of CERN LHC in the m_0 *vs.* $m_{1/2}$ parameter plane of the mSUGRA model, with $\tan\beta = 52$, $A_0 = 0$ and $\mu > 0$, assuming 100 fb^{-1} of integrated luminosity. The red (magenta) regions are excluded by theoretical (experimental) constraints discussed in the text. We show the reach in the 0ℓ, 1ℓ, OS, SS, 3ℓ, $\geq 4\ell$, γ and Z channels, as well as in the "inclusive" $\not{E}_T$ channel.

in the multi-lepton channels, there is again a suppression of reach at low m_0. This is because for very high $\tan\beta$, $m_{\tilde{\tau}_1}$ is so light that $\widetilde{W}_1$ dominantly decays to $\tilde{\tau}_1\nu_\tau$ rather than $\widetilde{Z}_1 W$, and likewise, $\widetilde{Z}_2 \to \tilde{\tau}_1\tau$ rather that $\widetilde{Z}_1 h$ or $\widetilde{Z}_1 Z$. As m_0 increases, the stau mass increases, and the $\widetilde{W}_1 \to \tilde{\tau}_1\nu_\tau$ decay mode becomes more suppressed, which increases the $\widetilde{W}_1 \to \widetilde{Z}_1 W$ branching fraction. The subsequent W boson decays from $\widetilde{W}_1 \to \widetilde{Z}_1 W$ lead to hard isolated leptons.

Our projections of the LHC reach, where they can be directly compared, are qualitatively similar to the results in Ref. [57]. Differences between the results can be attributed to the difference in the observability criteria ($S \geq 5\sqrt{S + B}$ used in Ref.[57] requires a minimum of

40

25 events to be compared with 10 events in our study, as well as a somewhat larger significance of the signal), and to the use of PYTHIA instead of ISAJET for event simulation.

3.3.2   The LHC reach in light of indirect constraints

A variety of low energy measurements have been used to obtain constraints on the parameter space of the mSUGRA model. These include the measured values of the cold dark matter density, the branching fraction $BF(b \rightarrow s\gamma)$, the value of the anomalous magnetic moment of the muon, $a_\mu = (g - 2)_\mu/2$, [3] and a lower limit on $BF(B_s \rightarrow \mu^+\mu^-)$. Unlike collider constraints which are much more direct, constraints from low energy measurements may be considerably more sensitive to details of the model, or to improvements in the theoretical calculation. Within a specific framework (*e.g.* mSUGRA), however, these indirect constraints exclude certain regions of parameter space, and also suggest other regions where future searches might be focussed.

Neutralino relic density:

Measurements of galactic rotation curves, binding of galactic clusters, and the large scale structure of the universe all point to the need for significant amounts of cold dark matter (CDM) in the universe. In addition, recent measurements of the power spectrum of the cosmic microwave background from WMAP and other data sets[42] lead to

- $\Omega_{CDM}h^2 = 0.1126^{+0.008}_{-0.009}$.

The upper limit derived from this is a true constraint on any stable relic from the Big Bang, such as the lightest neutralino of the mSUGRA model. Regions of mSUGRA parameter space which result in a relic density that violates this bound are excluded. A remarkable feature of the model is that there are regions of the parameter space where the neutralino density lies in the observed range, so that the neutralino makes up almost all the cold dark matter in the universe. We remark, however, that unlike the upper limit above, the corresponding lower limit is flexible, since there may be additional sources of CDM such as axions, or states associated with the hidden sector of the mSUGRA model and/or extra dimensions.

To estimate the relic density of neutralinos in the mSUGRA model, we use the recent calculation in Ref. [76]. All relevant neutralino annihilation and co-annihilation reactions are

---

[3]There is considerable theoretical uncertainty in the SM value of a_μ, so that caution must be exercised in interpreting the result of experiment E821.

included along with relativistic thermal averaging[77], which is important for obtaining the correct neutralino relic density in the vicinity of annihilations through s-channel resonances.

BF($b \to s\gamma$):

The branching fraction $BF(b \to s\gamma)$ has recently been measured by the BELLE[78], CLEO[79] and ALEPH[80] collaborations. Combining statistical and systematic errors in quadrature, these measurements give $(3.36 \pm 0.67) \times 10^{-4}$ (BELLE), $(3.21 \pm 0.51) \times 10^{-4}$ (CLEO) and $(3.11 \pm 1.07) \times 10^{-4}$ (ALEPH). A weighted averaging of these results yields $BF(b \to s\gamma) = (3.25 \pm 0.37) \times 10^{-4}$. The 95% CL range corresponds to $\pm 2\sigma$ away from the mean. To this we should add uncertainty in the theoretical evaluation, which within the SM dominantly comes from the scale uncertainty, and is about 10%. Together, these imply the bounds,

- $2.16 \times 10^{-4} < BF(b \to s\gamma) < 4.34 \times 10^{-4}$.

The evaluation of the SUSY contribution to this decay entails additional theoretical uncertainties, especially when $\tan\beta$ is large, so that this range should be relaxed somewhat. In our study, we show contours of $BF(b \to s\gamma)$ of 2, 3, 4 and 5×10^{-4}.

The calculation of $BF(b \to s\gamma)$ used here is based upon the program of Ref. [81]. In our calculations, we also implement the running b-quark mass including SUSY threshold corrections as calculated in ISAJET; these effects can be important at large values of the parameter $\tan\beta$[82]. Our value of the SM $b \to s\gamma$ branching fraction yields 3.4×10^{-4}, with a scale uncertainty of 10%.

Muon anomalous magnetic moment

The muon anomalous magnetic moment $a_\mu = (g-2)_\mu/2$ has been recently measured to high precision by the E821 experiment[83]: $a_\mu = 11659204(7)(5) \times 10^{-10}$. The most challenging parts of the SM calculation are the hadronic light-by-light[84] and vacuum polarization (HVP)[85] contributions and their uncertainties. Presently these results are in dispute. In the case of the HVP the use of tau decay data can reduce the error, but the interpretation of these data is somewhat controversial[86]. Thus, the deviation of the measurement from the SM depends on which prediction is taken into account. According to the recent analysis by Hagiwara et al.[85]:

- $11.5 < \delta a_\mu \times 10^{10} < 60.7$.

A different assessment of the theoretical uncertainties[85] using the procedure described in Ref.[87] gives,

- $-16.7 < \delta a_\mu \times 10^{10} < 49.1$.

Yet another determination has recently been made by Narison, includes additional scalar meson loops[88]. This, using $e^+e^- \rightarrow hadrons$ data to evaluate hadronic vacuum polarization contributions, yields

- $-3.9 < \delta a_\mu \times 10^{10} < 52.1$,

while using τ-decay data results in

- $-26.7 < \delta a_\mu \times 10^{10} < 30.1$.

The latter may include additional systematic uncertainties from how isospin breaking effects are incorporated.

In view of the theoretical uncertainty, we only present contours of δa_μ, as calculated using the program developed in [89], and leave it to the reader to decide the extent of the parameter region allowed by the data.

$B_s \rightarrow \mu^+\mu^-$ decay

The branching fraction of B_s to a pair of muons has been experimentally bounded by CDF[90]:

- $BF(B_s \rightarrow \mu^+\mu^-) < 2.6 \times 10^{-6}$.

If $\tan\beta \lesssim 20 - 25$, SUSY contributions to this decay are small and do not lead to new constraints on the parameter space. If $\tan\beta$ is large, the important SUSY contribution to this decay is mediated by the neutral states in the Higgs sector of supersymmetric models. While this branching fraction is very small within the SM ($BF_{SM}(B_s \rightarrow \mu^+\mu^-) \simeq 3.4 \times 10^{-9}$), the amplitude for the Higgs-mediated decay of B_s roughly grows as $\tan^3\beta$, [4] and hence can completely dominate the SM contribution if $\tan\beta$ is large. In our analysis we use the results from the last paper in Ref. [91] to delineate the region of mSUGRA parameters excluded by the CDF upper limit on its branching fraction.

In Fig. 3.6, we again show the m_0 *vs.* $m_{1/2}$ plot for $\tan\beta = 10$, $A_0 = 0$ and $\mu > 0$. This time, we exhibit contours for the low energy observables mentioned above, as mapped out in Ref. [87]. A χ^2 analysis of the indirect constraints was performed in Ref. [44], which helped to identify regions of parameter space allowed by all the combined indirect constraints.

---

[4]The $\tan^3\beta$ growth obtains if the tree-level value of m_b is fixed. For large values of $\tan\beta$, the radiative correction to m_b is important resulting in a deviation from the $\tan^3\beta$ growth.

Several regions emerge in the m_0 $vs.$ $m_{1/2}$ plane where the relic density can be within the WMAP range. At low m_0 and low $m_{1/2}$, neutralino annihilation through t-channel sleptons can occur with a high rate. Much of this so-called "bulk" region is largely excluded by the LEP2 Higgs bound (shown as the red contour), and in addition, $BF(b \rightarrow s\gamma)$, though in the acceptable range, is below its experimental central value. In this region, sparticles are very light, and a SUSY discovery by the CERN LHC should be easy.

One of the remaining regions allowed by relic density constraint is the very narrow strip adjacent to the "$\widetilde{Z}_1$ not LSP" region at low m_0, where stau co-annihilation is important[92]. We see that the reach of the LHC apparently covers much of the stau co-annihilation strip, up to $m_{1/2} \sim 1400$ GeV for 100 fb^{-1} of integrated luminosity. To determine the LHC reach needed to completely explore the stau co-annihilation strip, we show the relic density for fixed $m_{1/2}$ values $vs.$ m_0 in Fig. 3.7. In frame a), it is evident that the stau co-annihilation corridor yields a relic density in accord with WMAP results for $m_{1/2} \stackrel{<}{\sim} 900$ GeV. Thus, the LHC would completely explore the stau co-annihilation corridor for $\tan \beta = 10$.

The other region allowed by relic density constraint occurs at very large m_0 where μ becomes small: the HB/FP region[73, 74].[5] Here, the growing higgsino component of the neutralino allows for efficient annihilation into vector boson pairs[93, 39]. For very small μ values, then neutralino-chargino co-annihilation becomes important[94]. In this HB/FP region squarks are very heavy, and as $m_{1/2}$ increases, $m_{\tilde{g}}$ increases as well so that strongly interacting sparticle production cross sections decrease. Since μ is small, the light charginos and neutralinos are significantly higgsino-like, and can only be produced via electroweak interactions. We see that the reach of the LHC is limited to $m_{1/2} \sim 700$ GeV. For even higher $m_{1/2}$ values, and staying in the HB/FP region, one enters an area that is not accessible to LHC experiments, at least via the general purpose search strategies described here, even though the light charginos and neutralinos are expected to have masses less than 250-500 GeV. It would be interesting to examine whether it is possible to devise search strategies that exploit specific characteristics of the HB/FP region to extend the LHC reach. For instance, in the small $|\mu|$ region, decays of gluinos into third generation fermions are enhanced resulting

---

[5]The entire HB/FP region is not shown here: over part of this region, the evaluation of the μ parameter using ISAJET 7.64 is numerically unstable. This is corrected in ISAJET v7.65.
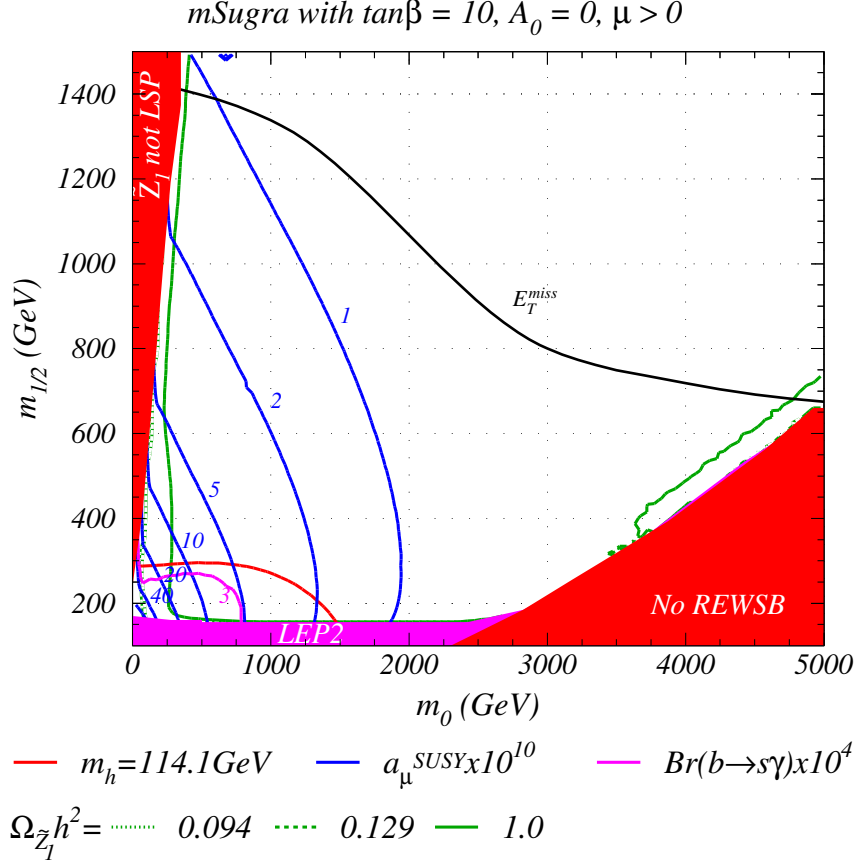
Figure 3.6. Contours of several low energy observables in the m_0 *vs.* $m_{1/2}$ plane of the mSUGRA model, for $\tan\beta = 10$, $A_0 = 0$ and $\mu > 0$. We show contours of CDM relic density (green), together with a contour of $m_h = 114.1$ GeV (red), contours of muon anomalous magnetic moment a_μ ($\times 10^{10}$) (blue) and contours of $b \to s\gamma$ branching fraction ($\times 10^4$) (magenta). Also shown is the maximal reach of the CERN LHC in the $\not{E}_T$+jets channel for 100 fb^{-1} of integrated luminosity.

in events with hard b and t quarks from the decay of heavy gluinos. Whether it is possible to extend the LHC reach in these event topologies merits further investigation.

Next, we show the contours for the same low energy observables as in Fig. 3.6, but for $\tan\beta = 30$, $A_0 = 0$ and $\mu > 0$ in Fig. 3.8. The larger value of $\tan\beta$ causes the values a_μ and $BF(b \to s\gamma)$ to deviate more from their SM values at low m_0 and $m_{1/2}$; the bulk region of relic density annihilation is disfavored by $BF(b \to s\gamma)$. This leaves only the stau co-annihilation corridor and the HB/FP region as phenomenologically viable. The LHC
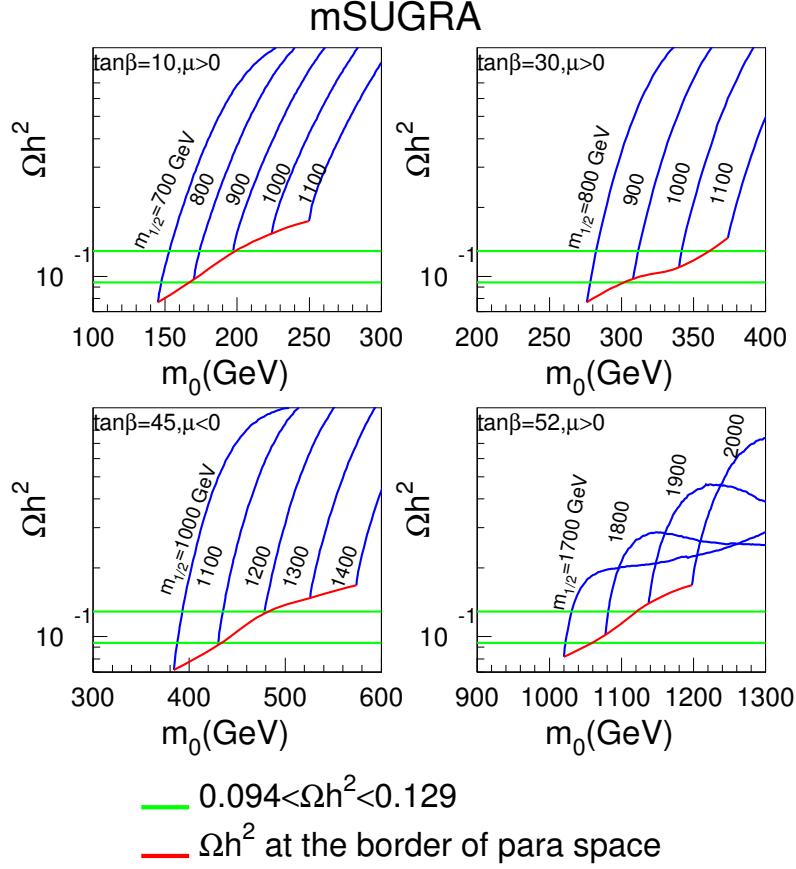
Figure 3.7. The relic density $\Omega_{\widetilde{Z}_1} h^2$ *vs.* m_0 for various fixed $m_{1/2}$ values in the stau co-annihilation corridor, for *a)* $\tan\beta = 10$, $\mu > 0$, *b)* $\tan\beta = 30$, $\mu > 0$, *c)* $\tan\beta = 45$, $\mu < 0$ and $\tan\beta = 52$, $\mu > 0$. We also show via green lines the 2σ WMAP limits on $\Omega_{\widetilde{Z}_1} h^2$.

reach contour remains similar to that for $\tan\beta = 10$. Again, we see that if SUSY has parameters in this plane, then LHC should see it unless $m_{1/2} > 700$ GeV with SUSY in the HB/FP region. In particular, the LHC should be able to cover the stau co-annihilation corridor for $\tan\beta = 30$, since it yields a relic density $\Omega_{\widetilde{Z}_1} h^2 < 0.129$ for $m_{1/2} \lesssim 1050$ GeV, while the LHC reach for low m_0 extends to $m_{1/2} \sim 1400$ GeV.

Fig. 3.9 illustrates the impact of the low energy observables, this time for $\tan\beta = 45$ and $\mu < 0$. The LHC reach is similar to the lower $\tan\beta$ cases, but now the low m_0 and $m_{1/2}$ bulk

Figure 3.8. The same as Fig. 3.6 but for $\tan\beta = 30$.

region is firmly excluded by both a_μ and $BF(b \to s\gamma)$, which are large negative, and large positive, respectively. We see, however, that a new region of low relic density has opened up: the $\widetilde{Z}_1\widetilde{Z}_1 \to A$, $H \to f\bar{f}$ annihilation corridor, where annihilation takes place especially through the very broad A width[93, 38]. In fact, we see that although the A annihilation corridor extends to very large $m_{1/2}$ values, the region allowed by WMAP is almost entirely accessible to LHC searches. A modest additional integrated luminosity beyond 100 fb^{-1} assumed in this study should cover this entire region. In addition, the stau co-annihilation corridor remains consistent with WMAP constraints up to $m_{1/2}$ values as high as 1200 GeV as shown in frame c) of Fig. 3.7, so that LHC should be able to completely explore this region. Finally, the HB/FP region can again be explored up to $m_{1/2} \sim 700$ GeV at the LHC.

Figure 3.9. The same as Fig. 3.6 but for $\tan\beta = 45$ and $\mu < 0$.

In Fig. 3.10, we show the same low energy contours in the m_0 *vs.* $m_{1/2}$ plane, but now for $\tan\beta = 52$ and $\mu > 0$. In this case, the low m_0 and $m_{1/2}$ bulk region is largely excluded because $BF(b \to s\gamma) < 2 \times 10^{-4}$. The WMAP constraints again restrict us to either the stau co-annihilation region at low m_0, or the HB/FP region at large m_0. We can see from Fig. 3.7d that the stau co-annihilation corridor extends to $m_{1/2} \sim 1870$ GeV, which is somewhat beyond the reach of the LHC for 100 fb^{-1} of integrated luminosity. Models with these high parameter values suffer from considerable fine-tuning, since the μ parameter, which has been invoked as a measure of fine-tuning[73], is beyond 1600 GeV for $m_{1/2} > 1400$ GeV, so that μ^2/M_Z^2 is large. In the HB/FP region, the LHC reach, via these channels, again cuts off at $m_{1/2} \sim 700$ GeV: once again, it would be worth exploring whether the SUSY signal can be
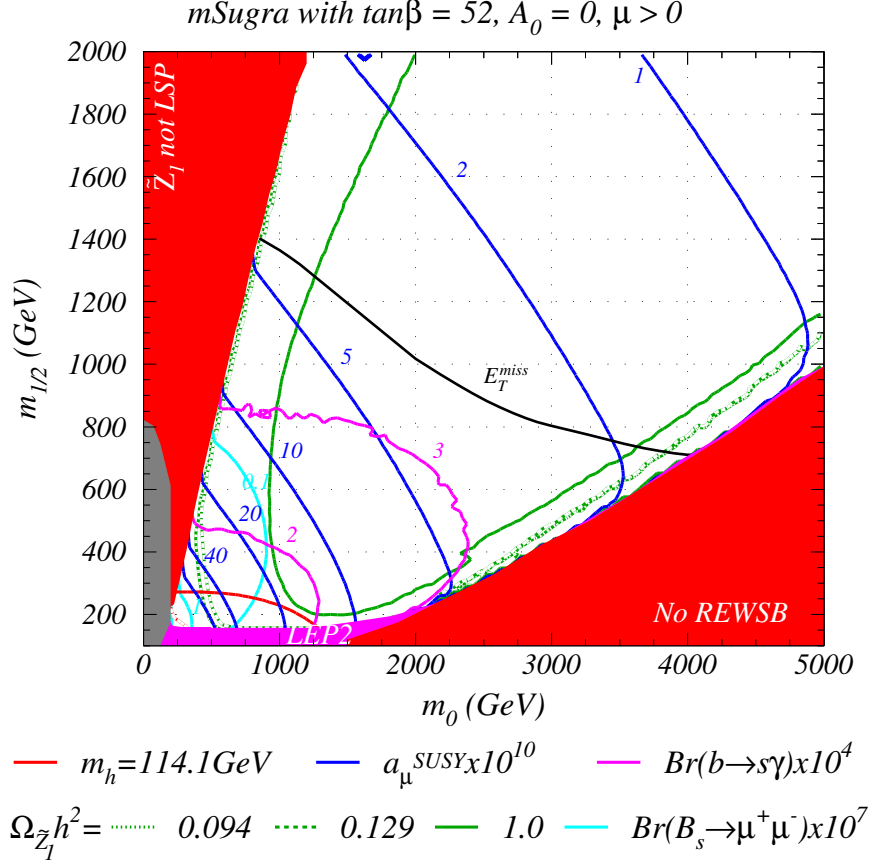
Figure 3.10. The same as Fig. 3.6 but for $\tan\beta = 45$.

picked up in other channels. If we increase $\tan\beta$ beyond 52, then the A, H-annihilation funnel re-enters the figure[44]. In Ref. [44], it is shown that this annihilation funnel can reach $m_{1/2}$ values as high as 1400 GeV for $m_0 \sim 3.5$ TeV and $\tan\beta = 56$. Thus, in this case, the LHC will not be able to access the complete A, H annihilation funnel.

3.4   Summary

We have updated assessments of the SUSY reach of the CERN LHC via E_T^{miss} and multilepton channels, and presented new results for the reach in channels with isolated photons or leptonically decaying Z bosons. We work within the framework of the mSUGRA model, and use ISAJET v7.64 together with the CMSJET fast detector simulation to model

the CMS detector, and assume an integrated luminosity of $100\,\text{fb}^{-1}$. Our results are presented over an expanded mSUGRA model parameter space to include the reach in the so-called HB/FP region at very large m_0, This region, together with the stau coannihilation corridor, and the annihilation funnel where LSPs annihilate via the A or H resonances, are strongly preferred by the recent data of the WMAP collaboration. The overall LHC reach turns out to be quite insensitive to $\tan\beta$. We find that experiments at the LHC will probe $m_{1/2} \overset{<}{\sim} 1400$ GeV for low m_0, and $m_{1/2} \sim 700$ for large m_0 in the HB/FP region. These values correspond to $m_{\tilde{g}} \sim 3000$ GeV and 1800 GeV, respectively.

We have also presented the reach in a variety of multi-lepton channels. The reach in these individual channels is, in general, sensitive to $\tan\beta$. We also show the reach in a channel including reconstructed $Z^0 \to \ell\bar{\ell}$ decays, and channels including isolated photons. The isolated photon signals may contain $h \to \gamma\gamma$ events at a low, but observable rate. Indeed the SUSY event sample may contain SM background-free $h \to \gamma\gamma$ events, though a very high integrated luminosity will be needed to identify the rate-limited h signal. In the HB/FP region, the photonic channels also have a slight enhancement from radiative neutralino decays $\widetilde{Z}_2 \to \widetilde{Z}_1\gamma$. For $m_{1/2} \overset{<}{\sim} 800(400)$ GeV and small (large) values of m_0, there should be observable signals in all these channels if new physics discovered at the LHC is to be interpreted as supersymmetry as realized in the mSUGRA model.

We have also examined the reach of the LHC in light of the recent assessment of direct (from LEP2) and indirect constraints on the mSUGRA model. The indirect constraints include the neutralino relic density $\Omega_{\widetilde{Z}_1}h^2$ from recent WMAP analyses together with accelerator measurements of $BF(b \to s\gamma)$, $a_\mu = (g-2)_\mu$ and the bound on $BF(B_s \to \mu^+\mu^-)$ (this bound is hardly constraining for the parameter planes that we have examined). For large values of $\tan\beta$, experimental values of $BF(b \to s\gamma)$ and a_μ disfavor negative values of the μ parameter unless m_0 and $m_{1/2}$ are also large, but for $\tan\beta \sim 10$, values of m_0 and $m_{1/2} \overset{>}{\sim} 400 - 500$ GeV are perfectly acceptable. For $\mu > 0$, m_0 would have to be rather small so that the relic density is either in the bulk annihilation region or in the stau coannihilation strip, or m_0 would have to be very large, in the HB/FP region. The CERN LHC can definitely explore all the bulk annihilation region, and can explore all the stau co-annihilation corridor unless $\tan\beta$ is very high. The LHC can explore the HB/FP region up to $m_{1/2} \sim 700$ GeV via the conventional SUSY search channels. However, the HB/FP

region appears to extend indefinitely to large $m_{1/2}$ and m_0 values, ultimately well beyond the LHC reach. For large $\tan\beta$, the A, H annihilation funnel enters the m_0 $vs.$ $m_{1/2}$ plane. The LHC with 100 fb^{-1} ought to be able to detect SUSY over this entire region, except for the case of very large $\tan\beta \sim 56$ with $\mu > 0$.

CHAPTER 4

LINEAR COLLIDER CAPABILITIES FOR SUPERSYMMETRY IN DARK MATTER ALLOWED REGIONS OF THE MSUGRA MODEL

4.1 Introduction

Our main goal in this chapter is to assess the reach of linear colliders for SUSY in the mSUGRA model[112, 113], paying particular attention to the HB/FP region. In the HB/FP region, since $|\mu|$ becomes small, charginos are light. This then implies that there would be a large rate for chargino pair production at e^+e^- linear colliders (LCs) operating with center-of-mass energy $\sqrt{s} \simeq 0.5 - 1$ TeV over most of the HB/FP region. However, since the $\widetilde{W}_1 - \widetilde{Z}_1$ mass gap also becomes small, it is not clear that linear collider experiments would access the entire kinematically allowed chargino pair production region. We note here that previous reach estimates of linear colliders for SUSY in the mSUGRA model extended only up to m_0 values as high as 800 GeV[112]– well below the HB/FP region. We find that a linear collider, using standard cuts for chargino pair events, can explore the low $m_{1/2}$ portion of the HB/FP region. To explore the high $m_{1/2}$ part of the hyperbolic branch, new specialized cuts are suggested. With these cuts, it appears possible to probe essentially all of the HB/FP region (up to $m_{1/2} = 1.6$ TeV) where charginos satisfy the LEP2 bounds, and where chargino pairs are kinematically accessible at a linear collider (LC). This then provides the first example of a SUSY parameter space region which is accessible to linear e^+e^- colliders, while likely remaining out of reach of LHC experiments! This is especially interesting since the HB/FP region is one of the three qualitatively different mSUGRA parameter space regions allowed by dark matter and other constraints.

If indeed a SUSY signal from charginos is detected, the next step would be to try and determine the associated weak scale parameters: μ, M_2 and $\tan\beta$[114]. We explore a particular case study in the low $m_{1/2}$ region of the HB/FP region, and show that at least in this case μ and M_2 should be measurable. This measurement would give a firm indication of the large higgsino content of the light chargino and $\widetilde{Z}_1$ and, together with the fact that sfermions are not detected either at the LC or at the LHC, provide a strong indication that SUSY in fact lies in the HB/FP region.

4.2 Reach of a Linear Collider in the mSUGRA model

In our signal and background computations, we use ISAJET 7.69[116] which allows for the use of polarized beams, and also allows for convolution of subprocess cross sections with electron parton distribution functions (PDFs) arising from both initial state bremsstrahlung and also beamstrahlung[117]. We use the ISAJET toy detector CALSIM with calorimetry covering the regions $-4 < \eta < 4$ with cell size $\Delta\eta \times \Delta\phi = 0.05 \times 0.05$. Electromagnetic energy resolution is given by $\Delta E_{em}/E_{em} = 0.15/\sqrt{E_{em}} \oplus 0.01$, while hadronic resolution is given by $\Delta E_h/E_h = 0.5/\sqrt{E_h} \oplus 0.02$, where $\oplus$ denotes addition in quadrature. Jets are identified using the ISAJET jet finding algorithm GETJET using a fixed cone size of $\Delta R = \sqrt{\Delta\eta^2 + \Delta\phi^2} = 0.6$, modified to cluster on energy rather than transverse energy. Clusters with $E > 5$ GeV and $|\eta(jet)| < 2.5$ are labeled as jets. Muons and electrons are classified as isolated if they have $E > 5$ GeV, $|\eta_\ell| < 2.5$, and the visible activity within a cone of $R = 0.5$ about the lepton direction is less than $max(E_\ell/10 \text{ GeV}, 1 \text{ GeV})$. Finally, jets originating from b-quarks are tagged as b-jets with an efficiency of 50%.

4.2.1 Review of previous reach assessment

The reach of a $\sqrt{s} = 0.5$ TeV LC for supersymmetry has previously been evaluated in Ref. [112] assuming an integrated luminosity of 20 fb^{-1}. Reach contours were presented for the case of the mSUGRA model in the m_0 *vs.* $m_{1/2}$ plane for $A_0 = 0$, $\tan\beta = 2$ and 10, and $\mu \gtrless 0$. The reach plots in that study were limited to $m_{1/2} < 600$ GeV and $m_0 < 800$ GeV, *i.e.* well outside the HB/FP region.

The region of the $m_0 - m_{1/2}$ plane where there should be an observable SUSY signal in LC experiments consists of three distinct pieces.

- At low m_0 with $m_{1/2} \sim 300 - 500$ GeV, slepton pair production occurs at large rates. The signal is a pair of opposite sign/same flavor leptons plus missing energy. Tsukamoto *et al.*[114] suggested cuts of *i*) 5 GeV $< E(\ell) < 200$ GeV, *ii*) 20 GeV $< E_{vis.} < \sqrt{s} - 100$ GeV, *iii*) $|m(\ell\bar{\ell}) - M_Z| > 10$ GeV, *iv*) $|\cos\theta(\ell^{\pm})| < 0.9$, *v*) $-Q_\ell \cos\theta_\ell < 0.75$, *vi*) $\theta_{acop} > 30°$, *vii*) $E_T^{mis} > 25$ GeV and *viii*) veto events with any jet activity. Here, $\theta_{acop} \equiv \pi - \cos^{-1}(\hat{p}_x^+ \hat{p}_x^- + \hat{p}_y^+ \hat{p}_y^-)$. The reach was evaluated by running with right-polarized electron beams where $P_L(e^-) = -0.9$. The beam polarization maximizes $\tilde{\ell}_R \bar{\tilde{\ell}}_R$ pair production, while minimizing background from $W^+ W^-$ production.

- At low $m_{1/2}$ values, chargino pair production occurs at a large rate. To search for chargino pairs, one may look for $1\ell + 2j + E^{mis}$ events. Following Ref. [114], it was required in Ref. [112] to have one isolated lepton plus two jets with *i*) 20 GeV $< E_{vis} < \sqrt{s} - 100$ GeV, *ii*) if $E_{jj} > 200$ GeV, then $m(jj) < 68$ GeV, *iii*) $E_T^{mis} > 25$ GeV, *iv*) $|m(\ell\nu) - M_W| > 10$ GeV for a W pair hypothesis, *v*) $|\cos\theta(j)| < 0.9$, $|\cos\theta(\ell)| < 0.9$, $-Q_\ell \cos\theta_\ell < 0.75$ and $Q_\ell \cos\theta(jj) < 0.75$, *vi*) $\theta_{acop}(WW) > 30°$ for a W pair hypothesis. The reach for $1\ell + 2j + \not{E}_T$ events from chargino pair production was evaluated using a left polarized beam with $P_L = +0.9$.

- Finally, there exists a small region around $m_0 \sim 200 - 500$ GeV and $m_{1/2} \sim 300 - 350$ GeV where neither slepton pairs nor chargino pairs are kinematically accessible, but where $e^+ e^- \to \widetilde{Z}_1 \widetilde{Z}_2$ is. In this case, the decay $\widetilde{Z}_2 \to \widetilde{Z}_1 h$ was usually found to be dominant. Since $h \to b\bar{b}$ with a large branching fraction, $b\bar{b} + \not{E}_T$ events were searched for with two tagged b-jets, $E_T^{mis} > 25$ GeV and $30° < \Delta\phi_{b\bar{b}} < 150°$. Imposing a missing mass cut $\not{m} > 340$ GeV eliminated almost all SM backgrounds, so that a signal cross section of 10 fb would yield 10 signal events for integrated luminosity 20 fb^{-1}, where the signal efficiency was found to be 6%. Beam polarization of $P_L = +0.9$ was used.

In the following, we refer to these as the "standard cuts".

The ultimate reach contours found in Ref. [112] generally track the boundary of the kinematically allowed regions for $\widetilde{W}_1$ and $\tilde{e}_R$ pair production. An exception occurs at low m_0 values where selectron pair production is dominant, but where $m_{\tilde{e}_R} \simeq m_{\widetilde{Z}_1}$. Then, the mass gap $m_{\tilde{e}_R} - m_{\widetilde{Z}_1}$ becomes so small that there was very little visible energy in the slepton pair events, resulting in very low detection efficiency, causing a turnover in the reach contours. For $\tan\beta$ values larger than those explored in Ref. [112], the large τ Yukawa coupling makes $\tilde{\tau}_1$ significantly lighter than $\tilde{e}_R$ so that close to the boundary of excluded region at small m_0 $\tilde{e}_R \bar{\tilde{e}}_R$ events may still be observable, while $\tilde{\tau}_1 \bar{\tilde{\tau}_1}$ events are not.

4.2.2   Updated reach results

In this section, we update previous reach projections[112] for a linear collider. We present reach projections for linear colliders with $\sqrt{s} = 0.5$ and 1 TeV of energy in the CM frame. We also expand the range of $m_{1/2}$ (to 1.6 TeV) and m_0 (to 8 TeV) beyond the values presented in Ref. [112]. This allows us to explore the entire stau co-annihilation strip, the A-annihilation funnel and the HB/FP region. In our analysis, we restrict ourselves to the trilinear SSB term $A_0 = 0$. For the most part, our results are qualitatively insensitive to variations in A_0. An exception occurs for particular A_0 choices which may greatly reduce the value of $m_{\tilde{t}_1}$, and lead to a top squark-neutralino co-annihilation region[118].

Our first results are presented in Fig. 4.1, where we show the m_0 $vs.$ $m_{1/2}$ plane for $\tan\beta = 30$, $\mu > 0$ and $A_0 = 0$. The left-most red region at low m_0 is disallowed because the LSP would become a stau. The right-most red region (large m_0) is mainly excluded by a lack of appropriate REWSB, although this includes as well points with no convergent RGE solution as generated by ISAJET. The precise location of the boundary of the large m_0 red region depends somewhat on the computer code, and also on the assumed fermion masses. The lower yellow region is excluded by LEP2 chargino searches, which require $m_{\widetilde{W}_1} > 103.5$ GeV. In addition, the region below the yellow contour gives a light (SM-like) Higgs boson with $m_h < 114.4$ GeV.

Using the standard dilepton cuts as described above, we find a SM background level of $\sigma_{SM} = 1.79$ fb (0.045 fb) for a LC with $\sqrt{s} = 0.5$ TeV (1.0 TeV) with right polarized beams using $P_L(e^-) = -0.9$.[1] It has been shown in Ref. [114] that backgrounds from

---

[1]In our assessment of SM backgrounds, we have evaluated only the backgrounds from $2 \to 2$ processes.

$2 \rightarrow 3$ processes such as $e^+e^- \rightarrow \nu\nu Z, e^+e^- Z$ or $e^\pm \nu W^\mp$ production or $2 \rightarrow 4$ processes such as $e^+e^- W^+W^-$ production are also efficiently removed by these cuts, at least for $\sqrt{s} = 500$ GeV. Although the cross sections for these processes grow with energy, we expect that these cuts will remove the *bulk* of these backgrounds also at $\sqrt{s} = 1000$ GeV; for instance, the dominant portion of the $eeWW$ background that comes from "$\gamma\gamma$" collisions will be removed by the acoplanarity and other cuts; much of the remaining cross section will have $p_T(WW) \leq M_W$ and will also be reduced, though not eliminated by these cuts. However, since these backgrounds have not been included in our evaluation it is possible that the statistical significance of the signal may be somewhat over-estimated for $\sqrt{s} = 1000$ GeV. The regions to the left of the lower (upper) blue contour yield a supersymmetric signal at the 5σ level assuming 100 fb^{-1} of integrated luminosity at the 0.5 (1) TeV LC. An increased reach for slepton pairs may be obtained by searching for ditau events originating from stau pair production. We show the kinematic limit for stau pair production by a dashed light-blue contour, which for $\tan\beta = 30$, lies somewhat above the blue dilepton reach contour.

In a later paper [115] we explore the ditau signal in more detail. We show that most of the kinematically accesible parameter space can be probed by using 2 tau-tagged jet signature and optimizing the cuts for each point in the parameter space. The regions where our method fails occur near the kinematical boundary due to very small stau pair production total cross section, and near the edge of the the allowed parameter space, where the mass gap between the $\tilde{Z}_1^0$ and $\tilde{\tau}_1$ becomes very small.

The green contour denotes the reach of a 0.5 or 1 TeV LC for SUSY via the $1\ell + 2j + \not{E}_T$ channel arising from chargino pair production, using the standard cuts given above. Unlike Ref. [112], we use $P_L = 0$, and find a background level of 15.5 fb (2.1 fb) for $\sqrt{s} = 0.5$ (1) TeV (the beam polarization is not important for this reach contour). For most of parameter space, the reach contours follow closely along the $m_{\widetilde{W}_1} = 250$ (500) GeV mass contours, indicating that chargino pair production can be seen with standard cuts almost to the kinematical limit for chargino pair production.

An exception occurs when m_0 becomes very large, in the HB/FP region. Around $m_0 \sim 4000$ GeV ($m_0 \sim 6000$ GeV) for $\sqrt{s} = 0.5$ TeV (1 TeV), the reach contour departs from the kinematic limit. The termination of the reach contour occurs because in this region, the superpotential parameter μ becomes very small, and the light chargino $\widetilde{W}_1$ and neutralino
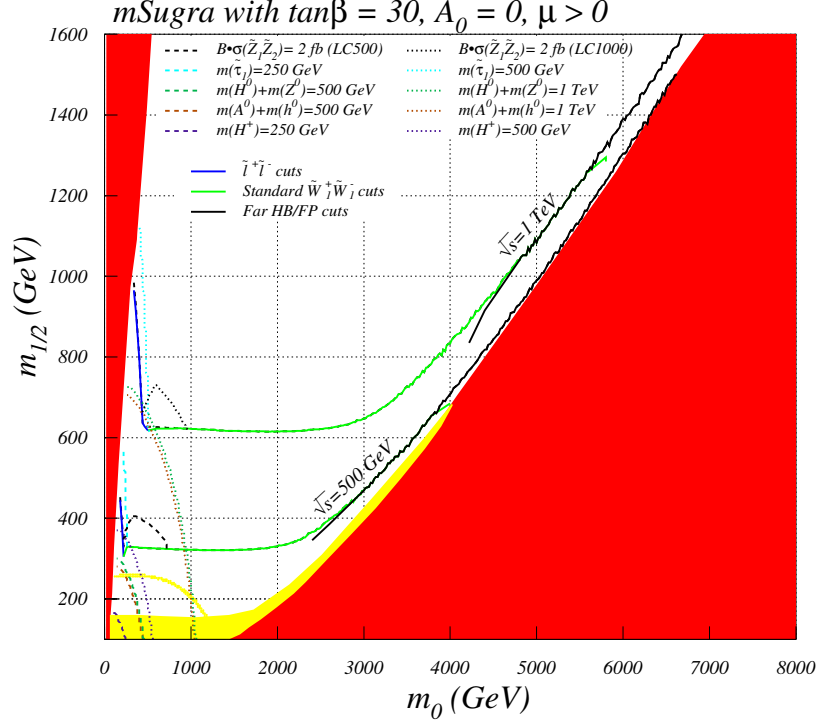
Figure 4.1. Reach of a linear collider for supersymmetry in the mSUGRA model for $\sqrt{s} = 500$ and 1000 GeV, for $\tan\beta = 30$, $A_0 = 0$ and $\mu > 0$. The reach via slepton pair production is denoted by the blue contour, while standard cuts for chargino pair production yield the green contour. Special chargino pair cuts yield the black contour in the HB/FP region. The red region is theoretically excluded, while the yellow region is excluded by LEP2 measurements. Below the yellow contour, $m_h \leq 114.4$ GeV.

$\widetilde{Z}_1$ become higgsino-like, and increasingly mass degenerate. The Q-value from $\widetilde{W}_1 \to \widetilde{Z}_1 f \bar{f}'$ decay (the fs are light SM fermions) becomes very small, and very little visible energy is released by the chargino decays. This causes the detection efficiency for $1\ell + 2j + \not{E}_T$ events to decrease sharply, leading to a corresponding reduction in the reach using the standard cuts.

To understand what is happening in the HB/FP region, we show relevant sparticle masses in Fig. 4.2a) for $m_{1/2} = 225$ GeV, $\tan\beta = 30$, $A_0 = 0$ and $\mu > 0$ versus the parameter m_0. As m_0 varies from 1400 GeV to nearly 2200 GeV, *i.e.* as we approach the HB/FP region for fixed $m_{1/2}$ with increasing m_0. As m_0 increases, $|\mu|$ is seen to be decreasing. Since the

value of $SU(2)$ gaugino mass M_2 is essentially fixed, the various chargino and neutralino masses also decrease, with the lighter ones becoming increasingly higgsino-like. The plot is terminated when the LEP2 limit $m_{\widetilde{W}_1} \geq 103.5$ GeV is reached. Of great importance is that the $\widetilde{W}_1 - \widetilde{Z}_1$ mass gap is also decreasing, although in this case it remains substantial out to the edge of parameter space.

In Fig. 4.2b), we show the total cross section for various chargino and neutralino production reactions versus m_0 as in frame a). At the lower m_0 values, $\sigma(\widetilde{W}_1^+\widetilde{W}_1^-)$ pair production dominates the total SUSY production cross section. As m_0 increases, and $|\mu|$ decreases, the other charginos and neutralinos become light as well, and many more reactions "turn on" in the HB/FP region. Although we will focus mainly on $\widetilde{W}_1^+\widetilde{W}_1^-$ pair production, it is important to note that many SUSY production reactions can occur in the HB/FP region, and can lead to an assortment of SUSY events from the production and cascade decays of the heavier chargino and neutralino states.

A similar plot is shown in Fig. 4.3, except this time for $m_{1/2} = 900$ GeV, $i.e.$ in the upper regions of the hyperbolic branch. In this case, M_2 is much larger than the case shown in Fig. 4.2, and so the heavier charginos and neutralinos remain inaccessible to a LC.

As m_0 increases, again $m_{\widetilde{W}_1}$ and $m_{\widetilde{Z}_1}$ decrease.[2] But in this case the $\widetilde{W}_1 - \widetilde{Z}_1$ mass gap is much smaller, reaching only several GeV at the limit of parameter space. Clearly, in this upper $m_{1/2}$ region of the hyperbolic branch, there will be little visible energy emerging from chargino 3-body decays, making detection of chargino pair events difficult using standard cuts. In addition, as shown in frame b), only $\widetilde{W}_1^+\widetilde{W}_1^-$ and $\widetilde{Z}_1\widetilde{Z}_2$ pair production occur, so fewer anomalous events are expected in the upper HB/FP region. Since $m_{\widetilde{Z}_2} \sim m_{\widetilde{W}_1}$, there will also be little visible energy from $\widetilde{Z}_2 \to \widetilde{Z}_1 f\bar{f}$ decay, so that $\widetilde{Z}_1\widetilde{Z}_2$ production will also be more difficult to observe. In the deep HB/FP region where $|\mu| \ll M_{1,2}$, one of the neutralinos is mainly higgsino-like with roughly equal components of $\tilde{h}_u$ and $\tilde{h}_d$. The other neutralinos, being orthogonal to these, thus either have equal magnitudes for their $\tilde{h}_u$ and $\tilde{h}_d$ content, or this content is small. In either case, the $Z\widetilde{Z}_i\widetilde{Z}_i$ coupling is dynamically suppressed[119]

---

[2]Since $|\mu|$ decreases very rapidly as m_0 increases and approaches the theoretical boundary of the HB/FP region, its precise value is not easy to obtain using numerical methods. The value of μ, of course, directly affects the chargino and neutralino masses. In this figure, we have smoothed out what appeared to be rather large numerical fluctuations in two of the bins.
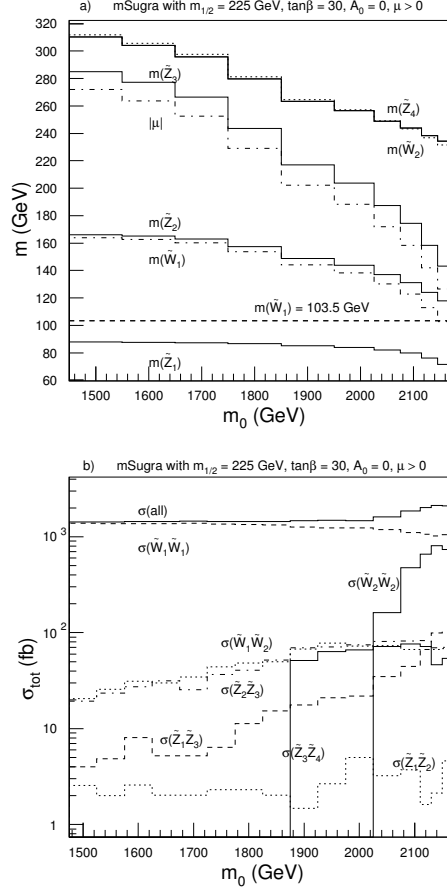
Figure 4.2. Plot of a). sparticle masses and b). sparticle pair production cross sections versus m_0 in the HB/FP region for $m_{1/2} = 225$ GeV, $\tan\beta = 30$, $A_0 = 0$ and $\mu > 0$ for a $\sqrt{s} = 500$ GeV e^+e^- collider.

in this region. This accounts for the strong suppression of $\sigma(\widetilde{Z}_2\widetilde{Z}_2)$ (recall that the electron sneutrino is very heavy) in Fig. 4.3b.

Coincidentally, the reach of a $\sqrt{s} = 0.5$ TeV LC in the $1\ell + 2j + \not{E}_T$ channel using the standard cuts terminates in the HB/FP region at nearly the same $m_{1/2}$ value as does the reach of the CERN LHC shown in Ref. [110], and again in Sec. 4 of this chapter. Meanwhile, the contour of chargino pair kinematic accessibility extends to much higher $m_{1/2}$ values, along
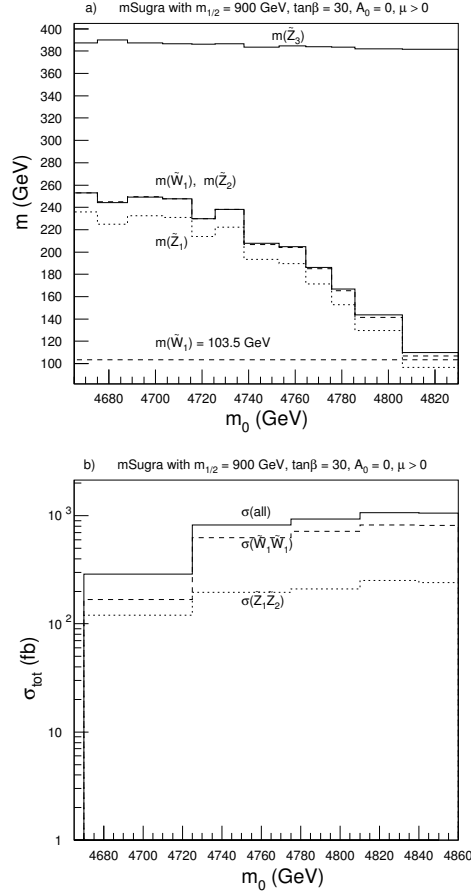
Figure 4.3. Plot of a). sparticle masses and b). sparticle pair production cross sections versus m_0 in the HB/FP region for $m_{1/2} = 900$ GeV, $\tan \beta = 30$, $A_0 = 0$ and $\mu > 0$ for a $\sqrt{s} = 500$ GeV e^+e^- collider.

the hyperbolic branch. This motivated us to examine strategies to extend the reach of a LC to the large $m_{1/2}$ part of the HB/FP region.

To find better suited signal selection cuts for the HB/FP region, we examine a particular case study for the mSUGRA point which is beyond the projected reach of the LHC[110]:

$$m_0, \ m_{1/2}, \ A_0, \ \tan \beta, \ sign(\mu) = \ 4625 \ \text{GeV}, \ 885 \ \text{GeV}, 0, \ 30, \ +1, \qquad (4.1)$$

for which various sparticle masses and parameters are listed in Table 4.1. We will refer to this as case 1. Not only is this point inaccessible at the LHC, but most of the sparticles are also

inaccessible to a LC, with the exception being the lighter charginos and neutralinos. While $m_{\widetilde{W}_1} = 195.8$ GeV, so that $\widetilde{W}_1^+\widetilde{W}_1^-$ pair production occurs at a large rate at a $\sqrt{s} = 0.5$ TeV e^+e^- collider, the $\widetilde{W}_1 - \widetilde{Z}_1$ mass gap is only 14.2 GeV, so little visible energy is released in chargino pair production events.

With this in mind, we generate SUSY events for this case study using ISAJET 7.69 for a linear collider with $\sqrt{s} = 0.5$ TeV and unpolarized beams, including bremsstrahlung and beamstrahlung for background events. The beamstrahlung parameters, defined in Ref. [117], are taken to be $\Upsilon = 0.1072$ with beam length $\sigma_z = 0.12$ mm.

Table 4.1. Masses and parameters in GeV units for case 1 for m_0, $m_{1/2}$, A_0, $\tan\beta$, $sign\mu =$ 4625 GeV, 885 GeV, 0, 30, +1 in the mSUGRA model. The spectrum is obtained using ISAJET v7.69.

parameter	value (GeV)
M_2	705.8
M_1	372.2
μ	185.9
$m_{\tilde{g}}$	2182.7
$m_{\tilde{u}_L}$	4893.9
$m_{\tilde{e}_L}$	4656.1
$m_{\widetilde{W}_1}$	195.8
$m_{\widetilde{W}_2}$	743.5
$m_{\widetilde{Z}_1}$	181.6
$m_{\widetilde{Z}_2}$	196.2
$m_{\widetilde{Z}_3}$	377.3
$m_{\widetilde{Z}_4}$	760.0
m_A	3998.3
m_h	122.0
$\Omega_{\widetilde{Z}_1}h^2$	0.0104
$BF(b \to s\gamma)$	3.34×10^{-4}
Δa_μ	0.6×10^{-10}

In Fig. 4.4a) we show the distribution of $E_{visible}$ from events with 1-lepton and two jets expected at a $\sqrt{s} = 500$ GeV LC. The solid black histogram represents the SUSY case study, which peaks at very low $E_{visible}$, as expected from the low energy release from chargino decays. The small number of events around $E_{visible} = 250$ GeV is from Zh production.

61
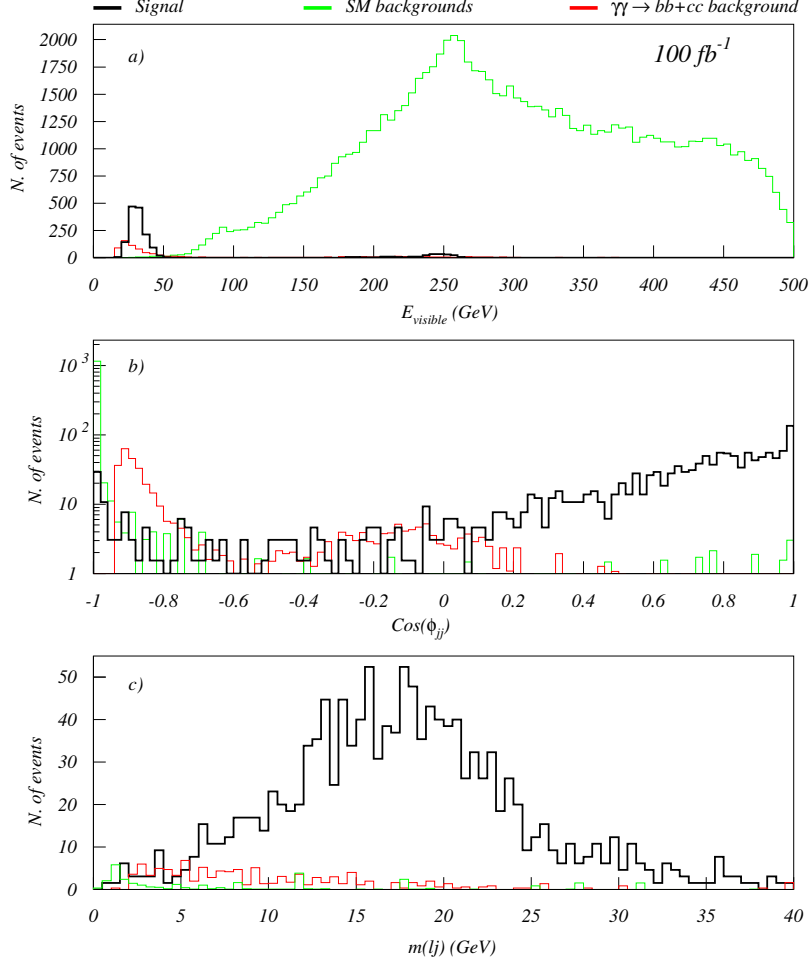
Figure 4.4. Distribution in *a*) $E_{visible}$ for mSUGRA signal (black histogram) with (m_0, $m_{1/2}$, A_0, $\tan\beta$, $sign(\mu)$= 4625 GeV, 885 GeV, 0, 30, 1) after cuts in the first row of Table 4.2. We take $\sqrt{s} = 500$ GeV and an integrated luminosity of 100 fb^{-1}, and adopt beamstrahlung parameters $\Upsilon = 0.1072$ and $\sigma_z = 0.12$ mm. The ISAJET SM background is shown by the green histogram, while the background from $\gamma\gamma \to c\bar{c}$, $b\bar{b}$ is shown in red. In *b*), we show the distribution in transverse plane dijet opening angle requiring, in addition, that 20 GeV$< E_{visible} < 100$ GeV. In *c*), we show the distribution in $m(\ell j)$, after the aditional requirement $\cos\phi(jj) > -0.6$. The jet entering the $m(\ell j)$ distribution is the one that is closest in angle to the lepton direction.

The green histogram shows the sum of all $2 \rightarrow 2$ SM backgrounds as generated by ISAJET. The large $E_{visible}$ component of these arises from WW, ZZ and $t\bar{t}$ production, where some energy is lost due to associated neutrino emissions. The SM background distribution extends to low $E_{visible}$ values, and has a visible shoulder at $E_{visible} \sim M_Z$ due to processes such as $e^+e^- \rightarrow Z \rightarrow b\bar{b}, c\bar{c}$, where the Z can be made by convoluting the subprocess reaction with the electron PDF, and the lepton from the decay of the heavy flavor is accidently isolated. The bulk of the $2 \rightarrow 2$ SM background can be eliminated by requiring low values of $E_{visible}$. In this case we require

$$20 \; GeV < E_{visible} < 100 \; GeV. \tag{4.2}$$

The upper limit is chosen to be well above the case 1 signal distribution endpoint to accommodate later scans over all mSUGRA parameter space, including points which allow larger $\widetilde{W}_1 - \widetilde{Z}_1$ mass gaps, and somewhat harder $E_{visible}$ distributions. We also show a red histogram which shows the results of the evaluation of the background from $e^+e^- \rightarrow e^+e^- c\bar{c}$, $e^+e^- b\bar{b}$ processes when both initial leptons escape detection when being scattered at a very small angle. We evaluated this background, which mainly arises from photon photon collisions, using the PYTHIA event generator[120]. In the case of $b\bar{b}$ production, the isolated lepton arises from semi-leptonic $b \rightarrow c\ell\nu$ decay, and the jets come one from a b quark, and the other from the charm quark.

In $\gamma\gamma \rightarrow b\bar{b}$ events, the b and $\bar{b}$ will typically emerge back-to-back in the transverse plane. Thus, in Fig. 4.4b) we plot the distribution in $\cos\phi(jj)$, where $\phi(jj)$ is the transverse dijet opening angle. The signal is distributed over a range of $\cos\phi(jj)$ values, and actually peaks at $\cos\phi(jj) \sim 1$. The background peaks at $\cos\phi(jj) \sim -1$, so we require a cut of

$$\cos\phi(jj) > -0.6. \tag{4.3}$$

Finally, any surviving background arising from $b\bar{b}$ or $c\bar{c}$ production followed by semileptonic heavy flavor decay is likely to have a jet-lepton invariant mass bounded by the heavy flavor mass (at least at parton level). In Fig. 4.4c) we show the distribution in $m(\ell j)$ where we form the invariant mass from the jet which is closest to the isolated lepton in space angle. Some additional background removal at low cost to signal is gained by requiring

$$m(\ell j_{near}) > 5 \; GeV. \tag{4.4}$$

63

At this point, the distribution is clearly dominated by signal. The cross sections in fb after each cut for signal and background are shown in Table 4.2, where we include in addition background from the $2 \to 4$ process $e^+e^- \to \ell\nu q\bar{q}'$ (evaluated using CompHEP[121]). In the $2 \to 4$ calculation we eliminate Feynman diagrams such as WW pair production which are already accounted for as $2 \to 2$ processes in ISAJET. The $2 \to 4$ processes are negligible after the $E_{visible}$ cut. For all frames of Fig. 4.4 we have assumed 100 fb^{-1} total integrated luminosity.

In this analysis we have neglected the beamstrahlung when calculating the $2 \to 4$ SM bakcgrounds. As we have shown later in Ref. [115], the inclusion of beamstrahlung into background calculations can have a profound effect. The $\gamma\gamma \to b\bar{b}$ and $\gamma\gamma \to c\bar{c}$ cross sections after the listed cuts are $\overset{<}{\sim} 40$ times larger when including beamstrahlung! However, after an additional cut $|\cos\theta_j| < 0.8$ is applied to both jets, one reduces the background to the same level as in the calculation done using PYTHIA without much loss of the signal. Therefore all the results of this chapter still hold true.

Table 4.2. Cross section after cuts in fb for mSUGRA case 1 signal and ISAJET SM backgrounds, two photon background $\gamma\gamma \to c\bar{c}$, $b\bar{b}$ and the $2 \to 4$ process $e^+e^- \to \ell\nu_\ell q\bar{q}'$. We take $\sqrt{s} = 0.5$ TeV collider CM energy. The corresponding background for $\sqrt{s} = 1$ TeV case is listed in parenthesis.

cuts	case 1	ISAJET BG	$\gamma\gamma \to c\bar{c}, bb$	$\ell\nu q\bar{q}'$
η, E, ΔR	16.2	897.1 (483)	9.2 (6.2)	448 (712)
20 $GeV < E_{vis} < 100$ GeV	14.4	12.6 (3.5)	5.4 (4.9)	0.16 (0.08)
$\cos\phi(jj) > -0.6$	13.5	0.34 (0.2)	1.1 (1.1)	0.04 (0.02)
$m(\ell j) > 5$ GeV	12.9	0.17 (0.1)	0.8 (0.8)	0.04 (0.02)

We now require a 5σ signal for SUSY events above the total SM background as listed in Table 4.2, for 100 fb^{-1} of integrated luminosity and scan mSUGRA points in the HB/FP region of Fig. 4.1. The new result is the black contour, below which the mSUGRA parameter space is accessible by the LC at 5σ level. One can see that this contour pushes the reach of the LC to much higher values of $m_{1/2}$. The contour peters out at low $m_{1/2}$ values, where the visible energy arising from chargino pair production is typically much higher than the 100 GeV maximum required by our cuts. However, this low $m_{1/2}$ region is already well covered by the standard chargino search cuts listed at the beginning of this section. The

new cuts for the far HB/FP region work for e^+e^- colliders with $\sqrt{s} = 1$ TeV as well. The $\sqrt{s} = 1$ TeV reach contour extends even beyond the limits of parameter space shown in Fig. 4.1.

To complete our SUSY reach contours, we also examined the reach of a LC for SUSY via the $e^+e^- \to \widetilde{Z}_1\widetilde{Z}_2$ reaction in the non-HB/FP part of parameter space, where neither chargino pair production nor slepton pair production is kinematically accessible. In this case, we follow Ref. [112] in asking for $b\bar{b} + \not{\!E}_T$ events from $e^+e^- \to \widetilde{Z}_1\widetilde{Z}_2$ production followed by $\widetilde{Z}_2 \to \widetilde{Z}_1 h$, where $h \to b\bar{b}$. In Ref. [112], no background was found after a series of cuts listed at the beginning of this section. Here, we do not perform complete event generation at every point in parameter space, but instead require that

$$\sigma(e^+e^- \to \widetilde{Z}_1\widetilde{Z}_2) \times BF(\widetilde{Z}_2 \to \widetilde{Z}_1 h) > 2 \text{ fb}, \qquad (4.5)$$

which should yield ~ 10 signal events for 100 fb^{-1} of integrated luminosity assuming an efficiency of $5-6\%$ as found in Ref. [112]. The resulting reach contour is shown in Fig. 4.1 as the black contour linking the slepton pair reach to the chargino reach contour. It gives some additional parameter space reach to a LC, although it is in a dark matter *disfavored* region of parameter space (unless $\tan\beta$ is large, and the H, A-annihilation funnel cuts through it). There is a turnover in the $e^+e^- \to \widetilde{Z}_1\widetilde{Z}_2$ reach contour at low m_0; this occurs because in this region, $\widetilde{Z}_2 \to \tilde{\tau}_1\bar{\tau}$ decay becomes accessible, resulting in a suppression of the $\widetilde{Z}_2 \to \widetilde{Z}_1 h$ branching fraction. However, the $\widetilde{Z}_2 \to \tilde{\tau}_1\bar{\tau}$ signal may also be detectable; if so, the gap caused by the turn-over just mentioned would be filled.

Finally, we show the kinematic limit for $e^+e^- \to ZH$ (green-dashed or dotted contours), $e^+e^- \to Ah$ (orange dashed or dotted contours) and $e^+e^- \to H^+H^-$ (purple dashed or dotted contours). The dashes are for $\sqrt{s} = 0.5$ TeV, while dotted are for $\sqrt{s} = 1$ TeV. For $\tan\beta = 30$, these contours always lie below the sparticle reach contours, so if heavier SUSY Higgs bosons are seen (at least in the channels mentioned above), sparticles should also be seen if SUSY is realized as in the mSUGRA framework.

In Fig. 4.5, we show LC reach contours for the same mSUGRA parameter plane as in Fig. 4.1, except this time $\tan\beta = 10$. Qualitatively, many of the reach contours are similar to the $\tan\beta = 30$ case of Fig. 4.1, and in particular, the new cuts designed to access the far HB/FP region again allow the LC reach to extend into the high $m_{1/2}$ section of the hyperbolic

65
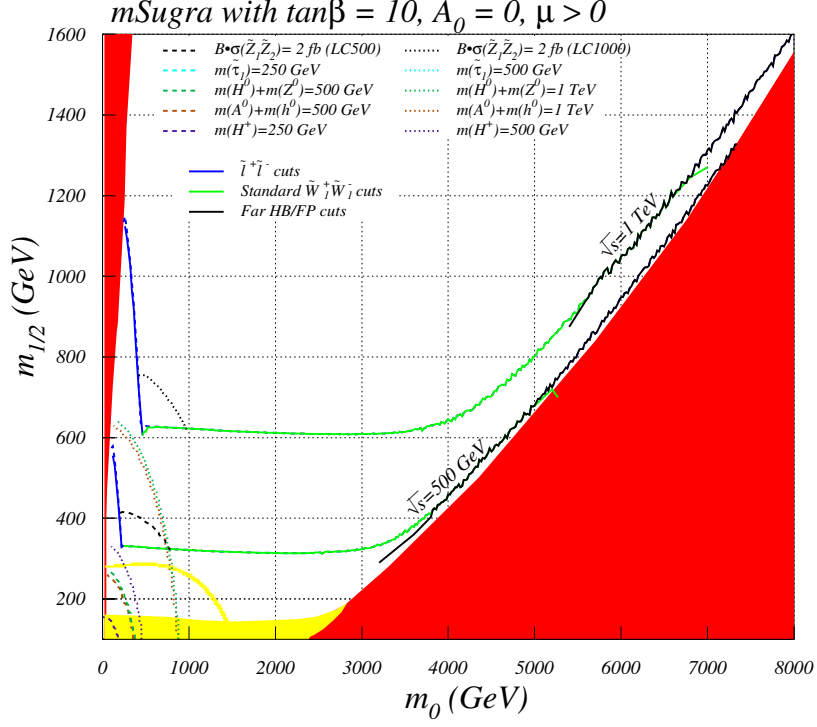
Figure 4.5. Reach of a linear collider for supersymmetry in the mSUGRA model for $\sqrt{s} = 500$ and 1000 GeV, for $\tan\beta = 10$, $A_0 = 0$ and $\mu > 0$. The colors on the various regions and on the different contours are as in Fig. 4.1.

branch. One difference for $\tan\beta = 10$ results is that the $\tilde{\tau}_1^+\tilde{\tau}_1^-$ kinematic reach contour now lies nearly atop the selectron/smuon reach contour using the dilepton cuts described at the beginning of this section.

In Fig. 4.6, we show the same reach contours in the m_0 *vs.* $m_{1/2}$ plane, but this time for $\tan\beta = 45$ and $\mu < 0$. The standard slepton pair and chargino pair production reach contours are similar to the low $\tan\beta$ cases. In this case, the far HB/FP region cuts allow the reach to be extended, although the reach contour terminates in the part of the red region where the numerical solutions to the renormalization group equations do not converge as per the criteria in ISAJET. A tiny region remains inaccessible to our new cuts, between the black solid contours and the dashed contours that depicts the kinematic limit for chargino pair production.
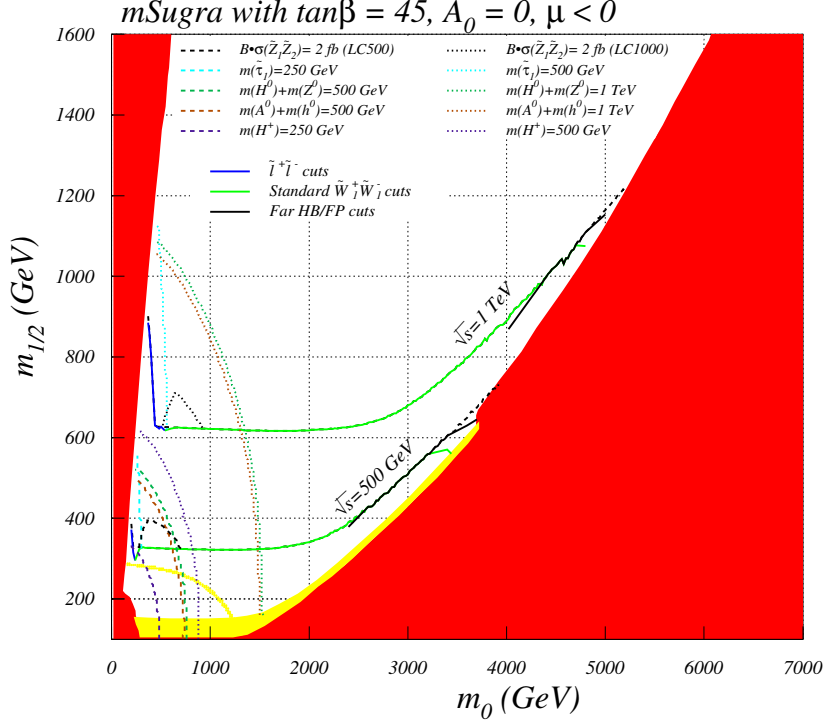
Figure 4.6. Reach of a linear collider for supersymmetry in the mSUGRA model for $\sqrt{s} = 500$ and 1000 GeV, for $\tan\beta = 45$, $A_0 = 0$ and $\mu < 0$. The colors on the various regions and on the different contours are as in Fig. 4.5.

Another feature of the $\tan\beta = 45$ plot is that the stau pair kinematic region has expanded even more beyond where signals for $\tilde{e}_R$ and $\tilde{\mu}_R$ may be accessible in the dilepton channel. In addition, for this large value of $\tan\beta$, the heavy Higgs bosons are much lighter than the low $\tan\beta$ cases[27], and now there exist regions of parameter space where ZH and Ah production may be accessible, while sparticles are not: indeed such a situation would point to a large value of $\tan\beta$ which would of course be independently measureable from the properties of the detected Higgs bosons[122]. These regions all occur well below the reach of the LHC for SUSY, which will be shown in Sec. 4. Thus, if nature chooses $\tan\beta = 45$ in an mSUGRA-like model, and the LC sees only Higgs bosons beyond the SM, it is likely that the existence of SUSY would already have been established by LHC experiments.
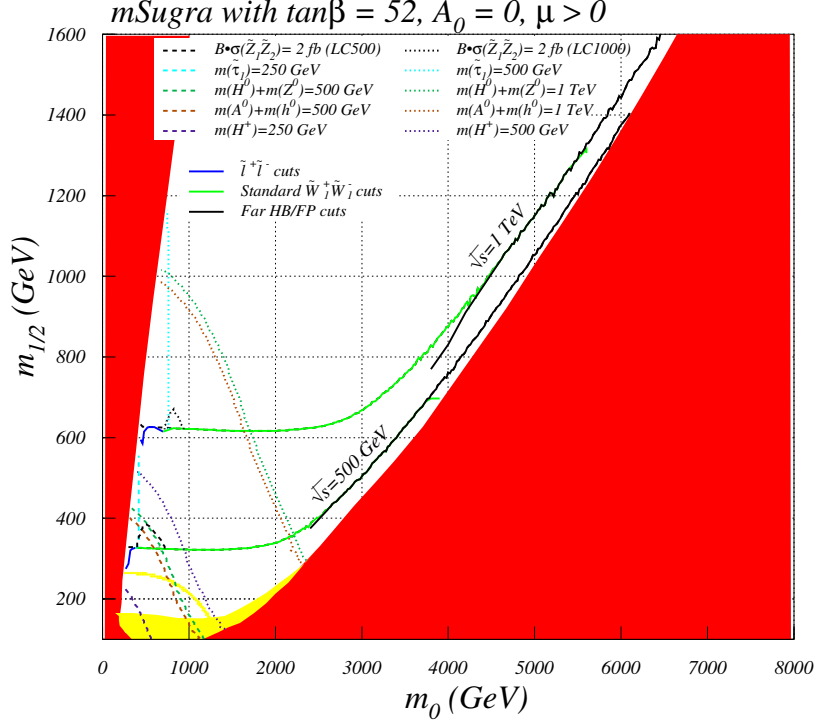
Figure 4.7. Reach of a linear collider for supersymmetry in the mSUGRA model for $\sqrt{s} = 500$ and 1000 GeV, for $\tan\beta = 52$, $A_0 = 0$ and $\mu > 0$. The colors on the various regions and on the different contours are as in Fig. 4.5.

In Fig. 4.7, we show our final LC reach plot, taking $\tan\beta = 52$ with $\mu > 0$. In this case, there is still substantial reach for chargino pairs via the standard cuts, and the special cuts for the far HB/FP region again allow extended reach into this area. For this large a value of $\tan\beta$, the dilepton reach contour has been completely consumed by the expanding forbidden region on the left where $\tilde{\tau}_1$ becomes the LSP. In addition, the $e^+e^- \to \widetilde{Z}_1\widetilde{Z}_2$ reach region has shrunk due to the increased branching fraction for $\widetilde{Z}_2 \to \tilde{\tau}_1\tau$ decay. However, the kinematic reach for stau pairs has greatly increased, and becomes especially important for very large $\tan\beta$, especially if nature has chosen to reduce LSP dark matter from the early universe via co-annihilation with staus.

4.3 Comparison of LC reach with Tevatron, LHC and $\Omega_{\widetilde{Z}_1} h^2$

In this section, we present an overview of the reach of a LC in comparison to the reach for sparticles that can be obtained by the Fermilab Tevatron and the CERN LHC. In addition, we show regions of relic neutralino dark matter density in accord with the recent WMAP measurements.

Our first results are shown in Fig. 4.8 which shows the same parameter space plane as in Fig. 4.5. In this case, however, we plot the composite reach plot of a $\sqrt{s} = 0.5$ and 1 TeV LC for discovery of sparticles assuming 100 fb^{-1} of integrated luminosity. The LC reach plots now consist of combined 1.) slepton pair reach via dileptons (we also show the kinematically accesible stau pair production contour, if it is beyond the slepton reach), 2.) the chargino pair reach via $1\ell + 2j + \not{\!\!E}_T$ events, with either the standard cuts or the cuts specialized for searches in the HB/FP region, and 3.) the region of $\widetilde{Z}_1\widetilde{Z}_2 \to b\bar{b} + \not{\!\!E}_T$. In addition, we superimpose on this plot the reach of the Fermilab Tevatron for SUSY via the clean trilepton signal originating from $p\bar{p} \to \widetilde{W}_1\widetilde{Z}_2 X \to 3\ell + \not{\!\!E}_T + X$, where X denotes assorted hadronic debris. The Tevatron reach was extended into the HB/FP region in Ref. [109]; we show the optimistic reach assuming a 3σ signal with 25 fb^{-1} of integrated luminosity. In addition, we show the reach of the CERN LHC as derived in Ref. [110], assuming 100 fb^{-1} of integrated luminosity. We have also added to the plot the green region, which denotes parameter space points with relic density $\Omega_{\widetilde{Z}_1} h^2 < 0.129$, as required by the recent WMAP measurements.[3] The relic density calculation[123] includes all relevant neutralino annihilation and co-annihilation processes in the early universe using the CompHEP program. It also implements relativistic thermal averaging of the annihilation cross section times velocity, which is useful to get the appropriate relic density in the vicinity of s-channel poles (where the annihilating neutralinos may have substantial velocities) using the formulae of Gondolo and Edsjo[124].

The dark matter allowed region splits into three distinct regions for $\tan\beta = 10$. On the far left of the plot at low m_0 is the stau co-annihilation region, which blends into the bulk annihilation region at low $m_{1/2}$ values. Note that the bulk region is largely below the LEP2 $m_h = 114.4$ GeV contour. We also see that the stau co-annihilation region extends

---

[3]The WMAP allowed region including the lower bound would appear as a very narrow strip following the border of the green region.

to $m_{1/2}$ values as high as ~ 900 GeV. For $\tan\beta = 10$, we see that a $\sqrt{s} = 0.5$ TeV e^+e^- collider should be able to scan much of the stau co-annihilation region, while a $\sqrt{s} = 1$ TeV machine can cover it entirely (as can the LHC). Another region of relic density is the small strip at constant $m_{1/2} \sim 100$ GeV, where neutralinos can annihilate through the narrow s-channel pole from the light Higgs boson h. This region can be covered by all the colliders, including the Fermilab Tevatron. Finally, adjacent to the REWSB excluded region at large m_0 is shown the dark matter allowed region in the HB/FP region, where the LSP has a significant higgsino component, which facilitates neutralino annihilation to WW and ZZ pairs in the early universe. The Fermilab Tevatron reach does not extend into this regime. The $\sqrt{s} = 0.5$ TeV LC can explore the kinematically allowed portion of the lower HB/FP region (which is the region favored by the fine-tuning analysis of Ref.[36]) via standard cuts and the cuts specialized to the far HB/FP region. The $\sqrt{s} = 1$ TeV colider can explore *all* the HB/FP region which is dark matter allowed, until $m_{1/2}$ becomes greater than ~ 900 GeV. The portion of the HB/FP region with $m_{1/2} > 900$ GeV, while allowed by dark matter as well as other experimental constraints, becomes more difficult to reconcile with fine-tuning considerations.

The new cuts proposed in Sec. 2 allow the LC SUSY search region to extend well beyond the reach of the CERN LHC, which extends only to $m_{1/2} \sim 700$ GeV. The LHC reach is limited in the high $m_{1/2}$ part of the hyperbolic branch because sfermions and gluinos are too heavy to be produced at an appreciable rate. Chargino and neutralino pairs can still be produced at the LHC in the high $m_{1/2}$ part of the hyperbolic branch, but the soft visible energy emanating from chargino and neutralino decay makes detection above background very difficult. The high $m_{1/2}$ part of the hyperbolic branch yields a first example of a region of mSUGRA model parameter space where *sparticles can be discovered at a LC, whereas the CERN LHC reach for sparticles has petered out.* Moreover, this additional reach area comes in precisely at a very compelling dark matter allowed region of the mSUGRA model.

In Fig. 4.9, we show the same plot, except this time for $\tan\beta = 30$. Many features of the plot are qualitatively similar to the $\tan\beta = 10$ case. In this case, the stau co-annihilation corridor now extends up to $m_{1/2}$ values as high as 1050 GeV. The entire stau co-annihilation corridor can potentially be explored by a $\sqrt{s} = 1$ TeV LC, but only if a stau pair search is made in addition to the dilepton search. In this case, the Tevatron reach extends just to the

Figure 4.8. Reach of a $\sqrt{s} = 0.5$ and 1 TeV LC for sparticles in the mSUGRA model for $\tan\beta = 10$, $A_0 = 0$ and $\mu > 0$. We also show the reach of the Fermilab Tevatron assuming 10 fb^{-1} of integrated luminosity (for isolated trileptons) and the reach of the CERN LHC assuming 100 fb^{-1} of integrated luminosity. Finally, the green shaded region shows points where the relic density $\Omega_{\widetilde{Z}_1} h^2 < 0.129$ as dictated by WMAP.

tip of the dark matter allowed HB/FP region. The LHC reach in the HB/FP region is again limited to $m_{1/2} < 700$ GeV values, while the $\sqrt{s} = 0.5$ and especially the $\sqrt{s} = 1$ TeV LC can explore much of the HB/FP region, even for $m_{1/2}$ values far in excess of 700 GeV.

The dark matter relic density is qualitatively different for the case of $\tan\beta = 45$, $\mu < 0$ shown in Fig. 4.10. Here, a large new dark matter allowed region has emerged, namely the A-annihilation funnel which is characteristic of the mSUGRA model at very large $\tan\beta$. As $\tan\beta$ increases, the derived value of m_A decreases, until a region where $m_A \simeq 2m_{\widetilde{Z}_1}$ arises, where neutralinos can efficiently annihilate through the very broad A and also the H s-channel resonances. It can be seen from the figure that the A-annihilation funnel region

71
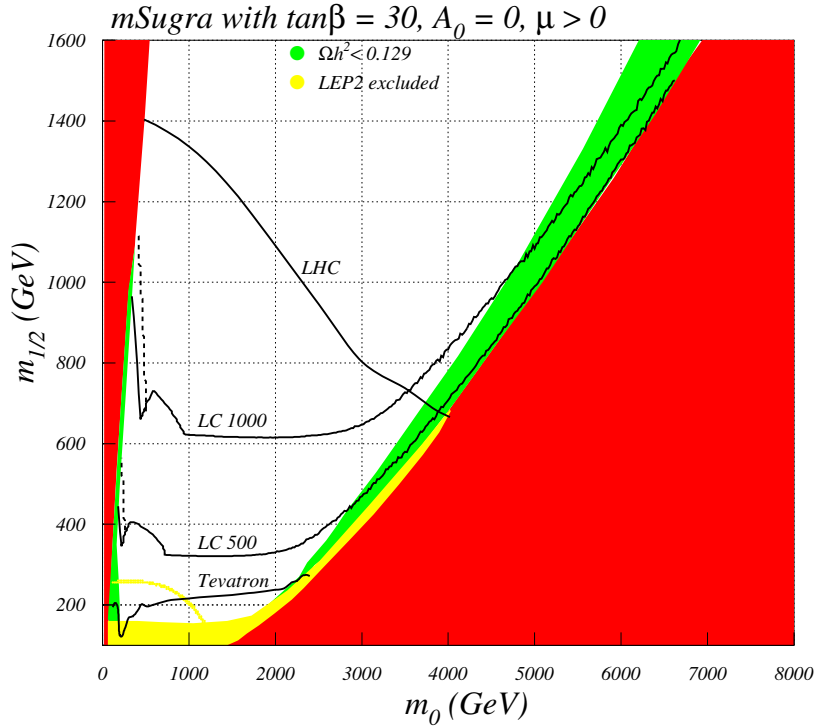
Figure 4.9. Reach of a $\sqrt{s} = 0.5$ and 1 TeV LC for sparticles in the mSUGRA model for $\tan\beta = 30$, $A_0 = 0$ and $\mu > 0$. We also show the reach of the Fermilab Tevatron assuming 10 fb^{-1} of integrated luminosity (for isolated trileptons) and the reach of the CERN LHC assuming 100 fb^{-1} of integrated luminosity. Finally, the green shaded region shows points where the relic density $\Omega_{\widetilde{Z}_1} h^2 < 0.129$ as dictated by WMAP. We denote the kinematic limit for stau pair production at LCs by a dashed black contour.

extends well beyond the reach of both the $\sqrt{s} = 0.5$ and 1 TeV LC. In addition, the stau co-annihilation strip rises to $m_{1/2}$ values that are also beyond the reach of a 1 TeV LC. The CERN LHC can explore essentially all of the A-annihilation funnel for this particular value of $\tan\beta$ and sign of μ. Also, in this case, the $\sqrt{s} = 0.5$ TeV LC can explore the HB/FP region only up to $m_{1/2} \sim 600$ GeV where the $m_{\widetilde{W}_1} = 250$ GeV contour intersects the excluded region. The 1 TeV LC has a reach that extends again well beyond the limit of the LHC reach in the HB/FP region.

In Fig. 4.11, we show the $\tan\beta = 52$ mSUGRA plane for $\mu > 0$. In this case, the effect of the A-annihilation funnel is just beginning to enter the m_0 *vs.* $m_{1/2}$ plane from the left, so

72
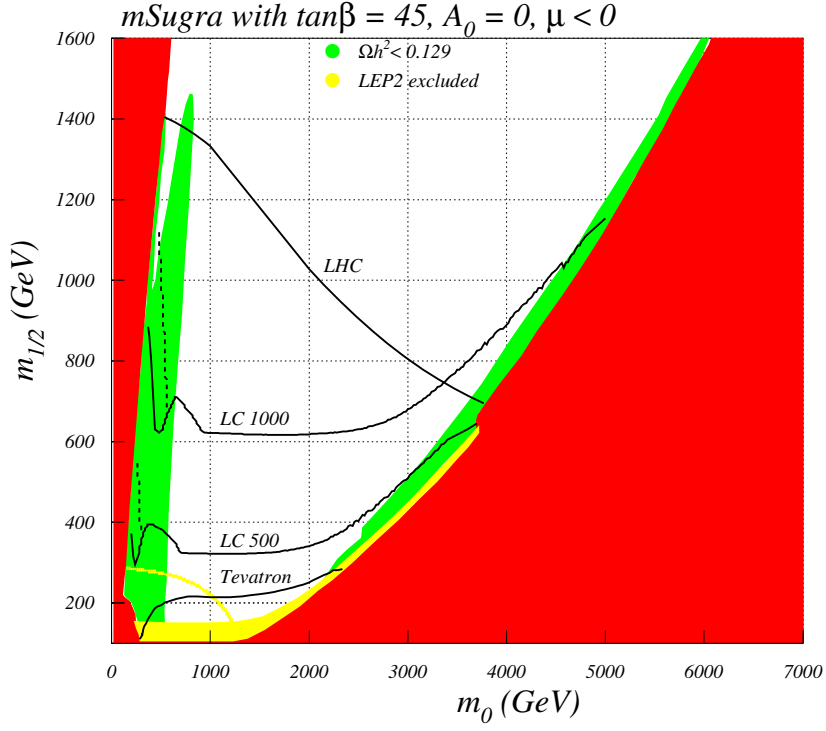
Figure 4.10. Reach of a $\sqrt{s} = 0.5$ and 1 TeV LC for sparticles in the mSUGRA model for $\tan\beta = 45$, $A_0 = 0$ and $\mu < 0$. We also show the reach of the Fermilab Tevatron assuming 10 fb^{-1} of integrated luminosity (for isolated trileptons) and the reach of the CERN LHC assuming 100 fb^{-1} of integrated luminosity. Finally, the green shaded region shows points where the relic density $\Omega_{\widetilde{Z}_1} h^2 < 0.129$ as dictated by WMAP. We denote the kinematic limit for stau pair production at LCs by a dashed black contour.

that points along the low m_0 forbidden region have a low relic density because neutralinos can annihilate via stau coannihilation, via t-channel slepton (mainly stau) exchange (low $m_{1/2}$) *and* partly due to annihilation through the s-channel A resonance. In this case, the A resonance corridor is actually off the plot, but since the A width is so large ($\Gamma_A \sim 25$ GeV for $m_{1/2} \sim 600$ GeV), the value of $2m_{\widetilde{Z}_1}$ can be a few partial widths away from resonance and still give significant contributions to the neutralino annihilation rate. For this large a $\tan\beta$ value, the stau co-annihilation strip reaches $m_{1/2}$ values far beyond the reach of LCs or even the LHC. In the HB/FP region, the new cuts presented in Sec. 2 again give the LCs a reach well beyond the LHC for $m_{1/2} > 700$ GeV.
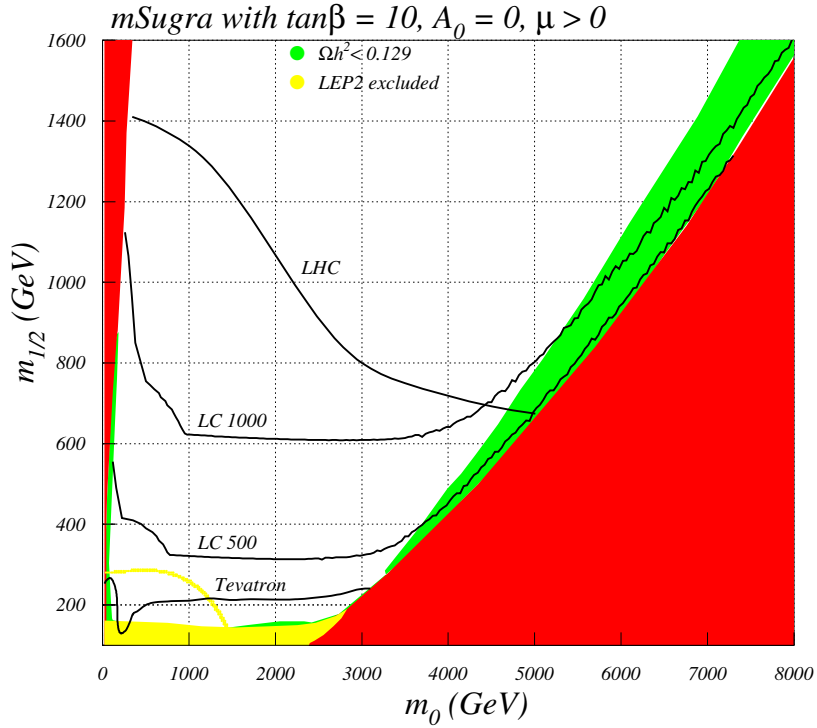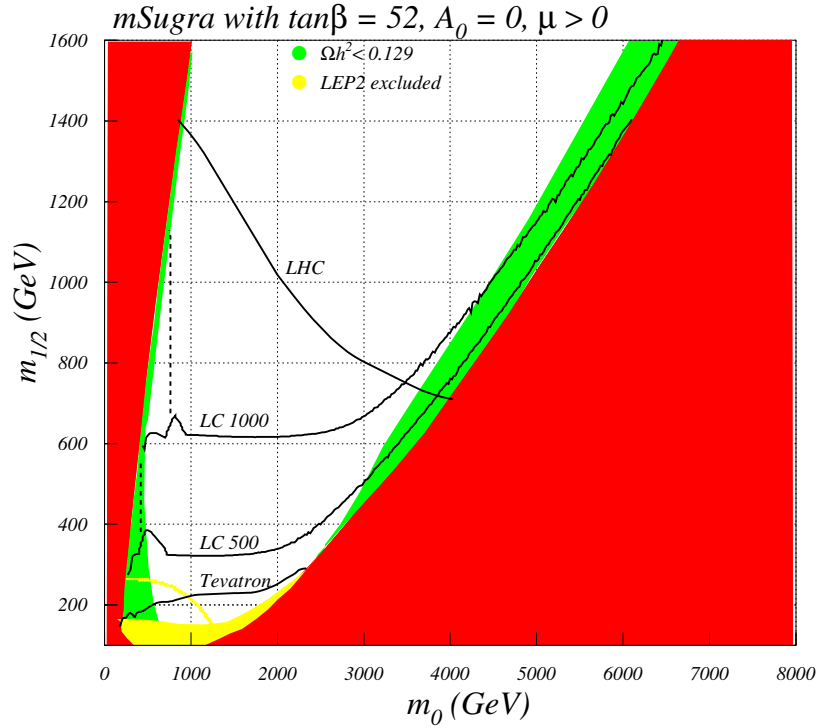
Figure 4.11. Reach of a $\sqrt{s} = 0.5$ and 1 TeV LC for sparticles in the mSUGRA model for $\tan\beta = 52$, $A_0 = 0$ and $\mu > 0$. We also show the reach of the Fermilab Tevatron assuming 10 fb^{-1} of integrated luminosity (for isolated trileptons) and the reach of the CERN LHC assuming 100 fb^{-1} of integrated luminosity. Finally, the green shaded region shows points where the relic density $\Omega_{\tilde{Z}_1} h^2 < 0.129$ as dictated by WMAP. We denote the kinematic limit for stau pair production at LCs by a dashed black contour.

4.4 Determination of Model Parameters in the HB/FP Region

Once a signal for supersymmetry is established at a LC, then the next task will be to scrutinize the signal to elucidate production and decay processes, extract sparticle masses, spins and other quantum numbers, and ultimately to determine parameters of the underlying model. Many groups have examined different case studies[125]. In this section, we will examine a case study in the low $m_{1/2}$ part of the HB/FP region in an attempt to extract the underlying parameters of the MSSM, which may in turn point to nature actually being described by parameters in the HB/FP region.

Toward this end, we consider Case 2, with the mSUGRA parameters set given by

$$m_0, \ m_{1/2}, \ A_0, \ \tan\beta, \ sign(\mu) = 2500 \text{ GeV}, 300 \text{ GeV}, 0, 30, +1.$$

Sample sparticle masses and parameters are given in Table 4.3. For these parameter choices, $|\mu| < M_2$, so that the light chargino and lightest neutralino have significant higgsino components. The chargino mass $m_{\widetilde{W}_1} = 113.1$ GeV, and is just beyond the reach of LEP2. The LSP mass is $m_{\widetilde{Z}_1} = 85.6$ GeV, so that the mass gap $m_{\widetilde{W}_1} - m_{\widetilde{Z}_1} = 27.5$ GeV. The $\widetilde{W}_1$ decays via 3-body modes into $\widetilde{Z}_1 f\bar{f}'$, where f and f' are SM fermions. The decays are dominated by the W boson exchange graphs, so that decays $\widetilde{W}_1 \to \widetilde{Z}_1 f\bar{f}'$ have similar branching fractions to $W \to f\bar{f}'$ decays.

Table 4.3. Masses and parameters in GeV units for Case 2 for $m_0, \ m_{1/2}, \ A_0, \ \tan\beta, \ sign\mu = $ 2500 GeV, 300 GeV, 0, 30, +1 in the mSUGRA model. The spectra is obtained using ISAJET v7.69.

parameter	value (GeV)
M_2	236.5
M_1	122.0
μ	121.6
$m_{\tilde{g}}$	833.2
$m_{\tilde{u}_L}$	2548.1
$m_{\tilde{e}_L}$	2503.9
$m_{\widetilde{W}_1}$	113.1
$m_{\widetilde{W}_2}$	274.8
$m_{\widetilde{Z}_1}$	85.6
$m_{\widetilde{Z}_2}$	135.0
$m_{\widetilde{Z}_3}$	142.2
$m_{\widetilde{Z}_4}$	281.5
m_A	2129.4
m_h	118.8
$\Omega_{\widetilde{Z}_1} h^2$	0.0423
$BF(b \to s\gamma)$	3.84×10^{-4}
Δa_μ	2.3×10^{-10}

We begin by generating $e^+e^- \to$ all SUSY particles for the signal, and generate SM backgrounds using all ISAJET SM processes. We first require all events to pass the standard chargino pair cuts for $1\ell + 2j + \not{E}_T$ events as detailed at the beginning of Sec. 2. Next,
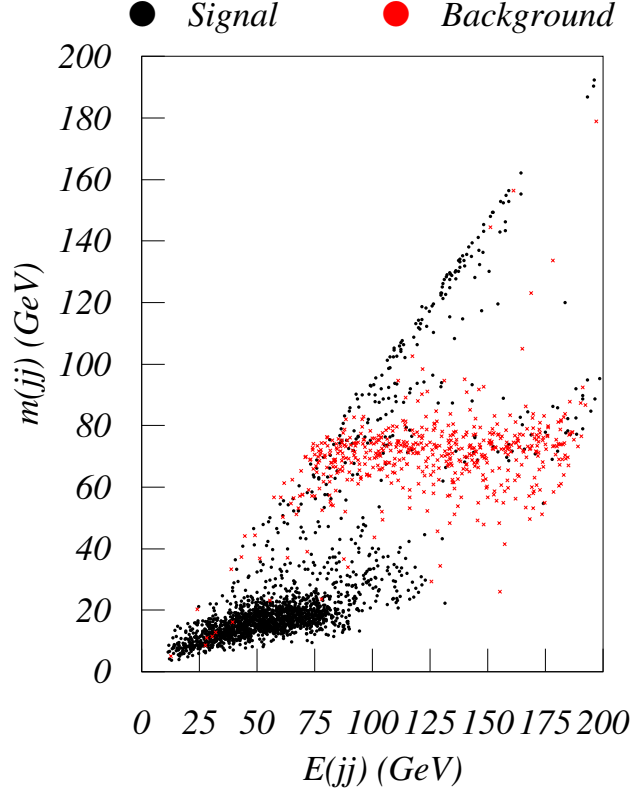
Figure 4.12. Scatter plot of SUSY signal events (black dots) and SM background (red x's) after standard cuts plus $\not{m} > 240$ GeV cuts, in the E_{jj} *vs.* $m(jj)$ plane. Chargino pair events occupy the low $m(jj)$ region.

following case study 4 of Ref. [112], we require missing mass $\not{m} > 240$ GeV. The resulting signal and also background events are plotted in Fig. 4.12 in the $E(jj)$ *vs.* $m(jj)$ plane. SUSY and Higgs boson events are denoted by black dots, while SM background events are denoted by red crosses. The chargino pair events populate the cluster at low $m(jj)$, since the dijet mass from chargino decay is bounded by the $\widetilde{W}_1 - \widetilde{Z}_1$ mass difference. If the chargino decays via $\widetilde{W}_1 \to W\widetilde{Z}_1 \to q\bar{q}'\widetilde{Z}_1$, we would expect that the $E(jj)$ distribution would have well-defined upper and lower endpoints that depend only on $m_{\widetilde{W}_1}$ and $m_{\widetilde{Z}_1}$ (and, of course M_W), as in case study 1 of Ref. [114].

In the HB/FP region, the $\widetilde{W}_1 - \widetilde{Z}_1$ mass gap is small, and the decay to on-shell W is kinematically inaccessible. We can, however, adapt this strategy by forcing "two-body kinematics" on these events by first selecting events in narrow bins in $m(jj)$ and studying separately their $E(jj)$ distributions. This is done in Fig. 4.13, where we show the $E(jj)$ distribution for $m(jj)$ bins of width 4 GeV, centered at 8, 12, 16 and 20 GeV, corresponding to an integrated luminosity of 100 fb^{-1}. This is the "data". The energy of the dijet cluster is bounded by

$$\gamma(E^*_{jj} - \beta p^*_{jj}) \leq E(jj) \leq \gamma(E^*_{jj} + \beta p^*_{jj}), \tag{4.6}$$

where $E^*_{jj} = (m^2_{\widetilde{W}_1} + m^2(jj) - m^2_{\widetilde{Z}_1})/2m_{\widetilde{W}_1}$, $p^*_{jj} = \sqrt{E^{*2}_{jj} - m^2(jj)}$, $\gamma = E_{\widetilde{W}_1}/m_{\widetilde{W}_1}$, $\beta = p^*_{jj}/E^*_{jj}$ and $E_{\widetilde{W}_1} = \sqrt{s}/2$, up to energy mismeasurement errors, jet clustering, particle losses, bremsstrahlung and finite width bins in $m(jj)$.

The corresponding "theoretical predictions" shown by the smooth curve are obtained by generating a much larger sample of the same events and fitting this larger sample (corresponding to an integrated luminosity of 600 fb^{-1}) to the function,

$$F(E, m_{\widetilde{W}_1}, m_{\widetilde{Z}_1}; A, B, C, D) = N \left\{ 1 + \exp\left[\frac{E_{min} + A - E}{B\sigma_{E_{min}}} \right] \right\}^{-1} \left\{ 1 + \exp\left[\frac{-E_{max} + C + E}{D\sigma_{E_{max}}} \right] \right\}^{-1}, \tag{4.7}$$

where E_{min} and E_{max} are calculated for each bin in $m(jj)$ taking the central $m(jj)$ value in that bin, and input values for $m_{\widetilde{W}_1}$ and $m_{\widetilde{Z}_1}$; $\sigma_{E_{min}}$ ($\sigma_{E_{max}}$) is the absolute value of the difference between E_{min} (E_{max}) at the highest $m(jj)$ value in each $m(jj)$ bin and E_{min} (E_{max}) for $m(jj)$ at the center of this bin. The small contribution from the SM background has also been included.

The parameters A, B, C and D are separately determined for each bin in $m(jj)$ and serve to fit the shapes of the corresponding distributions, while N is adjusted to give the normalization near the maximum of E_{jj} distribution corresponding to an integrated luminosity of 100 fb^{-1}.

Next, we proceed to perform a χ^2 fit to obtain $m_{\widetilde{W}_1}$ and $m_{\widetilde{Z}_1}$ from our synthetic data sample, using the fitted function (4.7) for the theoretical prediction [4] for chargino and

---

[4]Of course, the parameters E_{min}, $\sigma_{E_{min}}$, E_{max} and $\sigma_{E_{max}}$ depend on $m_{\widetilde{W}_1}$ and $m_{\widetilde{Z}_1}$ via (4.6) and the equations following that. We assume that the parameters A, B, C and D do not change.
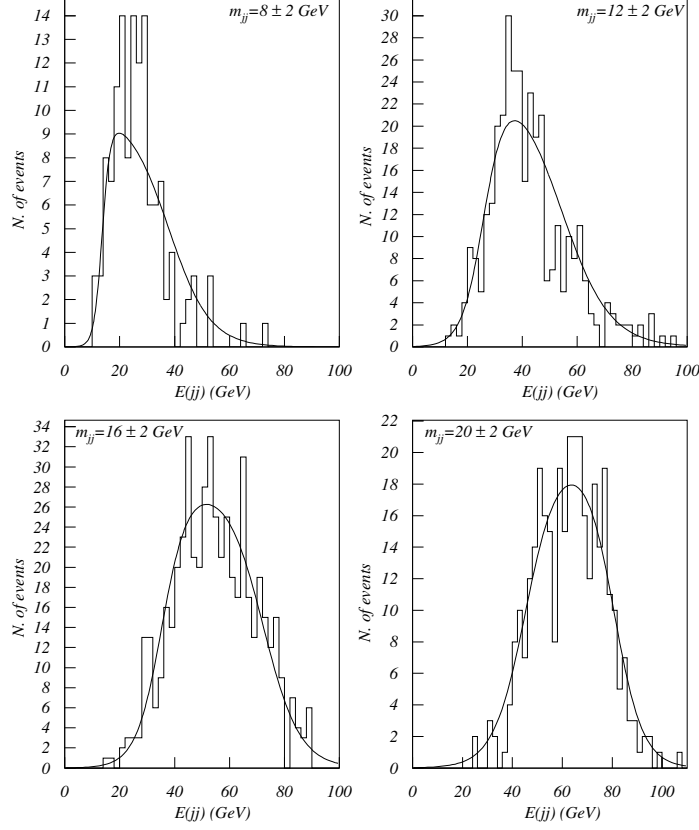
Figure 4.13. Distribution of E_{jj} for $\ell + 2 - jet$ events after standard cuts together with $\not{h} > 240$ GeV, with events restricted to narrow bins of $m(jj)$. The histograms show these distributions for the synthetic data sample while the solid line shows the corresponding theoretical expectation obtained as described in the text.

neutralino masses close to those for Case 2. In other words, for a grid of points in the $(m_{\widetilde{W}_1}, m_{\widetilde{Z}_1})$ plane, we evaluate,

$$\chi^2(m_{\widetilde{W}_1}, m_{\widetilde{Z}_1}) = \sum_{bins} \sum_E \left(\frac{F(E, m_{\widetilde{W}_1}(inp), m_{\widetilde{Z}_1}(inp)) - F(E, m_{\widetilde{W}_1}, m_{\widetilde{Z}_1})}{\sqrt{F(E, m_{\widetilde{W}_1}, m_{\widetilde{Z}_1})}} \right)^2 \qquad (4.8)$$

where $\sum_{bins}$ means that we sum over all four bins in $m(jj)$, and $\sum_E$ denotes the summation over all bins in E_{jj} and find the values of chargino and neutralino masses for which this quantity is minimized. These best fit values, together with the regions where
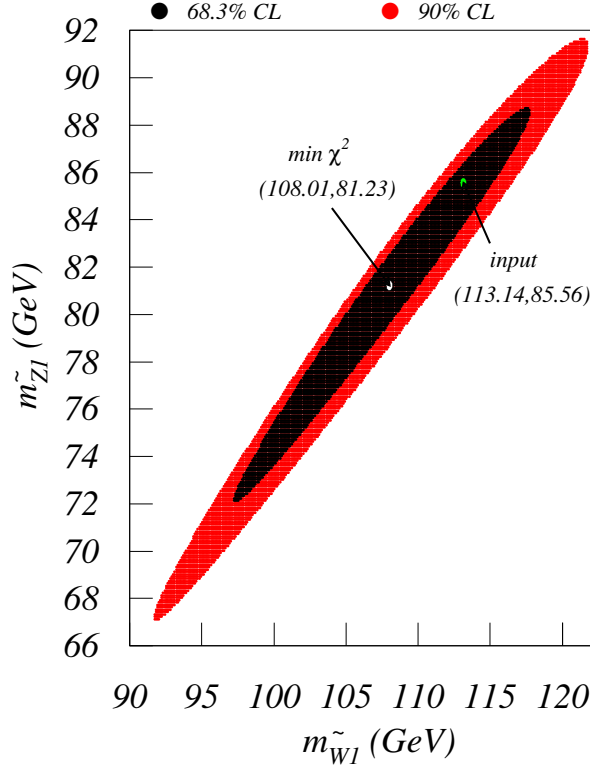
Figure 4.14. Fits to $m_{\widetilde{W}_1}$ and $m_{\widetilde{Z}_1}$ and the associated error ellipses for Case 2 in the text.

$\Delta\chi^2 \leq 2.3$ (68.3% CL) and ≤ 4.6 (90% CL) are shown in Fig. 4.14. We see that it is possible to determine $m_{\widetilde{W}_1}$ and $m_{\widetilde{Z}_1}$ at approximately the 10% level.

Having determined the values of $m_{\widetilde{W}_1}$ and $m_{\widetilde{Z}_1}$, the next step is to examine what we can say about the underlying MSSM parameters μ, M_2 and $\tan\beta$ that enter the chargino mass matrix. To determine three unknowns, we need to experimentally determine one more quantity which we take to be the cross section for $1\ell + 2j + \not{E}_T$ events from chargino pair production. Almost all the signal arises from chargino pair production if we require $m(jj) < 25$ GeV and $E(jj) < 100$ GeV as in Fig. 4.12. For 100 fb^{-1} of integrated luminosity, we find 1649 events, which translates to a measurement of $\sigma(e^+e^- \to \widetilde{W}_1^+\widetilde{W}_1^-) = 16.5 \pm 0.4$ fb

(after all the cuts), or 2.5% statistical error. Other systematic errors will be present, although these may be controllable by precision measurement of many SM processes. We perform a fit to the MSSM parameters using the values of $m_{\widetilde{W}_1}$, $m_{\widetilde{Z}_1}$ and $\sigma(\widetilde{W}_1^+\widetilde{W}_1^-)$ as determined above. We scan over MSSM model parameters, using 1-loop corrected mass relations for $m_{\widetilde{W}_1}$ and $m_{\widetilde{Z}_1}$ as given by ISAJET 7.69. In Fig. 4.15, we show the regions of a) the μ $vs.$ M_2 plane, b) the μ $vs.$ $\tan\beta$ plane and c) the M_2 $vs.$ $\tan\beta$ plane that are allowed at the 68.3% and 90% CL. In each case, we have held the parameter not shown in the plane fixed at its input value. The result in frame a) clearly shows that indeed $|\mu| << M_2$, providing strong support that the model parameters lie in the HB/FP region, and that the LSP has a significant higgsino component, enhancing the neutralino pair annihilation in the early universe.[5] While μ and M_2 can be well determined (at least for this case study), it is also evident from the figure that a precise determination of $\tan\beta$ is not possible in this case. This may not be so surprising, since in the HB/FP region, SUSY scalar masses that depend on Yukawa couplings and hence $\tan\beta$ are so heavy that they essentially decouple from observable physics, and the region is relatively invariant under changes in $\tan\beta$.

4.5   Summary

The recent constraint on the relic density of neutralinos obtained from WMAP measurements, together with earlier determinations of $BF(b \to s\gamma)$ and $(g-2)_\mu$ select out regions of parameter space of the mSUGRA model. In the stau co-annihilation region, the H, A-annihilation funnel and in the HB/FP regions, very high values of m_0 and $m_{1/2}$ consistent with all constraints are possible: moreover, the so-called bulk region where sparticles are light is disfavored. These considerations motivated us to re-assess the reach of various collider and non-accelerator search experiments for supersymmetry. In this chapter, we re-evaluate the reach of a $\sqrt{s} = 0.5$ and 1 TeV linear e^+e^- collider for SUSY in the context of the mSUGRA model, examining for the first time the reach in the HB/FP region. We find that a $\sqrt{s} = 1$ TeV LC can explore most of the stau co-annihilation region if $\tan\beta \stackrel{<}{\sim} 30$, although along with a dilepton search, a ditau search will also be needed. The H, A-annihilation funnel typically extends beyond the maximum reach of a LC. In the

---

[5]That $|\mu|$ is small can presumably also be determined by studying chargino production using polarized beams. Note that our determination does not require this capability.
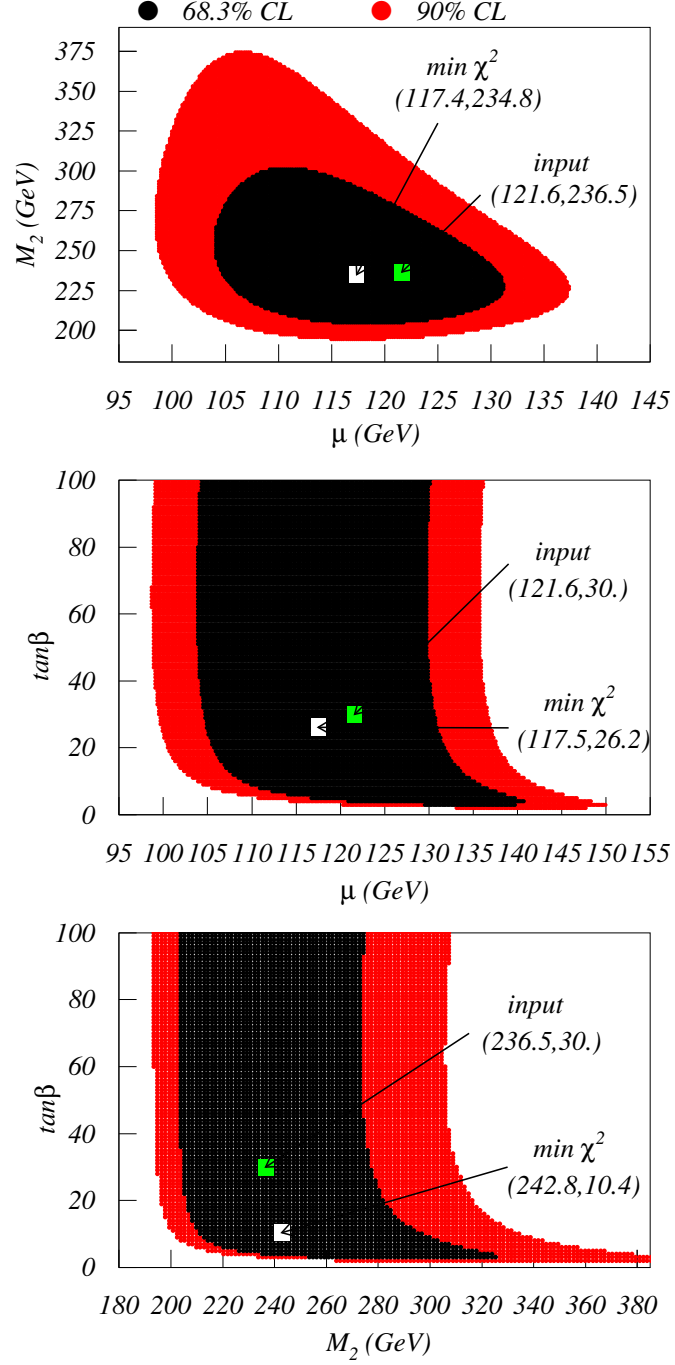
Figure 4.15. Fits to μ, M_2 and $\tan\beta$ from the measured values of $m_{\widetilde{W}_1}$, $m_{\widetilde{Z}_1}$ and $\sigma(\widetilde{W}_1^+\widetilde{W}_1^-)$, and the associated 68.3% and 90% CL regions for Case 2. The green squares denote the fitted values while the white squares show the corresponding input values of the parameters.

HB/FP region, chargino pairs may be kinematically accessible to a LC, but the energy release in chargino pairs can be small, reducing detection efficiency. Nonetheless, LCs should be able to probe much of the lower HB/FP region with standard chargino searches. In the upper HB/FP region, new cuts are proposed to allow signals from much of the small $\widetilde{W}_1 - \widetilde{Z}_1$ mass gap region to be observable above SM backgrounds. In this region, the reach of even a 500 GeV LC can exceed that of the CERN LHC! This is all the more important in that it occurs in a region of model parameter space which is allowed by all constraints, including those imposed by WMAP.

One should also stress that the LC's reach is also complementary to reach of direct dark matter search experiments (DDMS) even though both kinds of experiments similarly cover much of the HB/FP region [111]. The complementarity of a LC occurs for the region which is very close to the no REWSB border. In this region, the neutralino relic density is so low that DDMS experiments are not able to cover this part of the parameter space even though the higgsino component of neutralino is significant. This region can be probed by experiments at a LC.

If a supersymmetric signal is found, then the next obvious step will be to determine the underlying MSSM parameters. We have performed a case study in the low $m_{1/2}$ part of the hyperbolic branch. In this region, we show that a measurement of $m_{\widetilde{W}_1}$ and $m_{\widetilde{Z}_1}$ is possible at the 10% level. A measurement of the total chargino pair cross section to 2.5% allows a determination of MSSM parameters M_2 and μ, although $\tan\beta$ is more difficult to pin down. The resulting determination of M_2 and μ would point to a model with higgsino-like charginos and neutralinos. Together with absence (or low levels) of squark signals at the LHC, and the agreement of the chargino cross section with the expected s-channel contribution (pointing to heavy sneutrinos) these measurements would be indicative of an mSUGRA-type model in the HB/FP region. In case parameters are in the upper part of the hyperbolic branch, LC event characteristics may be sufficient at least to establish the production of massive particles, with associated decay products that are quite soft. An examination of how one would obtain information about the underlying scenario would be worthy of exploration.

CHAPTER 5

THE REACH OF THE FERMILAB TEVATRON
AND CERN LHC FOR
GAUGINO MEDIATED SUSY BREAKING
MODELS

5.1 Introduction

Supersymmetric models with weak scale supersymmetric matter are very compelling for a variety of reasons, most important of which is that they solve the gauge hierarchy problem[126]. However, it is safe to say that a compelling model for supersymmetry breaking has yet to emerge. Supergravity models based on SUSY breaking in a hidden sector[127] can give rise to weak scale soft SUSY breaking (SSB) terms with SUSY breaking communicated via gravitational interactions. However, there exists no compelling mechanism in supergravity to suppress the generation of non-universal SSB parameters that lead to unacceptably large flavor violation, sometimes in CP-violating processes. Alternatively, in models with gauge mediated SUSY breaking[10], universality of scalars with the same quantum numbers occurs naturally, but at the expense of the introduction of a messenger sector which acts to communicate SUSY breaking to the visible sector. Another intriguing alternative is anomaly-mediated SUSY breaking, an extra dimensional model wherein SUSY breaking on one brane is communicated to the visible sector brane via the superconformal anomaly[9]. The form of the scalar masses again allows a solution to the SUSY flavor (and CP) problems. Alas, the minimal version of this model leads to tachyonic slepton masses, although the tachyons can be exorcized in a variety of proposals[128].

An interesting alternative, also based on extra dimensions, is known as gaugino-mediated SUSY breaking (inoMSB)[11]. Like AMSB models, one postulates the existence of both

hidden and visible sector branes, spatially separated in an extra dimensional world. However, gauge superfields (and perhaps also Higgs superfields) are allowed to propagate in the bulk. Upon compactification of the extra dimensions, a tree level SSB gaugino mass is generated, but all scalar masses[1] and A (and perhaps B) terms are only generated at the loop level, and so are suppressed, and can be justifiably set to zero at the compactification scale. The gravitino can be made heavier than the gauginos; it then decouples and plays no role in our considerations.

Compactification is assumed to occur at or beyond the GUT scale, thus preserving the successful unification of gauge coupling constants[129]. Thus, at the compactification scale, we expect

$$m_{1/2} \neq 0; \quad m_0 \sim A_0 \simeq 0, \tag{5.1}$$

which are the same boundary conditions that arise in no-scale models[130]. If M_c is taken equal to the GUT scale, then evolution of soft SUSY breaking parameters leads in general to the tau slepton being the lightest SUSY particle (LSP), a result in conflict with cosmological considerations, since then the present day universe would be filled with charged relics, for which there exist stringent limits. A way out, proposed by Schmaltz and Skiba[129], is that $M_c > M_{GUT}$, and that above M_{GUT} some four-dimensional GUT gauge symmetry is valid, such as $SU(5)$ or $SO(10)$. In this case, the additional beyond-the-GUT-scale RGE running leads to large enough slepton masses at M_{GUT} that regions of parameter space exist [129, 131] with a neutralino LSP, in accord with cosmological constraints.

In the minimal gaugino mediation model, the bilinear SSB term $B \sim 0$. By minimizing the scalar potential of the MSSM at the weak scale, the weak scale value of B is related to the parameter $\tan\beta$. Thus, in minimal gaugino mediation, the value of $\tan\beta$ is predicted, and found for instance in Ref. [129] to be $\tan\beta \sim 9 - 22$. On a different track, the assumption of a GUT theory above M_{GUT} frequently implies relations amongst the Yukawa couplings of the theory, especially for the third generation. Thus, in minimal $SU(5)$ we expect $f_b = f_\tau$ for scales $Q > M_{GUT}$ and in minimal $SO(10)$ we expect $f_b = f_t = f_\tau$, where the f_i are Yukawa couplings. We adopt the computer program ISAJET v7.58 [45] for calculating RG evolution. Starting with $\overline{DR}$ fermion masses and gauge couplings at the weak scale, ISAJET calculates an iterative solution to the relevant set of RGEs of the MSSM by running between

---

[1]We assume that there are no Higgs fields in the bulk.

the weak and GUT scales. To test Yukawa coupling evolution, it is imperative to include SUSY loop corrections to fermion masses at the weak scale[132, 46]. It has been found that a high degree of $f_b - f_\tau$ Yukawa coupling unification at $Q = M_{GUT} \sim 2 \times 10^{16}$ can occur only for values of $\tan\beta \sim 30 - 50$, and $\mu < 0$. Similarly, a high degree of $f_b - f_\tau - f_t$ Yukawa unification only occurs for $\tan\beta \sim 50$ and $\mu < 0$[46, 133, 134, 135]. We adopt the criteria of Yukawa coupling unification as being more fundamental than the generation of tiny GUT scale values of B, so that $\tan\beta$ (and the sign of μ) are free parameters, although they are highly constrained by the requirement of $b - \tau$ unification.

In this chapter, we adopt as an example choice a model of gaugino mediation which reduces to a SUSY $SU(5)$ GUT at the compactification scale. Our goal is to calculate the spectrum of superpartners at the weak scale, so that collider scattering events may be generated. We then evaluate the reach of both the Tevatron $p\bar{p}$ and CERN LHC pp colliders for inoMSB models. In Sec. 5.2 we discuss our results for the spectrum of SUSY particles expected in inoMSB including $SU(5)$ gauge symmetry below M_c. In Sec. 5.3, we present our results for the reach of the Fermilab Tevatron for inoMSB models. In Sec. 5.4 we present similar results for the CERN LHC. Finally, we present our conclusions in Sec. 5.5.

5.2   Sparticle mass spectrum

If the scale at which SSB terms are generated is substantially higher than M_{GUT} (but smaller than M_P) then renormalization group (RG) evolution induces a non-universality at the GUT scale. The effect can be significant if large representations are present. Here, we assume that supersymmetric $SU(5)$ grand unification is valid at mass scales $Q > M_{GUT} \simeq 2 \times 10^{16}$ GeV, extending at most to the reduced Planck scale $M_P \simeq 2.4 \times 10^{18}$ GeV. Below $Q = M_{GUT}$, the $SU(5)$ model breaks down to the MSSM with the usual $SU(3)_C \times SU(2)_L \times U(1)_Y$ gauge symmetry. This model is well described in the work of Polonsky and Pomarol[136].

In the $SU(5)$ model, the $\hat{D}^c$ and $\hat{L}$ superfields are elements of a $\bar{\mathbf{5}}$ superfield $\hat{\phi}$, while the $\hat{Q}$, $\hat{U}^c$ and $\hat{E}^c$ superfields occur in the $\mathbf{10}$ representation $\hat{\psi}$. The Higgs sector is comprised of three super-multiplets: $\hat{\Sigma}(\mathbf{24})$ which is responsible for breaking $SU(5)$, plus $\hat{\mathcal{H}}_1(\bar{\mathbf{5}})$ and $\hat{\mathcal{H}}_2(\mathbf{5})$ which contain the usual Higgs doublet superfields $\hat{H}_d$ and $\hat{H}_u$ respectively, which occur

in the MSSM. The superpotential is given by

$$\hat{f} = \mu_\Sigma tr\hat{\Sigma}^2 \ + \ \frac{1}{6}\lambda' tr\hat{\Sigma}^3 + \mu_H\hat{\mathcal{H}}_1\hat{\mathcal{H}}_2 + \lambda\hat{\mathcal{H}}_1\hat{\Sigma}\hat{\mathcal{H}}_2$$
$$+ \ \frac{1}{4}f_t\epsilon_{ijklm}\hat{\psi}^{ij}\hat{\psi}^{kl}\hat{\mathcal{H}}_2^m + \sqrt{2}f_b\hat{\psi}^{ij}\hat{\phi}_i\hat{\mathcal{H}}_{1j}, \tag{5.2}$$

where a sum over families is understood. f_t and f_b are the top and bottom quark Yukawa couplings, λ and λ' are GUT Higgs sector self couplings, and μ_Σ and μ_H are superpotential Higgs mass terms.

Supersymmetry breaking is parametrized by the SSB terms:

$$\mathcal{L}_{soft} \ = \ -m_{\mathcal{H}_1}^2|\mathcal{H}_1|^2 - m_{\mathcal{H}_2}^2|\mathcal{H}_2|^2 - m_\Sigma^2 tr\{\Sigma^\dagger\Sigma\} - m_5^2|\phi|^2 - m_{10}^2 tr\{\psi^\dagger\psi\} - \frac{1}{2}M_5\bar{\lambda}_\alpha\lambda_\alpha$$
$$+ \ \left[B_\Sigma\mu_\Sigma tr\Sigma^2 + \frac{1}{6}A_{\lambda'}\lambda' tr\Sigma^3 + B_H\mu_H\mathcal{H}_1\mathcal{H}_2 + A_\lambda\lambda\mathcal{H}_1\Sigma\mathcal{H}_2 \right.$$
$$+ \ \left. \frac{1}{4}A_t f_t\epsilon_{ijklm}\psi^{ij}\psi^{kl}\mathcal{H}_2^m + \sqrt{2}A_b f_b\psi^{ij}\phi_i\mathcal{H}_{1j} + h.c. \right], \tag{5.3}$$

where the fields without the carets denote the appropriate scalar components. The various soft masses and gauge and Yukawa couplings evolve with energy according to the 15 renormalization group equations given in Ref. [136, 131].

To generate the weak scale MSSM mass spectrum, one begins with the input parameters

$$\alpha_{GUT}, \ f_t, \ f_b, \ \lambda, \ \lambda' \tag{5.4}$$

stipulated at $Q = M_{GUT}$, where $f_b = f_\tau$ is obtained from the corresponding mSUGRA model. The first three of these can be extracted, for instance, from ISASUGRA by finding points in mSUGRA parameter space with $f_b = f_\tau$. The couplings $\lambda(M_{GUT})$ and $\lambda'(M_{GUT})$ are additional inputs, where $\lambda(M_{GUT}) \gtrsim 0.7$ [137] to make the triplet Higgsinos heavy enough to satisfy experimental bounds on the proton lifetime. The gauge and Yukawa couplings can be evolved via the RGEs to determine their values at $Q = M_c$. Assuming universality at M_c, we impose

$$m_{10} \ = \ m_5 = m_{\mathcal{H}_1} = m_{\mathcal{H}_2} = m_\Sigma \equiv m_0 = 0$$
$$A_t \ = \ A_b = A_\lambda = A'_\lambda \equiv A_0 = 0, \tag{5.5}$$
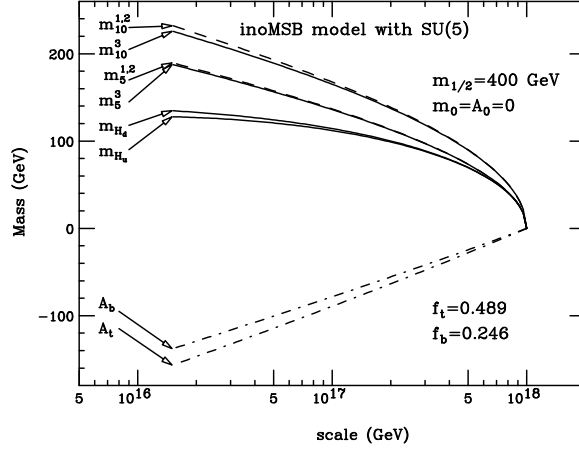
Figure 5.1. Evolution of SSB masses in the $SU(5)$ model from M_c to M_{GUT}, for $\tan\beta = 35$, $\mu < 0$, $\lambda = 1.0$ and $\lambda' = 0.1$, for $m_{1/2} = 400$ GeV.

as boundary conditions that define our $SU(5)$ inoMSB framework. We then evolve all the $SU(5)$ soft masses from M_c to M_{GUT}. The MSSM soft breaking masses at M_{GUT} are specified via

$$m_Q^2 = m_U^2 = m_E^2 \equiv m_{10}^2\,,$$
$$m_D^2 = m_L^2 \equiv m_5^2\,, \tag{5.6}$$
$$m_{H_d}^2 = m_{\mathcal{H}_1}^2\,, \quad m_{H_u}^2 = m_{\mathcal{H}_2}^2\,,$$

which can serve as input to ISAJET [45] via the $NUSUGi$ keywords. Yukawa couplings induce an inter-generation splitting amongst the scalars. Since there is no splitting amongst the gaugino masses, the gaugino masses may be taken to be $M_1 = M_2 = M_3 \equiv m_{1/2}$ where $m_{1/2}$ is stipulated most conveniently at the GUT scale.

In Fig. 5.1, we show the evolution of the various SSB parameters of the MSSM, starting with the inoMSB boundary conditions. Here, the unified gaugino mass is taken to be 400 GeV at $Q = M_{GUT}$. The compactification scale is taken to be $M_c = 10^{18}$ GeV, with $\tan\beta = 35$, $\mu < 0$, $\lambda = 1.0$ and $\lambda' = 0.1$[2]. We see that RG evolution results in GUT scale scalar masses and A-parameters that are substantial fractions of $m_{1/2}$; *i.e.* although we have

---

[2]Varying the parameters λ and λ' typically induces small changes only in *third* generation scalar masses, so that other sparticle masses should not be very sensitive to variations in these parameters.
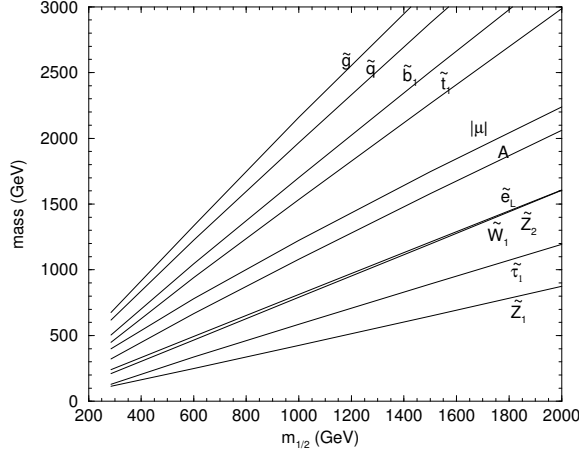
Figure 5.2. Mass values of various SUSY particles and μ parameter in the $SU(5)$ inoMSB model with $\tan\beta = 35$ and $\mu < 0$ versus the GUT scale common gaugino mass $m_{1/2}$. The lighter chargino and $\widetilde{Z}_2$ are essentially degenerate, and $\tilde{e}_L$ is slightly heavier.

inoMSB boundary conditions at the scale M_c, there are substantial deviations from these at M_{GUT}. While the inter-generation splitting is small, the splittings between the **5** and the **10** dimensional matter multiplets, as well as between these and the Higgs multiplets is substantial.

In Fig. 5.2, we show values of various sparticle and Higgs masses, plus the μ parameter, as a function of $m_{1/2}$ for $\tan\beta = 35$ and $\mu < 0$. In this plot, we adopt the values of $f_t = 0.489$, $f_b = f_\tau = 0.246$, $g = 0.703$ at the scale $M_{GUT} = 1.52 \times 10^{16}$ GeV. The output values of m_{10} and m_5 for first and third generations, and m_{H_u} and m_{H_d} serve as GUT scale inputs for ISAJET to generate the weak scale sparticle masses shown in the figure. We cut off the curves at $m_{1/2} = 285$ GeV below which $m_{\tilde{\tau}_1}$ becomes less than $m_{\widetilde{Z}_1}$. Note that the lower limit on $m_{1/2}$ implies that $m_{\widetilde{W}_1} \gtrsim 200$ GeV. The following pattern of sparticle masses occurs:

$$m_{\widetilde{Z}_1} < m_{\tilde{\ell}_R} < m_{\widetilde{W}_1} < m_{\tilde{\ell}_L} < m_A < m_{\tilde{t}_1} < m_{\tilde{b}_1} < m_{\tilde{q}} < m_{\tilde{g}}. \tag{5.7}$$

The large value of $|\mu|$ that occurs means that the $\widetilde{Z}_1$ is mainly bino-like, and a good candidate for cold dark matter[129].

Specific sparticle masses for an $m_{1/2} = 400$ GeV case study are shown in Table 5.1, along with an mSUGRA model with a universal GUT scale mass squared that is a weighted

88

Table 5.1. GUT scale SSB parameters and weak scale sparticle masses and parameters (GeV) for mSUGRA and inoMSB case studies with $m_{1/2} = 400$ GeV, $\tan\beta = 35$ and $\mu < 0$.

parameter	mSUGRA	inoMSB
$m_{10}(1)$	205.2	233.3
$m_{10}(3)$	205.2	226.8
$m_5(1)$	205.2	190.5
$m_5(3)$	205.2	188.5
m_{H_d}	205.2	134.9
m_{H_u}	205.2	128.0
A_t	-148.4	-157.9
A_b	-148.4	-139.0
$f_t(M_{GUT})$	0.497	0.489
$f_b(M_{GUT})$	0.287	0.246
$m_{\tilde{g}}$	916.6	919.5
$m_{\tilde{u}_L}$	836.5	843.8
$m_{\tilde{d}_R}$	805.5	801.8
$m_{\tilde{t}_1}$	622.0	629.4
$m_{\tilde{b}_1}$	691.2	689.6
$m_{\tilde{\ell}_L}$	340.6	331.8
$m_{\tilde{\ell}_R}$	256.3	279.8
$m_{\tilde{\nu}_e}$	331.1	322.1
$m_{\tilde{\tau}_1}$	193.0	210.5
$m_{\widetilde{W}_1}$	303.5	304.9
$m_{\widetilde{Z}_2}$	303.3	304.8
$m_{\widetilde{Z}_1}$	162.4	162.5
m_h	117.7	117.7
m_A	376.1	379.8
m_{H^+}	386.8	390.3
μ	-515.1	-539.3

average of the corresponding inoMSB values. Many aspects of the spectra shown are similar. However, it is noteworthy that the splitting of the **10** and **5** dimensional representations in inoMSB lead to increased right slepton and decreased left-slepton masses relative to the mSUGRA case. Such a splitting may be measureable at linear e^+e^- colliders; we discuss this further in Sec. 5.5.

5.3　Reach of the Tevatron collider

From the spectra shown in Fig. 5.2, we see that first and second generation squarks and gluinos have masses of at least 600 GeV, and hence are inaccessible [138] to Tevatron searches due to low production cross sections. Sleptons [61] and third generation squarks [139] are also too heavy to be searched for at the Tevatron. However, charginos and neutralinos may be light enough that $\widetilde{W}_1\widetilde{W}_1$ and $\widetilde{W}_1\widetilde{Z}_2$ production serve as the main SUSY production mechanisms at the Tevatron.

Since $m_{\widetilde{W}_1} > m_{\tilde{\tau}_1}$, while $m_{\widetilde{W}_1} < m_{\tilde{\ell}_L}$, the chargino dominantly decays via $\widetilde{W}_1 \to \tilde{\tau}_1\nu_\tau$. The neutralino $\widetilde{Z}_2$ is mainly wino-like, and so has only a small coupling to $\tilde{\ell}_R$. Thus, even though the decay mode $\widetilde{Z}_2 \to \tilde{\ell}_R\ell$ is open, the decay mode $\widetilde{Z}_2 \to \tilde{\tau}_1\tau$ is dominant. Thus, we expect signals rich in tau leptons.

The two most promising avenues to explore for Tevatron reach consist of a clean trilepton search[140], where the focus is on soft trileptons originating from tau decays, or for trilepton events where in fact one or more of the identified leptons is a hadronic tau[27].

To estimate the Tevatron reach for inoMSB models with soft trileptons, we adopt the cuts SC2 advocated in the last of Refs. [55, 56, 54]. These cuts have been optimized to maintain signal while rejecting backgrounds coming from WZ production, $t\bar{t}$ production and $W^*\gamma^*$ and W^*Z^* production, where the starred entries correspond to off-shell processes. The cuts include requiring three isolated[3] leptons (either es or μs) with $p_T(\ell_1, \ell_2, \ell_3) > 11$, 7, 5 GeV respectively, and with $|\eta(\ell)| < 2$, but including at least one lepton with $p_T > 11$ GeV within $|\eta| < 1$. In addition, a missing energy cut $\not{E}_T > 25$ GeV is required. Furthermore, a Z veto $m(\ell\bar{\ell}) < 81$ GeV and a virtual photon veto $m(\ell\bar{\ell}) > 20$ GeV is required for opposite sign/same flavor dilepton pairs. A transverse mass veto 60 GeV $< M_T(\ell, \not{E}_T) < 85$ GeV is also required to reject on and off shell backgrounds including W bosons. The background estimate is then 1.05 fb.

In Fig. 5.3, we show the isolated trilepton cross section after cuts SC2, along with the signal levels needed to achieve a 5σ signal at 2 fb^{-1} of integrated luminosity, and a 5σ or 3σ signal at 25 fb^{-1}. We see that the trilepton signal level corresponds to $\overset{<}{\sim}$ 1 trilepton

---

[3]Leptons with $p_T \geq 5$ GeV are defined to be isolated if the hadronic E_T in a $\Delta R =0.4$ cone about the lepton is smaller than 2 GeV.
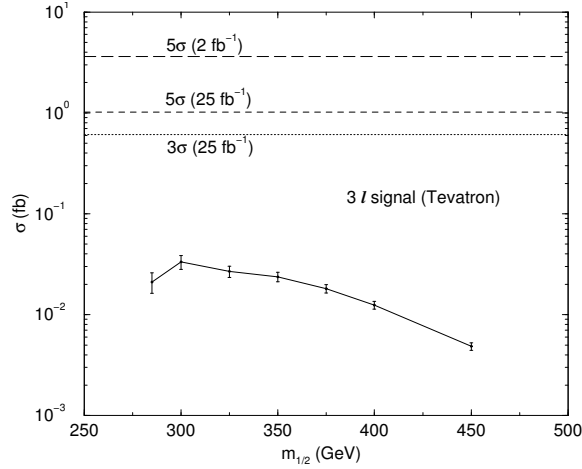
Figure 5.3. Cross section after cuts SC2 of Ref. [54] for trilepton events at the Fermilab Tevatron. The horizontal lines denote the minimum cross section for the signal to be observable.

event even with an integrated luminosity of 25 fb^{-1} and so appears to be undetectable for the entire range of $m_{1/2}$.

The other possible signal channel is to look for trilepton events where one or more of the leptons is, in fact, a tau identified via its hadronic decay. These can be separated into $\ell\bar{\ell}\tau$ (opposite-sign), $\ell\ell\tau$ (same-sign), $\ell\tau\tau$ and $\tau\tau\tau$ channels. Signals including tau leptons were first examined in the context of large $\tan\beta$ in Ref. [27], and refined background estimates were presented in Ref. [141]. We adopt the cuts and backgrounds presented in Ref. [141] for our analysis. Following Ref. [141], we define tau jets to be hadronic jets with $|\eta| < 1.5$, net charge ± 1, one or three tracks in a $10°$ cone with no additional tracks in a $30°$ cone, $E_T > 5$ GeV, $p_T > 5$ GeV, plus an electron rejection cut. The cuts that we implement depend on the event topology, and include: two isolated ($E_T(cone) < 2$ GeV) leptons with $p_T > 8$ GeV and $p_T > 5$ GeV, and one identified tau jet with $p_T(\tau) > 15$ GeV for $\ell\bar{\ell}\tau$ and $\ell\ell\tau$ signatures; two tau jets with $p_T > 15$ GeV and $p_T > 10$ GeV and one isolated lepton with $p_T > 7$ GeV for $\ell\tau\tau$ signature; three tau jets with $p_T > 15, 10$ and 8 GeV, respectively for $\tau\tau\tau$ signature. For the $\ell\bar{\ell}\tau$ topology, following Ref. [141], we impose additional cuts for same flavor, opposite sign leptons: $|m(\ell\bar{\ell}) - M_Z| > 10$ GeV and $m(\ell\bar{\ell}) > 11$. To maximize the signal statistics we chose set "A)" from the paper [141]: $\not{E}_T > 20$ GeV and no jet veto requirement.

91
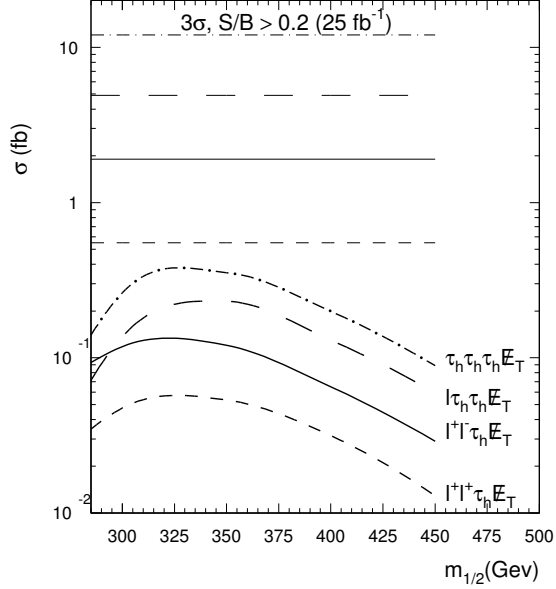
Figure 5.4. Cross section after cuts of Ref. [141] for trilepton events including identified hadronically decaying tau leptons at the Fermilab Tevatron. The horizontal lines denote the minimum cross section for the signal to be observable.

We consider a signal to be observable if *i*) the signal to background ratio, $S/B \geq 0.2$, *ii*) the signal has a minimum of five events, and *iii*) the signal satifies a statistical criterion $S \geq 5\sqrt{B}$.

Our results for signals including tau leptons are shown in Fig. 5.4. We use the background estimates from Ref. [141] to determine the minimum signal level for observability. These background cross sections for $\ell\bar{\ell}\tau$, $\ell\ell\tau$, $\ell\tau\tau$ and $\tau\tau\tau$ topologies are 10.7 fb, 0.85 fb, 60.4 fb and 24.7 fb, respectively. We clearly see that signal is, once again, too low to be detectable at luminosity upgrades of the Tevatron. We conclude that in this framework direct detection of sparticles will not be possible at the Tevatron.

5.4   Reach of the CERN LHC

At the CERN LHC, gluino and squark pair production reactions will be the dominant SUSY production reactions. Gluino and squark production will be followed by cascade decays

[142], in which a variety of jets, isolated leptons and missing energy will be produced. A variety of signals emerge, and can be classified by the number of isolated leptons present. The signal channels include *i.*) no isolated leptons plus jets plus $\not{E}_T$ ($\not{E}_T$), *ii.*) single isolated lepton plus jets plus $\not{E}_T$ (1ℓ), *iii.*) two opposite sign isolated leptons plus jets plus $\not{E}_T$ (OS), *iv.*) two same sign isolated leptons plus jets plus $\not{E}_T$ (SS) and *v.*) three isolated leptons plus jets plus $\not{E}_T$ (3ℓ).

The reach of the CERN LHC for SUSY has been estimated for the mSUGRA model in Ref. [34, 58] at low $\tan\beta$ and in Ref. [143] at large $\tan\beta$. We adopt the cuts and background levels presented in Ref. [34] for our analysis of the signal channels listed above. Hadronic clusters with $E_T > 100$ GeV and $|\eta(\text{jet})| < 3$ within a cone of size $R = \sqrt{\Delta\eta^2 + \Delta\phi^2} = 0.7$ are classified as jets. Muons and electrons are classified as isolated if they have $p_T > 10$ GeV, $|\eta(\ell)| < 2.5$, and the visible activity within a cone of $R = 0.3$ about the lepton direction is less than $E_T(\text{cone}) = 5$ GeV.

Following Ref. [34], we required that the jet multiplicity, $n_{\text{jet}} \geq 2$, transverse sphericity $S_T > 0.2$, $E_T(j_1)$, and further, that $E_T(j_2) > E_T^c$ and $\not{E}_T > E_T^c$, where the cut parameter E_T^c is chosen to roughly optimize the signal from gluino and squark production. For the leptons we require $p_T(\ell) > 20$ GeV ($\ell = e$ or μ) and $M_T(\ell, \not{E}_T) > 100$ GeV for the 1ℓ signal. For the OS, SS and 3ℓ channels, we require that the two hardest leptons have $p_T \geq 20$ GeV. We have also applied the cut on the transverse plane angle $\Delta\phi(\vec{\not{E}}_T, j_c)$ between $\vec{\not{E}}_T$ and closest jet: $30° < \Delta\phi < 90°$, in the case of the $\not{E}_T$ channel, *i*).

Our results for the $\not{E}_T$ signal channel are shown in Fig. 5.5 for choices of the cut parameter $E_T^c = 100$, 300 and, for the $\not{E}_T$ and 1ℓ channels, also 500 GeV. The error bars denote the statistical uncertainty in our Monte Carlo calculation. The solid (dashed) horizontal mark on each curve denotes the minimum cross section needed for discovery, incorporating the three criteria listed in the last section, for an integrated luminosity of 10 (100) fb^{-1}. For those values of E_T^c where the reach is limited by the $S/B \geq 0.2$ requirement, increasing the integrated luminosity does not improve the reach, and we have no dashed horizontal line. Although the signal is largest for the softer cuts, larger E_T^c values (corresponding to harder cuts) are more effective in selecting signal events over background for very heavy squarks and gluinos. This is why the reach is maximized for the largest E_T^c value for which the signal still leaves an observable number of events. Thus, in the $\not{E}_T$ channel, the 5σ reach is found

Figure 5.5. Cross section after cuts of Ref. [34] for $\not{E}_T + jets$ events at the CERN LHC for E_T^c values of 100, 300 and 500 GeV. For each E_T^c value, the reach is given by the horizontal solid (dashed) line for 10 (100) fb^{-1} of integrated luminosity.

to be 925 (1100) GeV in the parameter $m_{1/2}$ for 10 (100) fb^{-1}. This corresponds to a reach in $m_{\tilde{g}}$ of 2000 (2400) GeV, respectively.

The corresponding situation for the 1ℓ channel is shown in Fig. 5.6. Once again, the largest reach is obtained for $E_T^c = 500$ GeV. We see that $m_{1/2} = 1000$ (1160) GeV should be accessible for 10 (100) fb^{-1} of integrated luminosity, corresponding to a reach in $m_{\tilde{g}}$ of 2150 (2500) GeV.

For channels with ≥ 2 leptons, we have conservatively restricted our analyis to E_T^c smaller than 300 GeV, because for larger values of this cut parameter, the estimates of the SM backgrounds may have considerable statistical fluctuations. The results for the opposite sign (OS) dilepton channel is shown in Fig. 5.7, where the reach with $E_T^c = 300$ GeV is found to be $m_{1/2} = 750$ (900) GeV for 10 (100) fb^{-1} of integrated luminosity, corresponding to a reach in $m_{\tilde{g}}$ of $\sim$1650 (1950) GeV. The expectation for the same sign (SS) dilepton channel is shown in Fig. 5.8, where the reach with $E_T^c = 300$ GeV is found to be $m_{1/2} = 800$ (925) GeV for 10 (100) fb^{-1} of integrated luminosity, corresponding to a reach in $m_{\tilde{g}}$ of 1700 (2000) GeV. Finally, for the 3ℓ channel shown in Fig. 5.9, the reach with $E_T^c = 300$ GeV is found to be essentially the same as that for the SS channel.

94

Figure 5.6. Cross section after cuts of Ref. [34] for $1\ell+\not{E}_T + jets$ events at the CERN LHC for E_T^c values of 100, 300 and 500 GeV. For each E_T^c value, the reach is given by the horizontal solid (dashed) line for 10 (100) fb^{-1} of integrated luminosity.
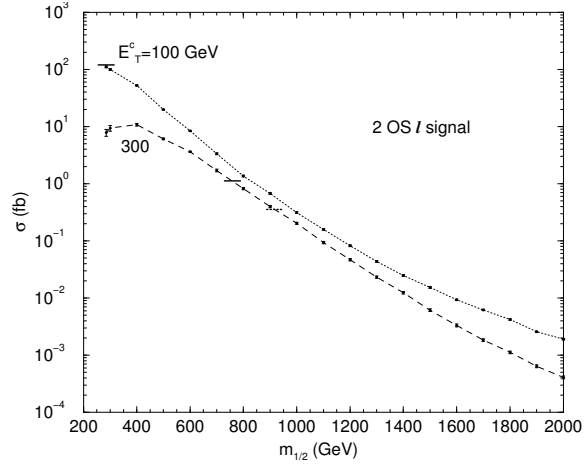
Figure 5.7. Cross section after cuts of Ref. [34] for OS dilepton$+ \not{E}_T + jets$ events at the CERN LHC for E_T^c values of 100 and 300 GeV. For each E_T^c value, the reach is given by the horizontal solid (dashed) line for 10 (100) fb^{-1} of integrated luminosity.

95
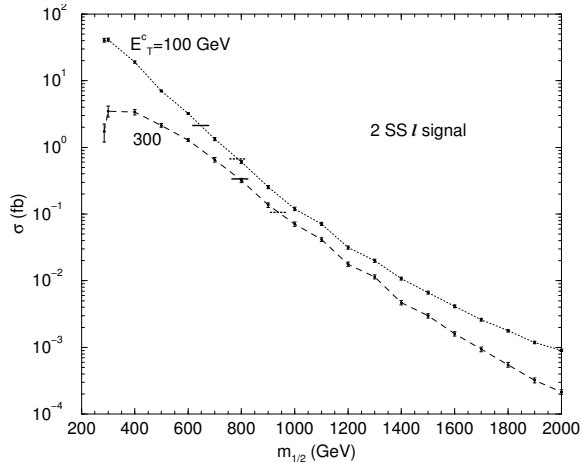
Figure 5.8. Cross section after cuts of Ref. [34] for SS dilepton+ $\not{E}_T + jets$ events at the CERN LHC for E_T^c values of 100 and 300 GeV. For each E_T^c value, the reach is given by the horizontal solid (dashed) line, for 10 (100) fb^{-1} of integrated luminosity.

Thus, for inoMSB, we expect a robust signal for SUSY in a variety of channels, with the 1ℓ channel offering the best ultimate reach for SUSY, corresponding to $m_{\tilde{g}}$ up to 2.1-2.5 TeV, for an integrated luminosity of 10-100 fb^{-1}.

5.5   Summary

In this chapter we have addressed the question of discovery reach for SUSY breaking models with gaugino mediated SUSY breaking. These models give rise to "no-scale" boundary conditions for SSB parameters. The boundary conditions are assumed valid at a scale M_c beyond the GUT scale, but somewhat below the Planck scale. A four dimensional SUSY GUT model is assumed valid at these high scales, and for definiteness, we chose a model based on $SU(5)$ gauge symmetry. Simple models based on $SO(10)$ gauge symmetry are more difficult to accommodate, since they must obey the more stringent condition of $t - b - \tau$ Yukawa coupling. Such Yukawa unified solutions are difficult to reconcile with the constraint of radiative EWSBW and no-scale type boundary conditions.

We found that the Fermilab Tevatron has *no reach* for sparticles in the inoMSB model. This occurs for several reasons. First, gluinos and squarks are beyond the reach of the
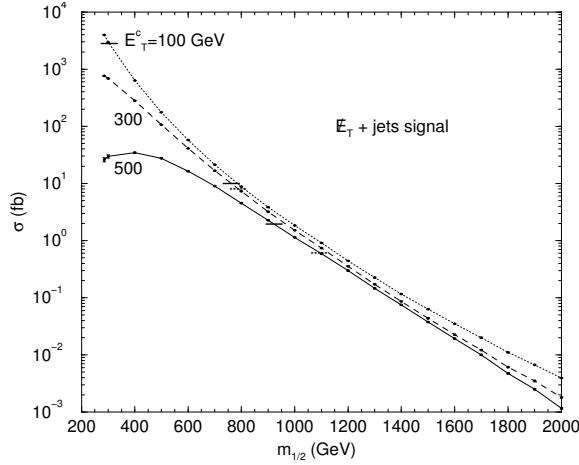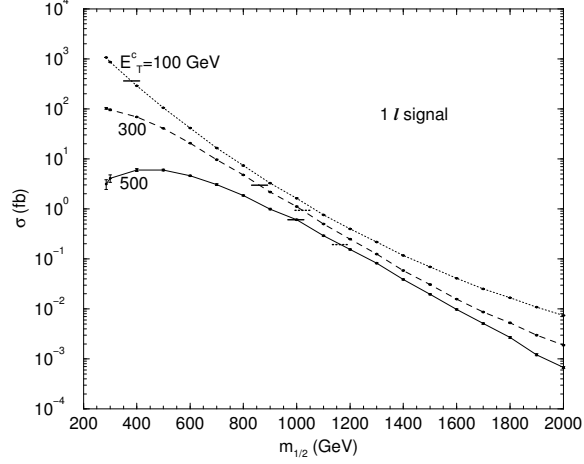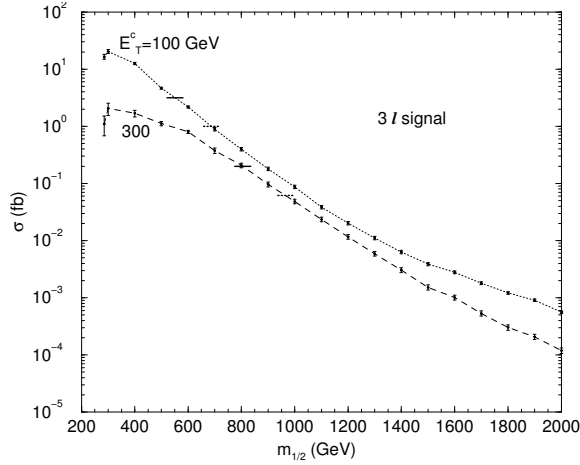
Figure 5.9. Cross section after cuts of Ref. [34] for $3\ell + \not{E}_T + jets$ events at the CERN LHC for E_T^c values of 100 and 300 GeV. For each E_T^c value, the reach is given by the horizontal solid (dashed) line for 10 (100) fb^{-1} of integrated luminosity.

Tevatron. Second, charginos and neutralinos dominantly decay to third generation leptons and sleptons, and taus are more difficult to detect that es and μs. Moreover, the lower limit on parameter space implies $m_{\widetilde{W}_1} \stackrel{>}{\sim} 200$ GeV, so there is not a lot of sparticle production cross section to begin with. Finally, since $m_{\tilde{\tau}_1} \simeq m_{\widetilde{Z}_1}$ at the lower values of allowed $m_{1/2}$, the stau decays give rise to very soft visible decay products, reducing greatly the efficiency to detect signals including hadronic taus.

On the other hand, the CERN LHC has a substantial reach for inoMSB models. In this case, we expect gluino and squark pair production to dominate, so that a variety of cascade decay signals will be present if $m_{1/2}$ is not too large. We find the greatest reach via the $\not{E}_T$ and 1ℓ channels, where there should be observable signals for gluinos as heavy as 2150 (2500) GeV for 10 (100) fb^{-1} of integrated luminosity. If gluinos are lighter than ~ 1700 (2000) GeV, there should be confirmatory signals also in the OS, SS and 3ℓ channels. These reach values are comparable to expectations within the mSUGRA framework, which is not surprising in that the sparticle mass spectra for the two models are not that different. Although we have performed our analysis assuming that there are no Higgs fields in the bulk, we expect that our conclusions about the LHC reach will be qualitatively unchanged even if this is not the case. The reason is that gaugino and scalar masses for the first two

generations are insensitive to our boundary condition $m_{H_u} = m_{H_d} = 0$. We also expect that our estimates of the SUSY reach of the LHC are insensitive to the couplings in the GUT Higgs sector.

The question then arises whether the inoMSB and mSUGRA models can be differentiated by collider experiments. The main spectral difference between the two models arises due to the non-universal GUT scale scalar masses arising in the inoMSB model. Most noticeably, the splitting between the **10** and **5** of $SU(5)$ gives rise to heavier right-sleptons and lighter left-sleptons in the inoMSB model compared to mSUGRA with a similar overall spectrum (see Table 5.1). Differentiation of the two models is a very difficult task to accomplish at the CERN LHC.

However, a method has recently been proposed to differentiate models with GUT scale scalar mass non-universality from the mSUGRA framework at e^+e^- linear colliders[144]. These authors have proposed that the measurable quantity

$$\Delta = m_{\tilde{e}_R}^2 - m_{\tilde{e}_L}^2 + \frac{m_{\widetilde{W}_1}^2}{2\alpha_2^2(m_{\widetilde{W}_1})} \left[\frac{3}{11}(\alpha_1^2(m_{\tilde{e}}) - \alpha_1^2(M_{GUT})) - 3(\alpha_2^2(m_{\tilde{e}}) - \alpha_2^2(M_{GUT})) \right], \quad (5.8)$$

could be used to differentiate the two classes of models. This quantity Δ is expected [4] to be small, within the range $-4000 \text{ GeV}^2 < \Delta < 2000 \text{ GeV}^2$ for mSUGRA, while it is expected to be much larger in the inoMSB framework. For instance, for the case study in Table 5.1, $\Delta \sim 15,000 \text{ GeV}^2$. The difference is sufficiently large so that the two models should be distinguishable via precision measurements at a linear e^+e^- collider where chargino and selectron masses can be determined to about 1-2%.

In conclusion, if nature has chosen to be described by inoMSB model with an $SU(5)$ gauge symmetry above the GUT scale, then we may expect a SUSY Higgs boson discovery at the luminosity upgrade of the Tevatron, but no sign of sparticles. Conversely, we would expect a SUSY discovery at the CERN LHC (unless sparticle masses are so heavy they are in the fine-tuned region of SUSY parameter space, with $m_{\tilde{g}} > 2500$ GeV). However, the underlying model will not be revealed until a sufficient data set has been accumulated at a linear e^+e^- collider, where precision measurements of sparticle masses would point to an inoMSB model with a $SU(5)$ GUT symmetry.

---

[4]Note that the theoretical expectation for Δ is slightly different than shown in Ref. [144] because the quantity S_{GUT} (defined therein) is now just $m_{\mathcal{H}_2}^2 - m_{\mathcal{H}_1}^2$.

CHAPTER 6

CONCLUSIONS

We have evaluated the reach of the Fermilab Tevatron collider for supersymmetry in the framework of the mSUGRA model. The best signature for SUSY appears to be trilepton events orginating from chargino/neutralino production, with subsequent leptonic decays. We have extended previous analyses into the large m_0 region, where significant regions of parameter space are accessible to the Tevatron search experiments. Tevatron experiments may be able to find evidence for SUSY up to $m_{1/2}$ values as high as 200-280 GeV depending on the ultimate integrated luminosity which is achieved.

We have updated our assessment of the SUSY reach of the CERN LHC via E_T^{miss} and multilepton channels, and presented new results for the reach in channels with isolated photons or leptonically decaying Z bosons. Our results are presented over an expanded mSUGRA model parameter space to include the reach in the so-called HB/FP region at very large m_0. This region, together with the stau coannihilation corridor, and the annihilation funnel where LSPs annihilate via the A or H resonances, are strongly preferred by the recent data of the WMAP collaboration. The overall LHC reach turns out to be quite insensitive to $\tan\beta$. We find that experiments at the LHC will probe $m_{1/2} \stackrel{<}{\sim} 1400$ GeV for low m_0, and $m_{1/2} \sim 700$ for large m_0 in the HB/FP region. These values correspond to $m_{\tilde{g}} \sim 3000$ GeV and 1800 GeV, respectively.

We have also presented the reach in a variety of multi-lepton channels. The reach in these individual channels is, in general, sensitive to $\tan\beta$. We also show the reach in a channel including reconstructed $Z^0 \rightarrow \ell\bar{\ell}$ decays, and channels including isolated photons. The isolated photon signals may contain $h \rightarrow \gamma\gamma$ events at a low, but observable rate. Indeed the SUSY event sample may contain SM background-free $h \rightarrow \gamma\gamma$ events, though a very high integrated luminosity will be needed to identify the rate-limited h signal. In the HB/FP region, the photonic channels also have a slight enhancement from radiative

neutralino decays $\widetilde{Z}_2 \to \widetilde{Z}_1\gamma$. For $m_{1/2} \overset{<}{\sim} 800(400)$ GeV and small (large) values of m_0, there should be observable signals in all these channels if new physics discovered at the LHC is to be interpreted as supersymmetry as realized in the mSUGRA model.

We have also examined the reach of the LHC in light of the recent assessment of direct (from LEP2) and indirect constraints on the mSUGRA model. The indirect constraints include the neutralino relic density $\Omega_{\widetilde{Z}_1}h^2$ from recent WMAP analyses together with accelerator measurements of $BF(b \to s\gamma)$, $a_\mu = (g-2)_\mu$ and the bound on $BF(B_s \to \mu^+\mu^-)$ (this bound is hardly constraining for the parameter planes that we have examined). For large values of $\tan\beta$, experimental values of $BF(b \to s\gamma)$ and a_μ disfavor negative values of the μ parameter unless m_0 and $m_{1/2}$ are also large, but for $\tan\beta \sim 10$, values of m_0 and $m_{1/2} \overset{>}{\sim} 400 - 500$ GeV are perfectly acceptable. For $\mu > 0$, m_0 would have to be rather small so that the relic density is either in the bulk annihilation region or in the stau coannihilation strip, or m_0 would have to be very large, in the HB/FP region. The CERN LHC can definitely explore all the bulk annihilation region, and can explore all the stau co-annihilation corridor unless $\tan\beta$ is very high. The LHC can explore the HB/FP region up to $m_{1/2} \sim 700$ GeV via the conventional SUSY search channels. However, the HB/FP region appears to extend indefinitely to large $m_{1/2}$ and m_0 values, ultimately well beyond the LHC reach. For large $\tan\beta$, the A, H annihilation funnel enters the m_0 $vs.$ $m_{1/2}$ plane. The LHC with 100 fb^{-1} ought to be able to detect SUSY over this entire region, except for the case of very large $\tan\beta \sim 56$ with $\mu > 0$.

The recent constraint on the relic density of neutralinos obtained from WMAP measurements, together with earlier determinations of $BF(b \to s\gamma)$ and $(g-2)_\mu$ select out regions of parameter space of the mSUGRA model. In the stau co-annihilation region, the H, A-annihilation funnel and in the HB/FP regions, very high values of m_0 and $m_{1/2}$ consistent with all constraints are possible: moreover, the so-called bulk region where sparticles are light is disfavored. These considerations motivated us to re-assess the reach of various collider and non-accelerator search experiments for supersymmetry. In this work, we re-evaluate the reach of a $\sqrt{s} = 0.5$ and 1 TeV linear e^+e^- collider for SUSY in the context of the mSUGRA model, examining for the first time the reach in the HB/FP region. We find that a $\sqrt{s} = 1$ TeV LC can explore most of the stau co-annihilation region if $\tan\beta \overset{<}{\sim} 30$, although along with a dilepton search, a ditau search will also be needed.

The H, A-annihilation funnel typically extends beyond the maximum reach of a LC. In the HB/FP region, chargino pairs may be kinematically accessible to a LC, but the energy release in chargino pairs can be small, reducing detection efficiency. Nonetheless, LCs should be able to probe much of the lower HB/FP region with standard chargino searches. In the upper HB/FP region, new cuts are proposed to allow signals from much of the small $\widetilde{W}_1 - \widetilde{Z}_1$ mass gap region to be observable above SM backgrounds. In this region, the reach of even a 500 GeV LC can exceed that of the CERN LHC! This is all the more important in that it occurs in a region of model parameter space which is allowed by all constraints, including those imposed by WMAP.

One should also stress that the LCs reach is also complementary to the reach of direct dark matter search experiments (DDMS) even though both kinds of experiments similarly cover much of the HB/FP region [111]. The complementarity of a LC occurs for the region which is very close to the no REWSB border. In this region, the neutralino relic density is so low that DDMS experiments are not able to cover this part of the parameter space even though the higgsino component of neutralino is significant. This region can be probed by experiments at a LC.

If a supersymmetric signal is found, then the next obvious step will be to determine the underlying MSSM parameters. We have performed a case study in the low $m_{1/2}$ part of the hyperbolic branch. In this region, we show that a measurement of $m_{\widetilde{W}_1}$ and $m_{\widetilde{Z}_1}$ is possible at the 10% level. A measurement of the total chargino pair cross section to 2.5% allows a determination of MSSM parameters M_2 and μ, although $\tan\beta$ is more difficult to pin down. The resulting determination of M_2 and μ would point to a model with higgsino-like charginos and neutralinos. Together with absence (or low levels) of squark signals at the LHC, and the agreement of the chargino cross section with the expected s-channel contribution (pointing to heavy sneutrinos) these measurements would be indicative of an mSUGRA-type model in the HB/FP region. In case parameters are in the upper part of the hyperbolic branch, LC event characteristics may be sufficient at least to establish the production of massive particles, with associated decay products that are quite soft. An examination of how one would obtain information about the underlying scenario would be worthy of exploration.

If nature has chosen to be described by inoMSB model with an $SU(5)$ gauge symmetry above the GUT scale, then we may expect a SUSY Higgs boson discovery at the luminosity

upgrade of the Tevatron, but no sign of sparticles. Conversely, we would expect a SUSY discovery at the CERN LHC (unless sparticle masses are so heavy they are in the fine-tuned region of SUSY parameter space, with $m_{\tilde{g}} > 2500$ GeV). However, the underlying model will not be revealed until a sufficient data set has been accumulated at a linear e^+e^- collider, where precision measurements of sparticle masses would point to an inoMSB model with a $SU(5)$ GUT symmetry.

REFERENCES

[1] M. E. Peskin and D. V. Schroeder, An Introduction to Quantum Field Theory, 1995.

[2] J. R. Ellis, Lectures given at European School of High-Energy Physics, Beatenberg, Switzerland, 26 Aug - 8 Sep 2001, hep-ph/0203114.

[3] D. Pierce, Talk given at the Theoretical Advanced Study Institute in Elementary Particle Physics (TASI 97): Supersymmetry, Supergravity and Supercolliders, Boulder, CO, 1-7 Jun 1997, hep-ph/9805497.

[4] S. Coleman and J. Mandula, *Phys. Rev.* **159** (1967) 1251.

[5] R. Haag, J. Lopuzanski and M. Sohnius, *Nucl. Phys.* **B 88** (1975) 257.

[6] H. Baer and X. Tata, Weak Scale Supersymmetry: From Superfields to Scattering Events, *to be published.*

[7] L. O'Raifeartaigh, *Nucl. Phys.* **B 96** (1975) 331.

[8] E. Cremmer, S. Ferrara, L. Girardello and A. Van Proeyen, *Nucl. Phys.* **B 212** (1983) 413.

[9] L. Randall and R. Sundrum, Nucl. Phys. **B557**, 79 (1999); G. F. Giudice, M. A. Luty, H. Murayama and R. Rattazzi, JHEP **9812**, 027 (1998).

[10] M. Dine, A. Nelson, Y. Nir and Y. Shirman, Phys. Rev. D**53**, 2658 (1996); for a review, see G. Giudice and R. Rattazzi, Phys. Rept. **322**, 419 (1999).

[11] D. E. Kaplan, G. D. Kribs and M. Schmaltz, Phys. Rev. D **62**, 035010 (2000); Z. Chacko, M. A. Luty, A. E. Nelson and E. Ponton, JHEP **0001**, 003 (2000)

[12] A. Chamseddine, R. Arnowitt and P. Nath, *Phys. Rev. Lett.* **49** (1982) 970; R. Barbieri, S. Ferrara and C. Savoy, *Phys. Lett.* **B 119** (1982) 343; N. Ohta, *Prog. Theor. Phys.* **70** (1983) 542; L. J. Hall, J. Lykken and S. Weinberg, *Phys. Rev.* **D 27** (1983) 2359; for reviews, see H. P. Nilles, *Phys. Rep.* **110** (1984) 1, and P. Nath, `hep-ph/0307123`.

[13] Joint LEP2 Supersymmetry Working Group, *Combined Chargino Results, up to 208 GeV*, `http://lepsusy.web.cern.ch/lepsusy/inos_moriond01/charginos_pub.html`.

[14] H. Baer, M. Drees, R. Godbole, J. Gunion and X. Tata, *Phys. Rev.* **D 44** (1991) 725; H. Baer, J. Sender and X. Tata, *Phys. Rev.* **D 50** (1994) 4517; H. Baer, P. Mercadante and X. Tata, *Phys. Rev.* **D 59** (1999) 015010; R. Demina, J. Lykken, K. Matchev and A. Nomerotski, *Phys. Rev.* **D 62** (2000) 035011.

[15] H. Baer, C. H. Chen, F. Paige and X. Tata, *Phys. Rev.* **D 49** (1994) 3283; H. Baer, B. Harris and M. H. Reno, *Phys. Rev.* **D 57** (1998) 5871.

[16] D. Dicus, S. Nandi and X. Tata, *Phys. Lett.* **B 129** (1983) 451; A. Chamseddine, P. Nath and R. Arnowitt, *Phys. Lett.* **B 129** (1983) 445.

[17] H. Baer and X. Tata, *Phys. Lett.* **B 155** (1985) 278.

[18] H. Baer, K. Hagiwara and X. Tata, *Phys. Rev. Lett.* **57** (1986) 294 and *Phys. Rev.* **D 35** (1987) 1598.

[19] R. Arnowitt and P. Nath, *Mod. Phys. Lett.* **A 2** (1987) 331.

[20] R. Barbieri, F. Caravaglios, M. Frigeni and M. Mangano, *Nucl. Phys.* **B 367** (1991) 28.

[21] H. Baer and X. Tata, *Phys. Rev.* **D 47** (1993) 2739.

[22] J. Lopez, D. Nanopoulos, X. Wang and A. Zichichi, *Phys. Rev.* **D 48** (1993) 2062 and *Phys. Rev.* **D 52** (1995) 142.

[23] H. Baer, C. Kao and X. Tata, *Phys. Rev.* **D 48** (1993) 5175.

[24] S. Mrenna, G. Kane, G. Kribs and J. Wells, *Phys. Rev.* **D 53** (1996) 1168.

[25] H. Baer, C. H. Chen, C. Kao and X. Tata, *Phys. Rev.* **D 52** (1995) 1565; H. Baer, C. H. Chen, F. Paige and X. Tata, *Phys. Rev.* **D 54** (1996) 5866; H. Baer, C. H. Chen, M. Drees, F. Paige and X. Tata, *Phys. Rev.* **D 58** (1998) 075008.

[26] K. Matchev and D. Pierce, *Phys. Rev.* **D 60** (1999) 075004.

[27] H. Baer, C. H. Chen, M. Drees, F. Paige and X. Tata, *Phys. Rev. Lett.* **79** (1997) 986 and *Phys. Rev.* **D 58** (1998) 075008; J. Lykken and K. Matchev, *Phys. Rev.* **D 61** (2000) 015001.

[28] H. Baer, M. Drees, F. Paige, P. Quintana and X. Tata, *Phys. Rev.* **D 61** (2000) 095007.

[29] V. Barger, C. Kao and T. Li, *Phys. Lett.* **B 433** (1998) 328; V. Barger and C. Kao, *Phys. Rev.* **D 60** (1999) 115015.

[30] The background was also independently computed by J. M. Campbell and R. K. Ellis, *Phys. Rev.* **D 60** (1999) 113006.

[31] K. Matchev and D. Pierce, *Phys. Lett.* **B 467** (1999) 225.

[32] S. Abel *et al.* (SUGRA Working Group Collaboration), `hep-ph/0003154`.

[33] A. Dedes, H. Dreiner, U. Nierste and P. Richardson, `hep-ph/0207026`.

[34] H. Baer, C. H. Chen, F. Paige and X. Tata, *Phys. Rev.* **D 52** (1995) 2746 and *Phys. Rev.* **D 53** (1996) 6241.

[35] K. Chan, U. Chattopadhyay and P. Nath, *Phys. Rev.* **D 58** (1998) 096004.

[36] J. Feng, K. Matchev and T. Moroi, *Phys. Rev. Lett.* **84** (2000) 2322 and *Phys. Rev.* **D 61** (2000) 075005.

[37] J. Ellis, T. Falk and K. Olive, *Phys. Lett.* **B 444** (1998) 367; J. Ellis, T. Falk, K. Olive and M. Srednicki, *Astropart. Phys.* **13** (2000) 181.

[38] M. Drees and M. Nojiri, *Phys. Rev.* **D 47** (1993) 376; H. Baer and M. Brhlik, *Phys. Rev.* **D 57** (1998) 567; H. Baer, M. Brhlik, M. Diaz, J. Ferrandis, P. Mercadante, P. Quintana and X. Tata, *Phys. Rev.* **D 63** (2001) 015007; A. Djouadi, M. Drees and J. Kneur, *J. High Energy Phys.* **0108** (2001) 055; J. Ellis, T. Falk, G. Ganis, K. Olive and M. Srednicki, *Phys. Lett.* **B 510** (2001) 236; L. Roszkowski, R. Ruiz de Austri and T. Nihei, *J. High Energy Phys.* **0108** (2001) 024; A. Lahanas and V. Spanos, *Eur. Phys. J.* **C 23** (2002) 185.

[39] J. Feng, K. Matchev and F. Wilczek, *Phys. Lett.* **B 482** (2000) 388 and *Phys. Rev.* **D 63** (2001) 045024; see also H. Baer and M. Brhlik, *Phys. Rev.* **D 57** (1998) 567.

[40] C. Boehm, A. Djouadi and M. Drees, *Phys. Rev.* **D 62** (2000) 035012; J. Ellis, K. Olive and Y. Santoso, *Astropart. Phys.* **18** (2003) 395.

[41] See also G. Belanger, F. Boudjema, A. Pukhov and A. Semenov, *Comput. Phys. Commun.* **149** (2002) 103; H. Baer, C. Balazs and A. Belyaev, *J. High Energy Phys.* **0203** (2002) 042 and `hep-ph/0211213`; J. Edsjo, M. Schelke, P. Ullio and P. Gondolo, JCAP **0304** (2003) 001.

[42] C. L. Bennett *et al.*, Preliminary Maps and Basic Results," arXiv:astro-ph/0302207; D. N. Spergel *et al.*, Determination of Cosmological Parameters," arXiv:astro-ph/0302209.

[43] H. Baer, C. Balázs, A. Belyaev, J. K. Mizukoshi, X. Tata and Y. Wang, *J. High Energy Phys.* **0207** (2002) 050 and `hep-ph/0210441`; for a review, see G. Eigen, R. Gaitskell, G. Kribs and K. Matchev, `hep-ph/0112312`.

[44] H. Baer and C. Balázs, JCAP **0305** (2003) 006.

[45] H. Baer, F. Paige, S. Protopopescu and X. Tata, `hep-ph/0001086`.

[46] D. Pierce, J. Bagger, K. Matchev and R. Zhang, *Nucl. Phys.* **B 491** (1997) 3.

[47] B. Allanach, S. Kraml and W. Porod, *J. High Energy Phys.* **0303** (2003) 016.

[48] F. Maltoni and T. Stelzer, *J. High Energy Phys.* **0302** (2003) 027.

[49] For recent reviews, see *e.g.* S. Martin, in *Perspectives on Supersymmetry*, edited by G. Kane (World Scientific), `hep-ph/9709356`; M. Drees, `hep-ph/9611409`; J. Bagger, `hep-ph/9604232`; X. Tata, *Proc. IX J. Swieca Summer School,* J. Barata, A. Malbousson and S. Novaes, Eds., `hep-ph/9706307`; S. Dawson, Proc. TASI 97, J. Bagger, Ed., `hep-ph/9712464`.

[50] H. Baer, C. Balázs, A. Belyaev, J. K. Mizukoshi, X. Tata and Y. Wang, *J. High Energy Phys.* **0207** (2002) 050 and `hep-ph/0210441`; for a review, see G. Eigen, R. Gaitskell, G. Kribs and K. Matchev, `hep-ph/0112312`.

[51] For a recent review, see K. Olive, arXiv:astro-ph/0301505 (2003).

[52] Joint HEP2 Supersymmetry Working Group, *Combined Chargino Results, up to 208 GeV*,
`http://alephwww.cern.ch/lepsusy/www/inos_moriond01/charginos.pub.html`.

[53] ALEPH, DELPHI, L3 and OPAL Colaborations, *Phys. Lett.* **B 565** (2003) 61.

[54] H. Baer, M. Drees, F. Paige, P. Quintana and X. Tata, *Phys. Rev.* **D 61** (2000) 095007.

[55] V. Barger, C. Kao and T. Li, Phys. Lett. **B433**, 328 (1998); V. Barger and C. Kao, Phys. Rev. D**60**, 115015 (1999).

[56] K. Matchev and D. Pierce, *Phys. Rev.* **D 60** (1999) 075004 and *Phys. Lett.* **B 467** (1999) 225

[57] S. Abdullin and F. Charles, *Nucl. Phys.* **B 547** (1999) 60.

[58] S. Abdullin *et al.* (CMS Collaboration), `hep-ph/9806366`.

[59] ATLAS Collaboration, "ATLAS Physics and Detector Performance Technical Design Report", LHCC 99-14/15.

[60] H. Baer, C. H. Chen, M. Drees, F. Paige and X. Tata, *Phys. Rev.* **D 59** (1999) 055014.

[61] H. Baer, C. H. Chen, F. Paige and X. Tata, *Phys. Rev.* **D 49** (1994) 3283; D. Denegri, W. Majerotto and L. Rurua, *Phys. Rev.* **D 58** (1998) 095010 and *Phys. Rev.* **D 60** (1999) 035008.

[62] H. Baer, C. H. Chen, F. Paige and X. Tata, *Phys. Rev.* **D 50** (1994) 4508.

[63] H. Baer, C. H. Chen and X. Tata, *Phys. Rev.* **D 55** (1997) 1466.

[64] S. Bityukov and N. Krasnikov, *Phys. Lett.* **B 469** (1999) 149 and `hep-ph/0102179`.

[65] H. Baer, A. Belyaev, T. Krupovnickas and X. Tata, *Phys. Rev.* **D 65** (2002) 075024.

[66] H. Baer, P. Mercadante, F. Paige, X. Tata and Y. Wang, *Phys. Lett.* **B 435** (1998) 109; H. Baer, P. Mercadante, X. Tata and Y. Wang, *Phys. Rev.* **D 62** (2000) 095007.

[67] H. Baer, J. K. Mizukoshi and X. Tata, *Phys. Lett.* **B 488** (2000) 367; A. Barr, C. Lester, M. Parker, A. Allanach and P. Richardson, *J. High Energy Phys.* **0303** (2003) 045.

[68] H. Baer, J. Ellis, G. Gelmini, D. Nanopoulos and X. Tata, *Phys. Lett.* **B 161** (1985) 175; G. Gamberini, *Z. Physik* **C 30** (1986) 605; H. Baer, V. Barger, D. Karatas and X. Tata, *Phys. Rev.* **D 36** (1987) 96; R. M. Barnett, J. F. Gunion and H. Haber, *Phys. Rev.* **D 37** (1988) 1892; H. Baer, X. Tata and J. Woodside, *Phys. Rev.* **D 42** (1990) 1568; A. Bartl, W. Majerotto, B. Mösslacher, N. Oshimo and S. Stippel, *Phys. Rev.* **D 43** (1991) 2214; H. Baer, M. Bisset, X. Tata and J. Woodside, *Phys. Rev.* **D 46** (1992) 303. A. Bartl, W. Majerotto and W. Porod, *Z. Physik* **C 64** (1994) 499; A. Djouadi, Y. Mambrini and M. Mühlleitner, *Eur. Phys. J.* **C 20** (2001) 563; J. Hisano, K. Kawagoe and M. Nojiri, `hep-ph/0304214`.

[69] M. Nojiri and Y. Yamada, *Phys. Rev.* **D 60** (1999) 015006;

[70] H. Baer, X. Tata and J. Woodside, *Phys. Rev.* **D 42** (1990) 1450.

[71] H. Haber and D. Wyler, *Nucl. Phys.* **B 323** (1989) 267; S. Ambrosanio and B. Mele, *Phys. Rev.* **D 55** (1997) 1399.

[72] H. Baer and T. Krupovnickas, *J. High Energy Phys.* **0209** (2002) 038.

[73] K. Chan, U. Chattopadhyay and P. Nath, *Phys. Rev.* **D 58** (1998) 096004.

[74] J. Feng, K. Matchev and T. Moroi, *Phys. Rev. Lett.* **84** (2000) 2322 and *Phys. Rev.* **D 61** (2000) 075005.

[75] S. Abdullin, A. Khanov and N. Stepanov, CMSJET, CMS TN/94-180 (2002).

[76] H. Baer, C. Balázs and A. Belyaev, *J. High Energy Phys.* **0203** (2002) 042 and `hep-ph/0211213`; see also H. Baer and M. Brhlik, *Phys. Rev.* **D 53** (1996) 597.

[77] P. Gondolo and G. Gelmini, *Nucl. Phys.* **B 360** (1991) 145; J. Edsjö and P. Gondolo, *Phys. Rev.* **D 56** (1997) 1879.

[78] K. Abe *et al.* (Belle Collaboration), *Phys. Lett.* **B 511** (2001) 151.

[79] D. Cronin-Hennessy *et al.* (CLEO Collaboration), *Phys. Rev. Lett.* **87** (2001) 251808.

[80] R. Barate *et al.* (Aleph Collaboration), *Phys. Lett.* **B 429** (1998) 169.

[81] R. Barate *et al.* (Aleph Collaboration), *Phys. Lett.* **B 429** (1998) 169; D. Cronin-Hennessy *et al.* (Cleo Collaboration), *Phys. Rev. Lett.* **87** (2001) 251808; K. Abe *et al.* (Belle Collaboration), *Phys. Lett.* **B 511** (2001) 151; theoretical results for $BF(b \to s\gamma)$ in the SM are contained in *e.g.* P. Gambino and M. Misiak, *Nucl. Phys.* **B 611** (2001) 338; supersymmetric contributions are shown in *e.g.* H. Baer and M. Brhlik, *Phys. Rev.* **D 55** (1997) 3201 and H. Baer, M. Brhlik, D. Castano and X. Tata, *Phys. Rev.* **D 58** (1998) 015007.

[82] G. Degrassi, P. Gambino and G. Giudice, *J. High Energy Phys.* **0012** (2000) 009. M. Carena, D. Garcia, U. Nierste and C. Wagner, *Phys. Lett.* **B 499** (2001) 141.

[83] G. W. Bennett *et al.* [Muon g-2 Collaboration], Phys. Rev. Lett. **89**, 101804 (2002) [Erratum-ibid. **89**, 129903 (2002)].

[84] M. Knecht and A. Nyffeler, *Phys. Rev.* **D 65** (2002) 073034; M. Knecht, A. Nyffeler, M. Perrottet and E. De Rafael, *Phys. Rev. Lett.* **88** (2002) 071802; M. Hayakawa and T. Kinoshita, `hep-ph/0112102`; I. Blokland, A. Czarnecki and K. Melnikov, *Phys. Rev. Lett.* **88** (2002) 071803; A. Nyffeler, `hep-ph/0209329`.

[85] K. Melnikov, *Int. J. Mod. Phys.* **A 16** (2001) 4591 (His updated analysis of the SM value of δa_μ was presented at the High Energy Physics Seminar, University of Hawaii, March 2002); F. Jegerlehner, `hep-ph/0104304`; K. Hagiwara, A. D. Martin, D. Nomura and T. Teubner, `hep-ph/0209187`.

[86] M. Davier, S. Eidelman, A. Hocker and Z. Zhang, *Eur. Phys. J.* **C 27** (2003) 497.

[87] H. Baer, C. Balázs, A. Belyaev, J. K. Mizukoshi, X. Tata and Y. Wang, *J. High Energy Phys.* **0207** (2002) 050 and `hep-ph/0210441`.

[88] S. Narison, `hep-ph/0303004`.

[89] H. Baer, C. Balázs, J. Ferrandis and X. Tata, *Phys. Rev.* **D 64** (2001) 035004.

[90] F. Abe *et al.*, (CDF Collaboration), *Phys. Rev.* **D 57** (1998) 3811.

[91] S. Rai Choudhury and N. Gaur, *Phys. Lett.* **B 451** (1998) 86; K. Babu and C. Kolda, *Phys. Rev. Lett.* **84** (2000) 228; A. Dedes, H. Dreiner and U. Nierste, *Phys. Rev. Lett.* **87** (2001) 251804; R. Arnowitt, B. Dutta, T. Kamon and M. Tanaka, *Phys. Lett.* **B 538** (2002) 121; J. K. Mizukoshi, X. Tata and Y. Wang, *Phys. Rev.* **D 66** (2002) 115003.

[92] J. Ellis, T. Falk, K. Olive and M. Srednicki, *Astropart. Phys.* **13** (2000) 181.

[93] See H. Baer and M. Brhlik, Ref. [38]

[94] K. Griest and D. Seckel, *Phys. Rev.* **D 43** (1991) 3191.

[95] H. Baer, C. Balazs, A. Belyaev, J. Mizukoshi, X. Tata and Y. Wang, *J. High Energy Phys.* **0207** (2002) 050 and `hep-ph/0210441`; for a review, see G. Eigen, R. Gaitskell, G. Kribs and K. Matchev, `hep-ph/0112312`.

[96] G. Bennett *et al.* (E821 Collaboration), *Phys. Rev. Lett.* **89** (2002) 101804; a recent theoretical evaluation is given in M. Davier, S. Eidelman, A. Hocker and Z. Zhang, *Eur. Phys. J.* **C 31** (2003) 503; a survey of contributions from supersymmetric models can be found in H. Baer, C. Balazs, J. Ferrandis and X. Tata, *Phys. Rev.* **D 64** (2001) 035004.

[97] For a review of WMAP implications for supersymmetric models, see A. Lahanas, N. E. Mavromatos and D. V. Nanopoulos, *Int. J. Mod. Phys.* **D 12** (2003) 1529.

[98] H. Goldberg, *Phys. Rev. Lett.* **50** (1983) 1419; J. Ellis, J. Hagelin, D. Nanopoulos, K. Olive and M. Srednicki, *Nucl. Phys.* **B 238** (1984) 453.

[99] G. Jungman, M. Kamionkowski and K. Griest, *Phys. Rept.* **267** (1996) 195.

[100] H. Baer and M. Brhlik, *Phys. Rev.* **D 53** (1996) 597.

[101] J. Ellis, T. Falk, G. Ganis, K. Olive and M. Srednicki, *Phys. Lett.* **B 510** (2001) 236.

[102] G. Anderson and D. Castano, *Phys. Rev.* **D 52** (1995) 1693 and *Phys. Lett.* **B 347** (1995) 300.

[103] See M. Davier *et al.*, Ref. [96].

[104] J. Ellis, K. Olive, Y. Santoso and V. Spanos, *Phys. Lett.* **B 565** (2003) 176; U. Chattopadhyay, A. Corsetti and P. Nath, *Phys. Rev.* **D 68** (2003) 035005; A. Lahanas and D. V. Nanopoulos, *Phys. Lett.* **B 568** (2003) 55.

[105] J. Ellis, K. Olive, Y. Santoso and V. Spanos, `hep-ph/0310356` (2003).

[106] J. Ellis, T. Falk and K. Olive, *Phys. Lett.* **B 444** (1998) 367; J. Ellis, T. Falk, K. Olive and M. Srednicki, *Astropart. Phys.* **13** (2000) 181.

[107] W. de Boer, M. Herold, C. Sander and V. Zhukov, `hep-ph/0309029`.

[108] H. Baer, T. Krupovnickas and X. Tata, *J. High Energy Phys.* **0307** (2003) 020.

[109] H. Baer, T. Krupovnickas and X. Tata, Ref.[108]; see also H. Baer, M. Drees, F. Paige, P. Quintana and X. Tata, *Phys. Rev.* **D 61** (2000) 095007; V. Barger and C. Kao, *Phys. Rev.* **D 60** (1999) 115015; K. Matchev and D. Pierce, *Phys. Lett.* **B 467** (1999) 225 for earlier work on the trilepton signal.

[110] H. Baer, C. Balazs, A. Belyaev, T. Krupovnickas and X. Tata, *J. High Energy Phys.* **0306** (2003) 054. For earlier work, see H. Baer, C. H. Chen, F. Paige and X. Tata, *Phys. Rev.* **D 52** (1995) 2746 and *Phys. Rev.* **D 53** (1996) 6241; H. Baer, C. H. Chen, M. Drees, F. Paige and X. Tata, *Phys. Rev.* **D 59** (1999) 055014; S. Abdullin and F. Charles, *Nucl. Phys.* **B 547** (1999) 60; S. Abdullin *et al.* (CMS Collaboration), `hep-ph/9806366`; B. Allanach, J. Hetherington, A. Parker and B. Webber, *J. High Energy Phys.* **08** (2000) 017.

[111] H. Baer, C. Balazs, A. Belyaev and J. O'Farrill, JCAP**0309** (2003) 007; see also V. A. Bednyakov, H. V. Klapdor-Kleingrothaus and S. Kovalenko, Phys. Rev. D **50**, 7128 (1994) [arXiv:hep-ph/9401262]; E. Diehl, G. L. Kane, C. F. Kolda and J. D. Wells, Phys. Rev. D **52**, 4223 (1995) [arXiv:hep-ph/9502399]; R. Arnowitt and P. Nath, Phys. Rev. D **54**, 2374 (1996) [arXiv:hep-ph/9509260]; H. Baer and M. Brhlik, Ref. [38]; M. Drees, M. Nojiri, D. P. Roy and Y. Yamada, *Phys. Rev.* **D 56** (1997) 276; A. Bottino, F. Donato, N. Fornengo and S. Scopel, Phys. Rev. D **63**, 125003 (2001) [arXiv:hep-ph/0010203]; J. R. Ellis, A. Ferstl and K. A. Olive, Phys. Rev. D **63**, 065016 (2001) [arXiv:hep-ph/0007113]; E. Accomando, R. Arnowitt, B. Dutta and Y. Santoso, Nucl. Phys. B **585**, 124 (2000) [arXiv:hep-ph/0001019]; M. E. Gomez and J. D. Vergados, Phys. Lett. B **512**, 252 (2001) [arXiv:hep-ph/0012020];A. B. Lahanas, D. V. Nanopoulos and V. C. Spanos, Phys. Lett. B **518**, 94 (2001) [arXiv:hep-ph/0107151];E. A. Baltz and P. Gondolo, Phys. Rev. Lett. **86**, 5004 (2001) [arXiv:hep-ph/0102147]; Y. G. Kim, T. Nihei, L. Roszkowski and R. Ruiz de Austri, JHEP **0212**, 034 (2002) [arXiv:hep-ph/0208069]; for a recent review and further references, see the review by C. Munoz, `hep-ph/0309346`.

[112] H. Baer, R. Munroe and X. Tata, *Phys. Rev.* **D 54** (1996) 6735.

[113] A. Djouadi, M. Drees and J. L. Kneur, Ref. [38]; See also R. Arnowitt, B. Dutta, T. Kamon and V. Khotilovich, `hep-ph/0308159`.

[114] T. Tsukamoto, K. Fujii, H. Murayama, M. Yamaguchi and Y. Okada, *Phys. Rev.* **D 51** (1995) 3153; see also JLC-1, KEK Report 92-16 (1992).

[115] H. Baer, T. Krupovnickas and X. Tata, `hep-ph/0405058` *submitted to JHEP.*

[116] H. Baer, F. Paige, S. Protopopescu and X. Tata, `hep-ph/0312045`.

[117] P. Chen, *Phys. Rev.* **D 46** (1992) 1186.

[118] This region appears in H. Baer, C. H. Chen, R. Munroe, F. Paige and X. Tata, *Phys. Rev.* **D 51** (1995) 1046. Co-annihilation calculations may be found in C. Boehm, A. Djouadi and M. Drees, *Phys. Rev.* **D 62** (2000) 035012; J. Ellis, K. Olive and Y. Santoso, *Astropart. Phys.* **18** (2003) 395; J. Edsjo, M. Schelke, P. Ullio and P. Gondolo, JCAP**0304** (2003) 001.

[119] M. Drees, C. S. Kim and X. Tata, *Phys. Rev.* **D 37** (1988) 784.

[120] T. Sjostrand *et al.,* *Comput. Phys. Commun.* **135** (2001) 238.

[121] CompHEP v.33.23, by A. Pukhov *et al.,* hep-ph/9908288 (1999)

[122] V. Barger, T. Han and J. Jiang, *Phys. Rev.* **D 63** (2001) 075002.

[123] H. Baer, C. Balazs and A. Belyaev, *J. High Energy Phys.* **0203** (2002) 042.

[124] J. Edsjo and P. Gondolo, *Phys. Rev.* **D 56** (1997) 1879; this is based on earlier work by G. Gelmini and P. Gondolo, *Nucl. Phys.* **B 351** (1991) 623.

[125] See Ref. [114, 112] and also M. Nojiri, K. Fujii and T. Tsukamoto, *Phys. Rev.* **D 54** (1996) 6756; M. N. Danielson *et al.,* SLAC-REPRINT-1996-010 *Prepared for 1996 DPF / DPB Summer Study on New Directions for High-Energy Physics (Snowmass 96), Snowmass, Colorado, 25 Jun - 12 Jul 1996*; see also J. Feng and M. Nojiri, `hep-ph/0210390` and R. Godbole, `hep-ph/0102191`.

[126] For recent reviews, see *e.g.* S. Martin, in *Perspectives on Supersymmetry*, edited by G. Kane (World Scientific), hep-ph/9709356; M. Drees, hep-ph/9611409 (1996); J. Bagger, hep-ph/9604232 (1996); X. Tata, *Proc. IX J. Swieca Summer School*, J. Barata, A. Malbousson and S. Novaes, Eds. hep-ph/9706307; S. Dawson, Proc. TASI 97, J. Bagger, Ed. hep-ph/9712464.

[127] A. Chamseddine, R. Arnowitt and P. Nath, Phys. Rev. Lett. **49**, 970 (1982); R. Barbieri, S. Ferrara and C. Savoy, Phys. Lett. **119B**, 343 (1982); L. J. Hall, J. Lykken and S. Weinberg, Phys. Rev. D**27**, 2359 (1983).

[128] See, for instance, A. Pomarol and R. Rattazzi, JHEP **05**, 013 (1999); E. Katz, Y. Shadmi and Y. Shirman, JHEP **08**, 015 (1999); R. Rattazzi, A. Strumia and J. Wells, Nucl. Phys. **B576**, 3 (2000); I. Jack and D. R. T. Jones, Phys. Lett. **B482**, 167 (2000).

[129] M. Schmaltz and W. Skiba, Phys. Rev. D**62**, 095005 (2000) and Phys. Rev. D**62**, 095004 (2000).

[130] A. B. Lahanas and D. V. Nanopoulos, Phys. Rept. **145**, 1 (1987).

[131] H. Baer, M. Diaz, P. Quintana and X. Tata, JHEP **0004**, 016 (2000).

[132] L. J. Hall, R. Rattazzi and U. Sarid, Phys. Rev. D**50**, 7048 (1994); R. Hempfling, Phys. Rev. D**49**, 6168 (1994); M. Carena, M. Olechowski, S. Pokorski and C. Wagner, Nucl. Phys. **B426**, 269 (1994).

[133] H. Baer, M. Diaz, J. Ferrandis and X. Tata, Phys. Rev. D**61**, 111701 (2000).

[134] W. de Boer, M. Huber, C. Sander and D. I. Kazakov, Phys. Lett. B **515**, 283 (2001).

[135] S. Komine and M. Yamaguchi, hep-ph/0110032 (2001).

[136] N. Polonsky and A. Pomarol, Phys. Rev. D **51**, 6532 (1995).

[137] R. Arnowitt and P. Nath, Phys. Rev. Lett. **69**, 725 (1992); J. Hisano, H. Murayama and T. Yanagida, Nucl. Phys. B **402**, 46 (1993).

[138] S. Abel *et al.* Report of SUGRA Working Group for Run II of the Tevatron, hep-ph/0003154 (2000).

[139] H. Baer, J. Sender and X. Tata, Phys. Rev. **D50**, 4517 (1994); J. Sender, Ph.D thesis, hep-ph/0010025; H. Baer, P. Mercadante and X. Tata, Phys. Rev. **D59**, 015010 (1999); R. Demina, J. Lykken, K. Matchev and A. Nomerotski, Phys. Rev. **D62**, 035011 (2000).

[140] H. Baer, K. Hagiwara and X. Tata, Phys. Rev. D**35**, 1598 (1987); R. Arnowitt and P. Nath, Mod. Phys. Lett. **A2**, 331 (1987); H. Baer and X. Tata, Phys. Rev. D**47**, 2739 (1993).

[141] J. Lykken and K. Matchev, Phys. Rev. D**61**, 015001 (1999).

[142] H. Baer, V. Barger, D. Karatas and X. Tata, Phys. Rev. **D36**, 96 (1987).

[143] H. Baer, C. H. Chen, M. Drees, F. Paige and X. Tata, Phys. Rev. D**59**, 055014 (1999).

[144] H. Baer, C. Balazs, S. Hesselbach, J. K. Mizukoshi and X. Tata, Phys. Rev. D**63**, 095008 (2001).

BIOGRAPHICAL SKETCH

Tadas Krupovnickas

Date of Birth   May 13, 1977

Citizenship   Lithuanian

Education   2000 - 2004 enrolled in a Ph.D. program in physics,
Florida State University (advisor Prof. Howard Baer)
1998-2000 M.Sc., Vilnius University (Lithuania), Physics
1994-1998 B.Sc., Vilnius University (Lithuania), Physics

Research and
Teaching Positions   2004 - Present, Research Associate,
Brookhaven National Laboratory, Upton, NY
2001 - 2004, Research Assistant,
Florida State University, Tallahassee, FL
2000-2001, Teaching Assistant in Physics,
Florida State University, Tallahassee, FL
1998-2000, Part-time engineer,
Institute of Theoretical Physics and Astronomy , Vilnius, Lithuania

Languages   Lithuanian (native), English, Russian

PUBLICATIONS IN REFEREED JOURNALS

1. Dibaryons as Canonically Quantized Biskyrmions, (with E. Norvaišas and D. O. Riska), Lith. J. Phys. **41**, 13 (2001).

2. The Reach of the Fermilab Tevatron and CERN LHC for Gaugino Mediated SUSY Breaking Models, (with H. Baer, A. Belyaev and X. Tata), Phys. Rev. D**65**, 075024 (2002).

3. Radiative Neutralino Decay in Supersymmetric Models, (with H. Baer), JHEP **0209**, 038 (2002).

4. Updated Reach of the CERN LHC and Constraints from Relic Density, $b \rightarrow s\gamma$ and a_μ in the mSUGRA Model, (with H. Baer, C. Balazs, A. Belyaev and X. Tata), JHEP**0306**, 054 (2003).

5. Reach of the Fermilab Tevatron for Minimal Supergravity in the Region of Large Scalar Masses, (with H. Baer and X. Tata), JHEP**0307**, 020 (2003).

6. Linear Collider Capabilities for Supersymmetry in Dark Matter Allowed Regions of the mSUGRA Model, (with H. Baer, A. Belyaev and X. Tata), JHEP**0402**, 007 (2004).

7. SUSY Normal Scalar Mass Hierarchy Reconciles $(g-2)_\mu$, $b \rightarrow s\gamma$ and Relic Density, (with H. Baer, A. Belyaev and A. Mustafayev), hep-ph/0403214 (*submitted to JHEP*).

8. Two Photon Background and the Reach of a Linear Collider for Supersymmetry in WMAP Favored Coannihilation Regions, (with H. Baer and X. Tata), hep-ph/0405058 (*submitted to JHEP*).

OTHER REPORTS

1. Deuteron and Dibaryons in the Skyrme Model, (with E. Norvaišas, A. Acus and D. O. Riska), AIP Conf. Proc. **603**, 369 (2001).

TALKS ON RESEARCH

1. SUSY at the LHC: mSUGRA and Beyond, at Pheno-03 meeting, UW-Madison, May 2003.

2. Linear Collider Capabilities in mSUGRA, at Pheno-04 meeting, UW-Madison, April 2004.

AWARDS

1. The 2004 Dirac-Hellman award in Theoretical Physics "for investigations into the capabilities of colliding beam experiments to detect supersymmetric matter".